# THE IMPACT OF CLIMATE VARIABILITY ON THE PHYSICAL PROPERTIES OF THE BLACK SEA FOR THE PERIOD 1971 – 2001

**A THESIS SUBMITTED TO**
**INSTITUTE OF MARINE SCIENCES**
**OF**
**MIDDLE EAST TECHNICAL UNIVERSITY**
**BY**

**MUHTEŞEM AKİF KORKMAZ**

**IN PARTIAL FULFILLMENT OF THE REQUIREMENTS**
**FOR**
**THE DEGREE OF MASTER OF SCIENCE**
**IN**
**PHYSICAL OCEANOGRAPHY**

**SEPTEMBER 2011**

**THE IMPACT OF CLIMATE VARIABILITY ON THE PHYSICAL PROPERTIES OF THE BLACK SEA FOR THE PERIOD 1971 – 2001**

submitted by **MUHTEŞEM AKİF KORKMAZ** in partial fulfilment of the requirements for the degree of **Master of Science in Graduate School of Marine Sciences, Middle East Technical University** by,

Prof. Dr. Ferit Bingel _____
Director, **Graduate School of Marine Sciences, METU**

Prof. Dr. Emin Özsoy _____
Head of Department, **Physical Oceanography**

Yrd. Doç. Dr. Barış Salihoğlu _____
Supervisor, **Graduate School of Marine Sciences, METU**

Dr. Heather Anne Cannaby _____
Co-supervisor, **Graduate School of Marine Sciences, METU**

**Examining Committee Members:**

Prof. Dr. Emin Özsoy _____
**Graduate School of Marine Sciences, METU**

Yrd. Doç. Dr. Barış Salihoğlu _____
**Graduate School of Marine Sciences, METU**

Dr. Heather Anne Cannaby _____
**Graduate School of Marine Sciences,** METU

Prof. Dr. Ahmet Erkan Kıdeyş _____
**Graduate School of Marine Sciences, METU**

Dr. Mustafa Koçak _____
**Graduate School of Marine Sciences, METU**

**Date:** September 05, 2011

**I hereby declare that all information in this document has been obtained and presented in accordance with academic rules and ethical conduct. I also declare that, as required by these rules and conduct, I have fully cited and referenced all material and results that are not original to this work.**

Name, Last name: Muhteşem Akif KORKMAZ

Signature :

# ABSTRACT

## THE IMPACT OF CLIMATE VARIABILITY ON THE PHYSICAL PROPERTIES OF THE BLACK SEA FOR THE PERIOD 1971 – 2001

KORKMAZ, M. Akif

M.Sc., Department of Physical Oceanography

Supervisor: Yrd. Doç. Dr. Barış Salihoğlu

Co-Supervisor: Dr. Heather Anne Cannaby

September 2011, 110 pages

Deep ventilation of the Black Sea is inhibited by a sharp salinity gradient within the upper water column, resulting in a shallow anoxic interface at around 100 – 200 m depth. Understanding biological and chemical processes within the boundary region between oxic and anoxic waters is fundamental to comprehend the biogeochemical response of the Black Sea to climate forcing. The structure and depth of the chemocline is largely determined by the physical processes which transport surface waters to depth. Here we investigate how the structure and stability of the upper water column responds to changes in climatic forcing over interannual to multidecadal time-scales. We report results from two hydrodynamic model reanalysis. The first, extending from 1971-1993 assimilates CTD data. The second, extending from 1992-2001, assimilates altimetry data. Model results are validated against CTD and satellite data and consistency between modeled surface properties and observations is demonstrated. A problem with the data assimilation scheme of the 1992 -2001 model run is identified, which results in model drift and an unrealistic water column structure at intermediate depths. Model results indicate a warming trend of 0.7 °C in sea surface temperature and a freshening trend of 0.4 in sea surface salinity between 1971 and 2001, with an associated increasing trend in the stability of the seasonal thermocline and a declining trend in surface mixed layer depth of 6.3 m. Trends are superimposed on a distinct multiannual variability characterized by

relatively warm and saline conditions between 1971 and 1984, relatively cool and fresh conditions between 1985 and 1993 and warm and fresh conditions post-1993. The period between 1985 and 1993 corresponds to higher NAO and EA/WR index values although these indices do not exhibit a similar ~decadal scale variability. Higher frequency interannual variability in water column characteristics is related to the NAO and EA/WR atmospheric indices. Despite the cool conditions prevalent during the 1990s, the persistent freshening trend caused a reduction in the density of mixed layer waters throughout the study period. A positive feedback is proposed between increasing SSTs, reduced vertical mixing and freshening of the surface layer which further increases the stability of the upper water column. CIL characteristics typically mirrored surface temperature characteristics and varied considerably between the relatively warm period during the early part of the study and the subsequent cool period. The mean thickness and temperature of the CIL between 1971 and 1981 were ~39 m and ~7.5 °C respectively, as compared to ~47 m and ~7.4 °C between 1982 and 1993. Freshening of the upper water column also resulted in an increase in the stability maxima that exists at the base of the CIL, suggesting reduced ventilation of the upper water column during winter.

Keywords: Black Sea, Climate variability, Climate change, Cold intermediate layer, Mixed layer, Surface temperature, Surface salinity.

# ÖZ

## İKLİM DEĞİŞKENLİĞİNİN 1971 - 2001 ARASINDA KARADENİZ FİZİKSEL ÖZELLİKLERİNE ETKİSİ

Yüksek Lisans, Fiziksel Oşinografi Bölümü

Tez yöneticisi: Yrd. Doç. Dr. Barış Salihoğlu

Eş tez yöneticisi: Dr. Heather Anne Cannaby

Eylül 2011, 110 sayfa

Karadeniz'in derin sularının havalandırılması, 100 – 160 m arası derinlikte sığ bir anoksik ara yüzle sonuçlanan, üst su tabakası içerisindeki keskin bir tuzluluk geçişi ile ketlenir. Oksik ve anoksik sular arasındaki sınır bölgesi içinde biyolojik ve kimyasal süreçlerin anlaşılması Karadeniz'in iklim etkisine biyo-jeo-kimyasal tepkisini anlamak için temeldir. Kemoklin yapısı ve derinliği, büyük ölçüde yüzey sularını derinlere taşıyan fiziksel süreçler tarafından belirlenir. Burada üst su kolonunun yapısı ve kararlılığının yıllar ve çok-yıllar zaman ölçeklerinde iklim etkisindeki değişime tepkisi incelenmektedir. İki hidrodinamik model tekrar analizleri rapor edilmektedir; İlki 1971 – 1993 yılları arasında uzanan CTD verisi özümseyen, ikincisi 1992 – 2001 yılları arasında uzanan altimetre verisi özümseyen. Model sonuçları, CTD ve uydu verilerine karşı doğrulanmış ve modellenen yüzey özellikleri ve gözlemler arasında tutarlılık göstermiştir. 1992 – 2001 arasını kapsayan ikinci model çalışması veri özümseme süreci ile ilgili bir problemle karşılaşılmış olup bu problem orta derinliklerde model sürüklenmesi ve gerçekçi olmayan bir su kolonu yapısı ile sonuçlanmıştır. Model sonuçları artan yüzey sıcaklıklarında 0.7 $C^o$ lik ısınma ve yüzey tuzluluğunda 0.4 lük bir azalma göstermektedir. Bununla ilişkili olarak mevsimsel termoklin kararlılığında bir artış ve yüzey karışmış tabaka derinliğinde 6.3 metrelik bir azalma yönelimi gözlenmiştir. Eğilimler 1971 ve 1984 yılları arasında nispeten sıcak ve tuzlu koşullar, 1985 ve 1993 yılları arasında nispeten serin ve az tuzlu koşullar ile 1993 yılı sonrasında sıcak ve az tuzlu koşullar

ile karakterize edilebilecek şekilde belirgin çok-yıllık değişkenlik üzerine bindirilmiş. 1985 ve 1993 arasındaki dönem yüksek NAO ve EA/WR indeks değerlerine tekabül etmesine rağmen bu endeksler benzer bir ~ on yıllık ölçekli değişkenlik sergilememektedir. Su kolonu yapısındaki yüksek frekanslı yıllar arası değişkenlik NAO ve EA/WR indeks değerleri ile ilişkilidir. 1990'larda sık görülen serin koşullara rağmen, ısrarlı tuzluluk azalma yönelimi, çalışma süresi boyunca, karışık tabakalı suların yoğunluğunda bir azalmaya neden olmuştur. Daha sonra üst su kolonunun kararlılığını arttıran yüzey sıcaklığı artışı, azalan dikey karışım ve yüzey tabakasının azalan tuzluluğu, arasında olumlu bir geri besleme sunulmuştur. CIL özellikleri genellikle yüzey sıcaklığı özelliklerini yansıtır ve çalışmanın ilk bölümündeki nispeten sıcak dönem sırasında ve sonrasındaki serin dönem arasında önemli farklılıklar gösterdi. CIL'in (Soğuk Ara Tabaka) ortalama kalınlığı ve sıcaklığı 1971 ve 1981 yılları arasında sırasıyla yaklaşık 39 metre ve 7.5 $C^o$; 1982 ile 1993 arasında sırasıyla yaklaşık 47 metre ve 7.4 $C^o$ 'dir. Üst su kolonunun azalan tuzluluğu aynı zamanda CIL'in tabanında yer alan kararlılık maksimumunun artışı ile sonuçlanarak kış mevsimi boyunca üst su tabakası havalanmasının azalmasını destekler.

Anahtar Kelimeler: Karadeniz, İklim değişkenliği, İklim değişikliği, Soğuk ara tabaka, Karışmış tabaka, Yüzey tuzluluğu, Yüzey sıcaklığı.

To AC / DC

## ACKNOWLEDGMENTS

I wish to express my deepest gratitude to my supervisor Assistant Prof. Dr. Barış Salihoğlu and co-supervisor Dr. Heather Anne Cannaby for their guidance throughout the research and during the preparation and writing of this work.

I would like to thank Özge Yelekçi and Dr. Esin Yalçın for their endless frienship.

Special thanks to Ersin Tutsak, Serdar Sakınan, Fırat Özgenel, Ercüment Atmaca, Kemal Acar for their psychological support.

I would like to extend my gratitute to my office mate Ceren Güraslan and housemate Ali Aydoğdu.

I would also like to thank my mother and my sister for supporting and encouraging me both within this study and throughout my life.

Finally I would like to thank to "SETÜSTÜ", all the staff and members of IMS for creating such a beautiful workplace.

This study was supported by the Scientific and Technological Research Council of Turkey (TÜBİTAK) Project No: 108-Y-114.

# TABLE OF CONTENTS

# LIST OF TABLES

## TABLES

# LIST OF FIGURES

## FIGURES

# CHAPTER 1
# INTRODUCTION

## 1.1 Aims and objectives

As stated in sections above, the Black Sea has been subject to a multitude of human induced environmental pressures including eutrophication, overfishing, pollution (from river inflows, dumping, extensive shipping, and mineral exploitation), damming of rivers, and the introduction of alien species Each of the above mentioned environmental pressures has directly contributed to degradation of the Black Sea ecosystem making it difficult to isolate the impact of climate induced changes. It is clear following the above discussion that the structure and depth of the chemocline is largely determined by the physical processes which transport surface waters to depth. Therefore understanding interannual variability in the physical structure of the water column is vital to understanding the biogeochemical response to changes in climatic forcing.

This study examines the hypothesis that sustained changes in the heat and salt content of the Black Sea over the past four decades has led to changes in the stability of the upper water column, affecting both the extent of deep ventilation during winter and the structure of the seasonal thermocline. Due to a lack of sustained observations a model reanalysis covering the period from 1971-2001 is used. First a validation of the model results against CTD and satellite SST measurements is presented, demonstrating the stability of the model and consistency between modelled and observed properties of the upper water column. Then interannual to multiannual scale variability and multidecadal scale trends in the physical properties and water column structure of the Black Sea are described and analysed, relating observed interannual variability and trends to climatic forcing. The main focus of this thesis is on how the properties of the mixed-layer, the seasonal thermocline and the CIL changed throughout the study period.

## 1.2 Black Sea Oceanography

### 1.2.1 Physical Characteristics

The Black Sea is an inland sea located between 41$^{o}$N – 46$^{o}$N and 28$^{o}$E – 42$^{o}$E, connected to the Sea of Marmara via the Bosporus Strait and the Azov Sea by the Kerch Strait (Figure 1.1). The Black Sea has a surface area of 423,000 km$^{2}$, a total volume of 547,000 km$^{3}$, and a maximum depth of nearly 2200 m (Oguz *et al*., 2005a). The average depth is estimated to be ~1240 m (Ross *et al*., 1974). As can be seen in Figure 1.2, the shelf edge slope is steep and the shelf edge is narrow except in the northwestern region and western costs between Sevastapol and the discharge of the Sakarya River. The average depth of the North Western shelf region, which comprises nearly 20 % of the total area of the basin, is about 50 m (Oguz *et al*., 2005a). The North Western shelf contains the three most important rivers entering the Black Sea, the Danube, the Dniester and the Dnieper Rivers. The Danube River contributes about half of the total river input to the Black Sea and the Dnieper and the Dniester Rivers contribute 1/6 of the total river input (Sur, 2004). The Black Sea fresh water budget comprises of ~350 km$^{3}$ yr$^{-1}$ fresh river input with nearly 350 km$^{3}$ yr$^{-1}$ precipitation and about 350 km$^{3}$ yr$^{-1}$ evaporation (Unluata *et al*., 1990). The positive water budget of the Black Sea is balanced by a net outflow through the Bosporus, while the salt budget is conserved at a steady state by the balance of salinities of the inflowing and outflowing water. There is a net outflow through the Bosporus amounting to ~600 km$^{3}$ yr$^{-1}$ with salinities within the range 16-18, and a net influx of ~ 300 km$^{3}$ yr$^{-1}$ with salinities in the range 35 – 37.5 (Ozsoy *et al*., 1986; Ozsoy *et al*., 1988; Latif *et al*., 1990).

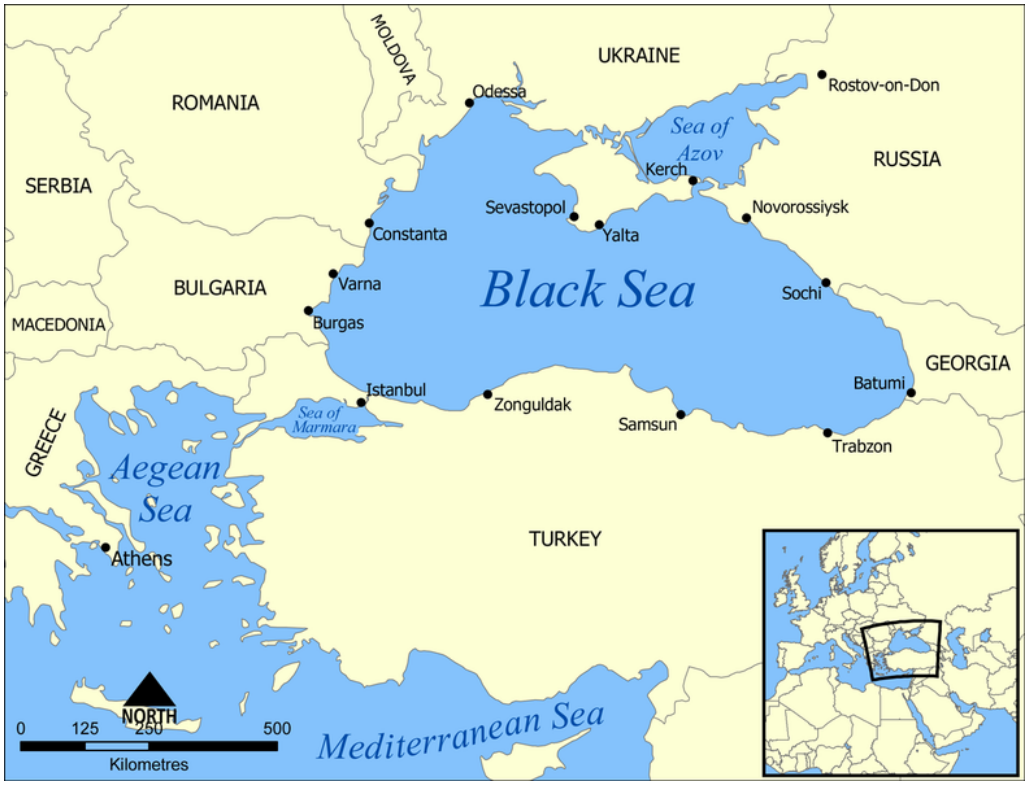


Figure 1.1 Location of the Black Sea (retrieved from http://en.wikipedia.org/wiki/Black_Sea)

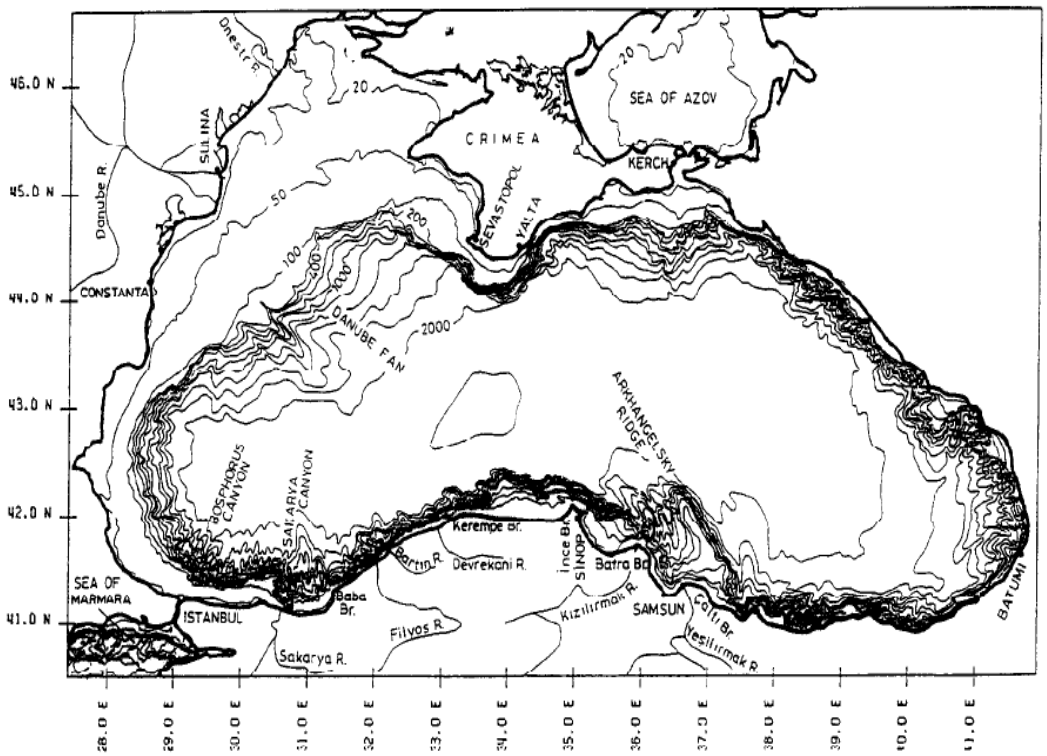


Figure 1.2. Black Sea bathymetry with important rivers (Ozsoy and Unluata, 1997).

#### 1.2.1.1 Water Column Structure

The Black Sea basin is flooded by saline Mediterranean water overlain by fresher water of riverine origin. As a result, a strong halocline exists around depths of 100 - 200 m (Ozsoy and Unluata, 1997). The salinity of the upper 30 – 40 m from the surface is about 18, with a seasonal variability in the range 0.5. Between the surface and ~200 m depth, salinity shows a relatively rapid increase to a value of nearly 21.4. Below 200 m depth salinity increases more gradually with depth, reaching a value of ~22.35 at 1700 m (Oguz and Tugrul, 1998). A typical salinity profile can be seen in Figure 1.3, taken from the World Ocean Atlas 2005.

The surface temperature of the Black Sea ranges seasonally from ~5 $^{o}$C to ~25 $^{o}$C. Below the seasonal thermocline there is a temperature minimum layer, typically characterised by water temperatures of less than 8 $^{o}$C, and with a core temperature of ~ 6 $^{o}$C. This feature is typically referred to as the Cold Intermediate Layer CIL (Ozsoy and Unluata, 1997). The lower boundary of the CIL ranges from 40 m depth in cyclonic regions to 160 m depth in anticyclonic regions. Below the CIL temperature gradually increases with depth, reaching ~9 $^{o}$C below depths of 1700 m. The water column shows a uniform and homogeneous structure below 1700 m due to geothermal heating from bottom, with an approximate energy input of 40 W m$^{-2}$ (Murray *et al*., 1991). A typical summer temperature profile, highlighting the CIL, can be seen in Figure 1.4, taken from the World Ocean Atlas 2005.

The process(s) leading to the formation of the CIL are not clearly understood and while a number of theories have been put forward over the years it now seems likely CIL formation is more complicated than previously thought and that a range of mechanisms may drive CIL formation throughout the Black Sea basin. As reported by Ozsoy and Unluata (1997), early Soviet oceanographers suggested that the CIL was formed by strong, local winter convection events. Other authors have suggested that CIL water originates from the Northwestern Shelf and Azov Sea, where extreme low temperatures occur in winter (Flippov, 1965; Toilmazin, 1985). It has also been suggested that the CIL is formed by down welling in the center of the cyclonic gyres

(Ovchinnicov and Popov, 1987). More recently, Ivanov *et al*. (1997) and Ozsoy and Unluata (1997) have suggested that all of the above mentioned processes may contribute to CIL formation.

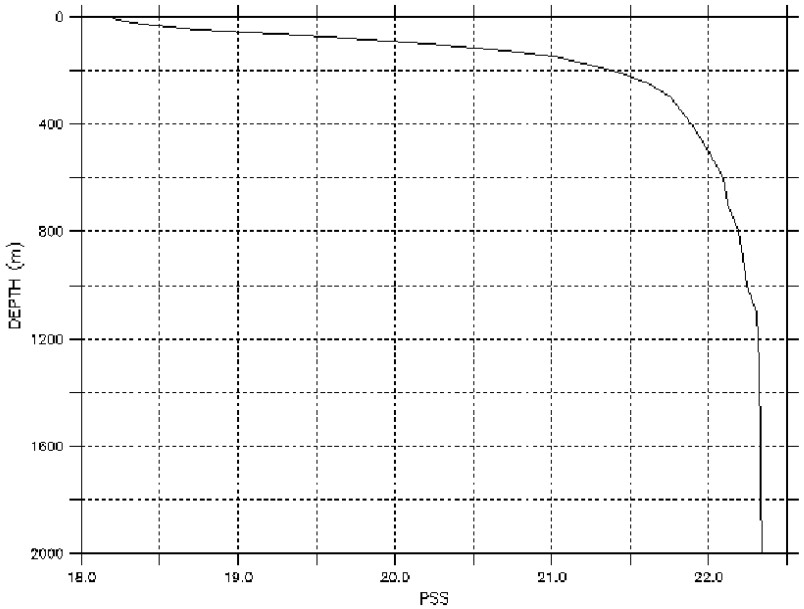


Figure 1.3. Example Black Sea salinity profile (35.5 E – 43.5 N, 1st of July 2005 at 12:00; World Ocean Atlas 2005).

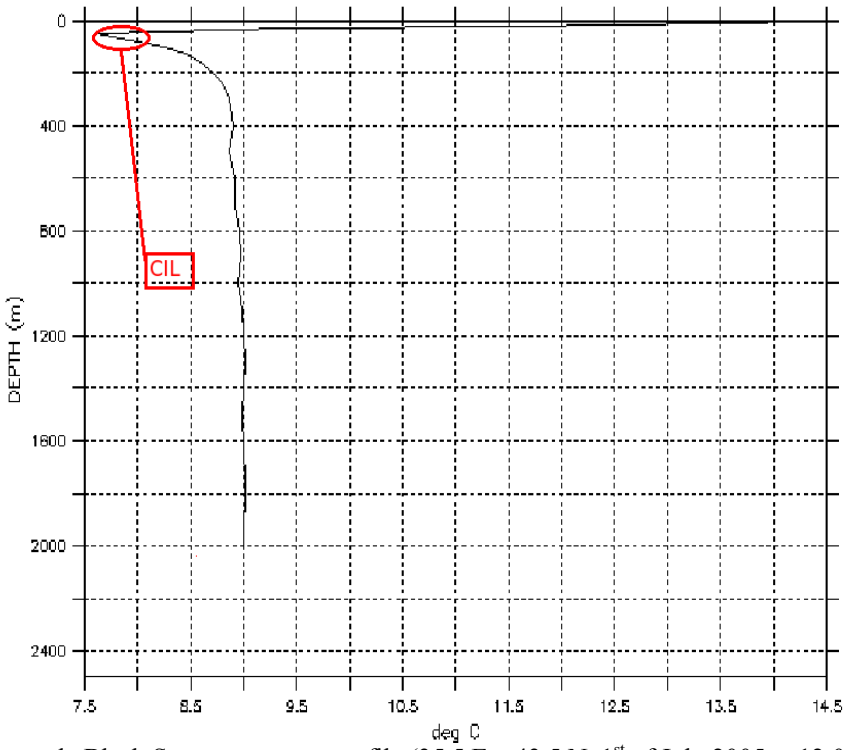


Figure 1.4. Example Black Sea temperature profile (35.5 E – 43.5 N, 1st of July 2005 at 12:00; World Ocean Atlas 2005). The subsurface temperature minimum layer known as the CIL is highlighted.

The Black Sea is characterised by shallow surface mixed-layer depths of less than 10 – 30 m in summer, while in the winter, the ML can reach up to 70 – 80 m. In this layer salinity is around 18 and temperature varies between 5 and 25 $^{o}$C with season and depth. As a result, mixed layer densities vary between 11 kg m$^{-3}$ and 14 kg m$^{-3}$. Below the ML there is a strong pycnocline associated with the sharp salinity gradient between 100 – 150 m depth. Since the water below the pycnocline is strongly affected by Mediterranean water from the Sea of Marmara, salinity, temperature and density gradually increase from 15 kg m$^{-3}$ to 17 kg m$^{-3}$ between the base of the pycnocline and 1700 m depth. Black Sea deep water is uniform and homogeneous with a temperature of 8.9 $^{o}$C, a salinity of 22.32 and a density of ~17 kg m$^{-3}$ (Murray *et al*., 1991; Ozsoy and Unluata, 1997). The density distribution of Black Sea waters can be clearly seen in the T-S diagram presented in Figure 1.5, together with that of the Marmara Sea water.

In conclusion, the Black Sea is highly stratified, consisting of two main water masses separated by a strong pycnocline which significantly limits vertical mixing. The vertical structure of the water column determines the vertical distribution of chemical and biological components, and the mechanisms of biogeochemical cycling, with implications for ecosystem functioning.

#### 1.2.1.2 General Circulation

The general basin scale circulation pattern of the Black Sea is illustrated in the form of a schematic diagram in Figure 1.6. The grey areas show regions where the maximum depth is less than 200 m. A cyclonic current following the 200 m contour is named the "Rim Current" (Oguz *et al*., 1993). The gyres encircled by the Rim Current are named the Western Gyre and the Eastern Gyre. A number of smaller quasi-permanent, anti-cyclonic eddies, including the prominent Batumi eddy in the southeast, are distributed between the Rim Current and the coasts. Bifurcation and convergence of the Rim Current at the west side of the basin is also illustrated in Figure 1.6 with a large anti-cyclonic eddy located to the north of the northwestern part of the Black Sea (Oguz *et al*., 2005a).

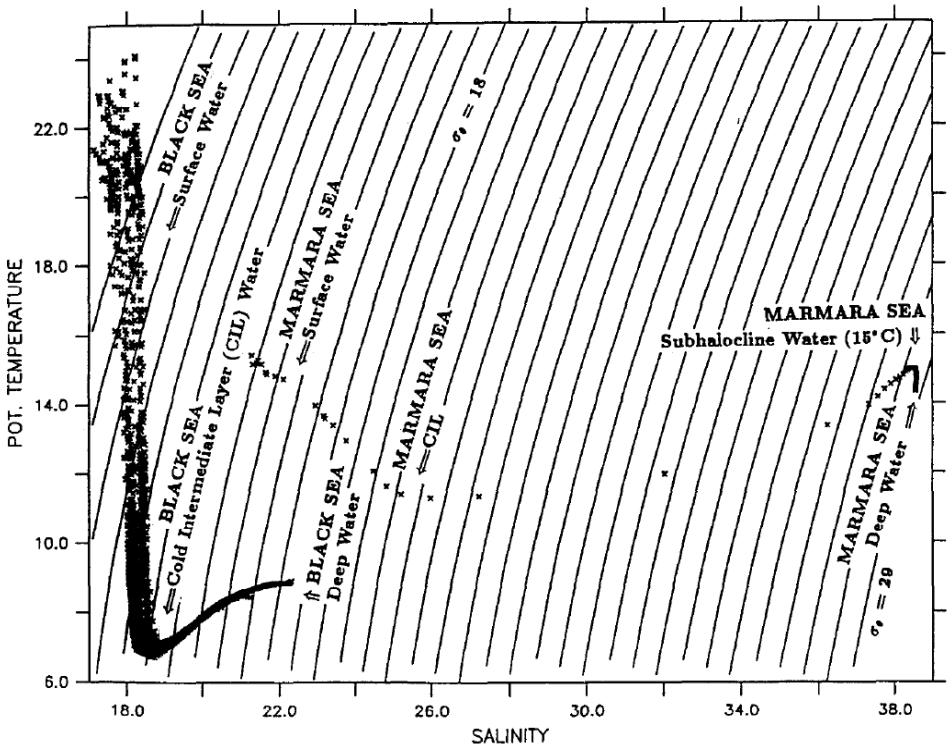


Figure 1.5. T-S diagram showing the characteristics of the Black Sea water as compared to the more saline Marmara Sea water from the cruise R/V Knorr Leg 4 in 1988 (Ozsoy and Unluata, 1997).

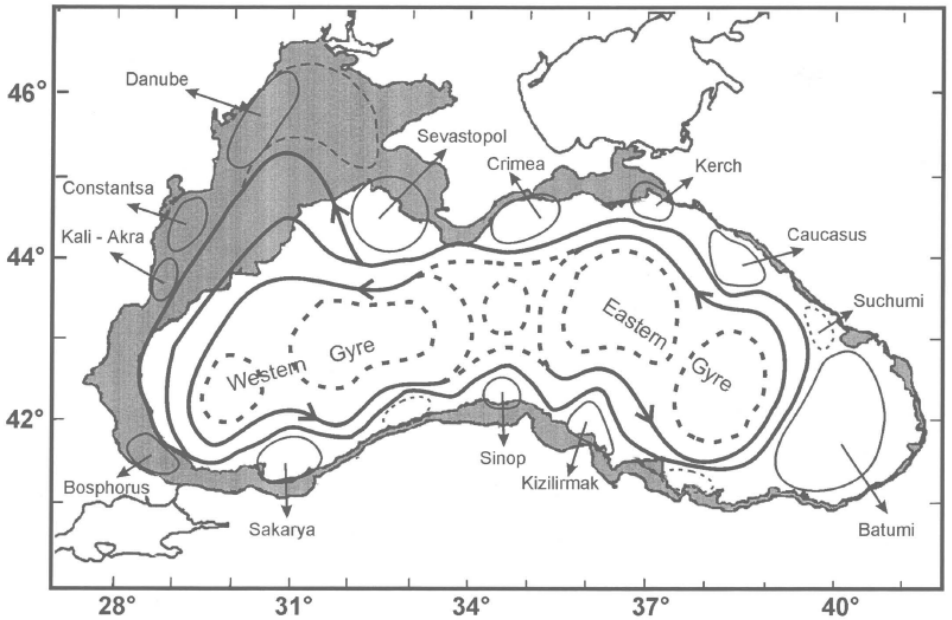


Figure 1.6. Schematic diagram illustrating the general circulation features of the Black Sea. Grey areas shows regions shallower than 200 m, thin (thick) lines show quasi-permanent anti-cyclonic (cyclonic) currents, dashed lines show recurrent currents (Oguz *et al*., 2005).

The average width of the Rim current is about 50 km with meanders that have length scales of nearly 100 – 200 km. These meanders show a standing structure in addition to impermanent and propagating characteristics (Ozsoy and Unluata, 1997). According to the ADCP (Acoustic Doppler Current Profiler) measurements of RV Bilim (April 1993; Oguz and Besiktepe, 1999), the speed of the Rim Current is about 50 – 100 cm $s^{-1}$ near the surface and at 150 – 300 m depth it has a speed of ~10 – 20 cm $s^{-1}$ (Oguz *et al*., 2005a). Although the gyres enclosed by the Rim Current are named the Eastern and Western gyres, recent studies shows that there are many centers of the gyres and the Rim current can penetrate into the central part of the Black Sea (Ozsoy and Unluata, 1997).

The driving forces of the cyclonic circulation of the Black Sea are not well explained and some modeling studies have addressed this question. Cyclonic currents seem to be forced mainly by the cyclonic wind patterns (Neumann, 1942; Moskalenko, 1976; Stanev *et al*., 1988; Rachev *et al*., 1991; Eremeev *et al*., 1992; Dzhioev and Sarkisyan, 1976; Demyshev, 1992; Trukhchev and Demin, 1992; Klimok and Makeshov, 1993). However, the numerical studies of Marchuk *et al*. (1975) and Stanev (1990) show thermohaline circulation driven by nonuniform seasonal surface fluxes can generate comparable currents (Ozsoy and Unluata, 1997).

The anti-cyclonic eddies surrounding the Rim Current have great importance for the transfer of materials between on-shore and off-shore regions and they follow the meanders of the Rim current. The quasi-permanent Batumi eddy deflects the Rim current away from the 200 m contour. Another significant quasi-permanent anti-cyclonic eddy is the Sevastapol eddy which is located behind the Crimean Peninsula relative to the Rim Current (Ozsoy and Unluata, 1997).

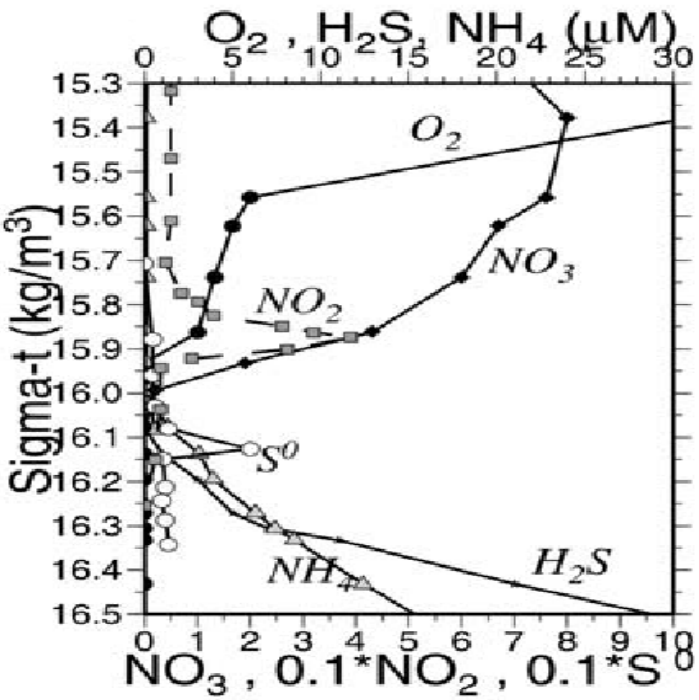


Figure 1 7. Vertical profiles of $O_2$, $NO_3$, $NO_2$, $S^0$, $H_2S$ and $NH_4$ for the upper 150 m of the Black Sea at the station 43° N, 34° E from cruise RV Knorr, 13 June 1988 (Oguz *et al*., 2001).

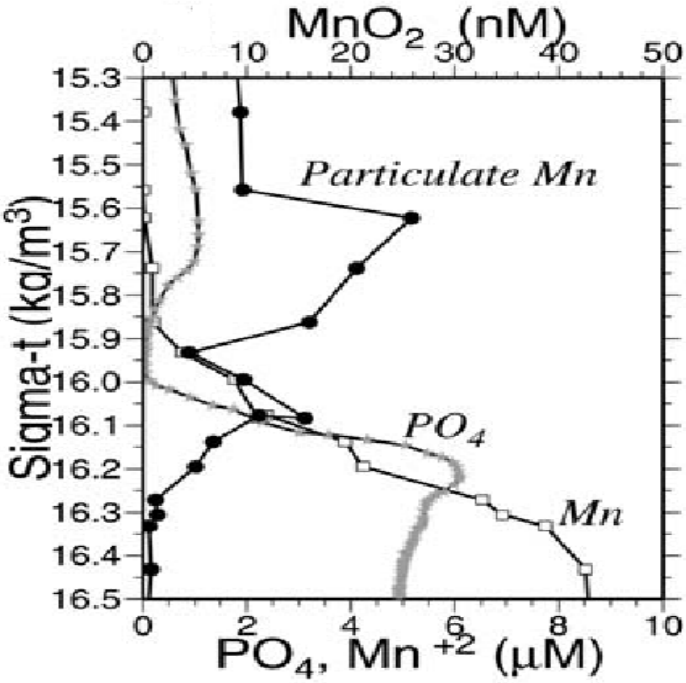


Figure 1.8. Vertical profiles of $MnO_2$, $PO_4$ and $Mn^{+2}$ for the upper 150 m of the Black Sea at the station 43° N, 34° E from cruise RV Knorr, 13 June 1988 (Oguz *et al*., 2001).

### 1.2.2 Biochemical Characteristics

The permanent pycnocline of the Black Sea forms a boundary between oxidised surface waters and deeper anoxic waters. The relatively shallow depth of the anoxic interface in the Black Sea results in unique processes of biogeochemical cycling (Oguz and Tugrul, 1998). In the anoxic layer there is no life except anaerobic bacteria due to high concentrations of $H_2S$. The euphotic zone, where the light level decreases up to 1% of surface intensity, has a maximum thickness of about 50 m and contains high oxygen concentrations of about 300 μM and high planktonic activity. Nearly 90 % of the sinking material is decomposed within this layer. Below the euphotic zone there is a layer 20 – 30 m thick which is aphotic but oxic. A small portion of sinking material reaches the anoxic zone, the upper limit of which is at nearly 100 m in offshore regions and at ~200 m depth in the onshore regions (Oguz *et al*., 2005). Between oxic and anoxic layers there is another layer which is called the 'suboxic layer' where both oxygen and $H_2S$ concentrations are below 5 μM. As can be seen in Figure 1.7, the upper limit of the suboxic layer is found at a density interface of 15.5 kg $m^{-3}$ and the lower limit is at around 16.2 kg $m^{-3}$. Below the anoxic interface ammonium and $H_2S$ increase with depth (Oguz and Tugrul, 1998; Oguz *et al*., 2005). According to Oguz *et al*. (1994) the lower level of the CIL overlaps with the upper level of the suboxic zone, which may explain the horizontal distribution of the oxic – suboxic transition (deeper in the cyclonic regions, shallower in the anti-cyclonic regions). The horizontal distribution of the lower level of the CIL and upper level of the anoxic zone (density interface of 16.2 kg $m^{-3}$) can be seen in Figures 1.9 and 10.

The Black Sea takes nutrients mainly from the Danube River, wet precipitation and nitrogen fixation. Danube sourced nutrients are transported by the Rim Current and feed the inner parts of the Rim current although some portion of nutrients are lost through the Bosporus with the winter surface outflow and sinking (Oguz *et al*. 2005). Figures 1.7 and 1.8 show examples of the vertical distribution of nutrients within the upper 150 m of the water column, as recorded during June 1988. Nitrate concentration peaks at around 15.5 kg $m^{-3}$ with maximum observed concentrations in

this example of 8 μM. Below this depth, nitrate starts to decrease to trace amounts within the upper limits of the anoxic zone. Nitrite concentrations exhibits peak values around the 15.85 kg $m^{-3}$ density surface, with a maximum value of nearly 0.5 μM in the example shown. Nitrite becomes depleted around the anoxic layer transition zone. In the anoxic zone, below $\sigma_t$~15.6 kg $m^{-3}$, the denitrification process becomes essential for organisms. In order to oxidize reduced ammonium and manganese, nitrate and nitrate are used. Nitrate is reduced to nitrogen while nitrite is produced as a byproduct. This process causes a decrease in nitrate in the suboxic zone and results in a peak in nitrite just above the anoxic layer, hence the peak nitrite zone is called the 'denitrification zone' (Oguz *et al*., 2005).

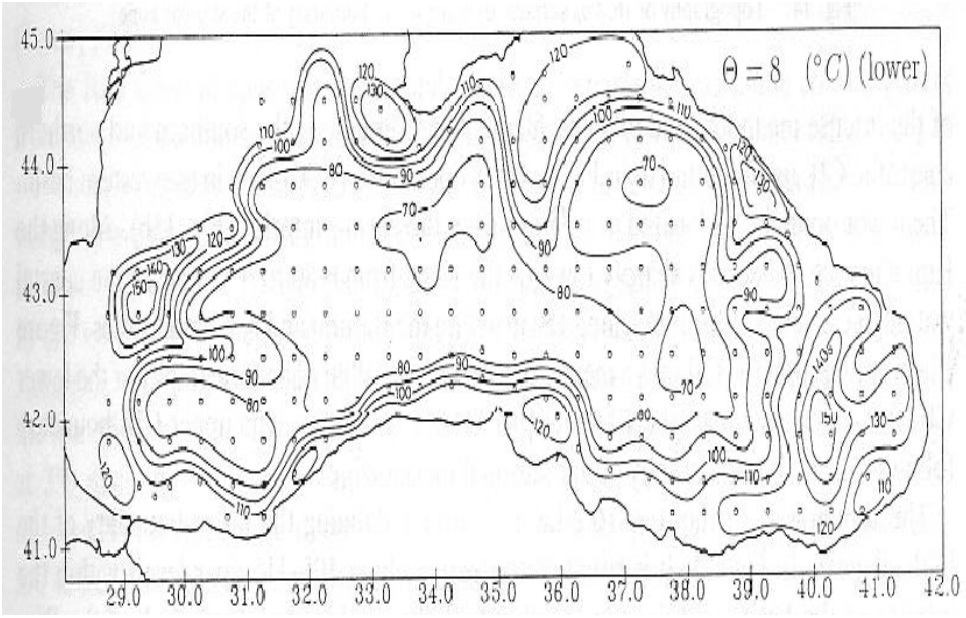


Figure 1.9. The lower limit of the CIL defined from the Hydroblack 1991 cruise (Oguz *et al*., 1994)

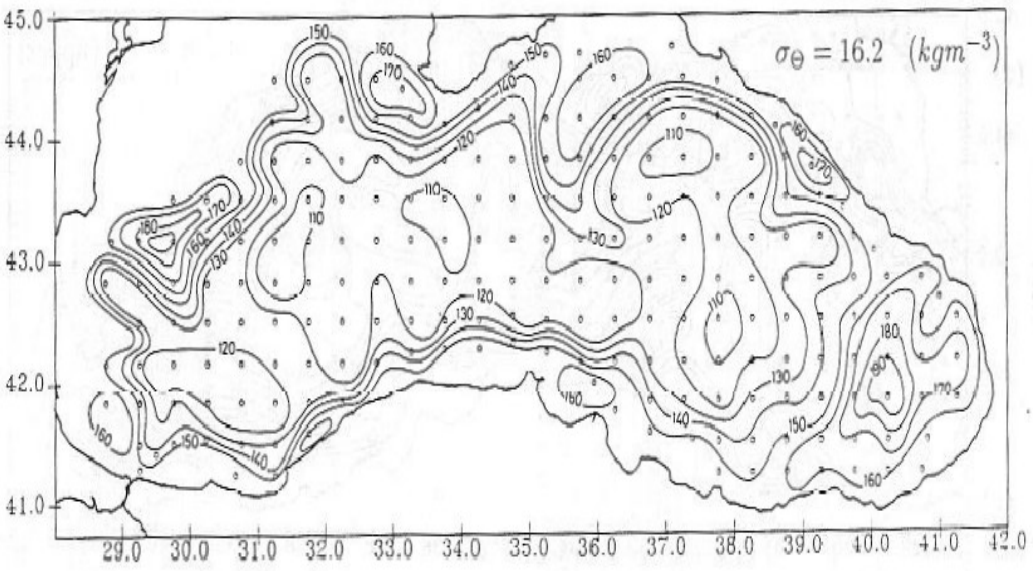


Figure 1.10. The upper limit of the anoxic zone from Hydroblack '91cruise (Oguz *et al*., 1994)

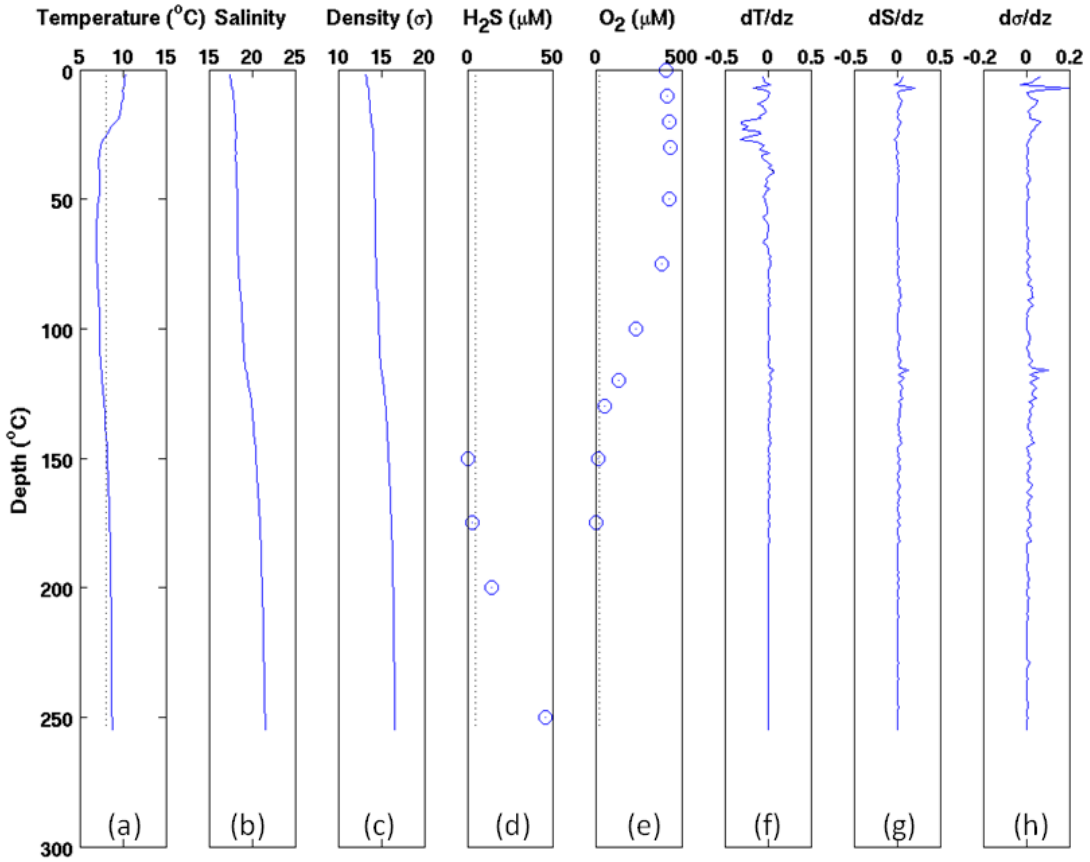


Figure 1.11. Sample profiles of (a) temperature, (b) salinity, (c) density, concentrations of (d) H2S and (e) O2, rate of change of (f) temperature, (g) salinity, (h) density in z direction (41.08 N, 38.00 E, 15.04.1990 extracted from Black Sea database; http://sfp1.ims.metu.edu.tr/).

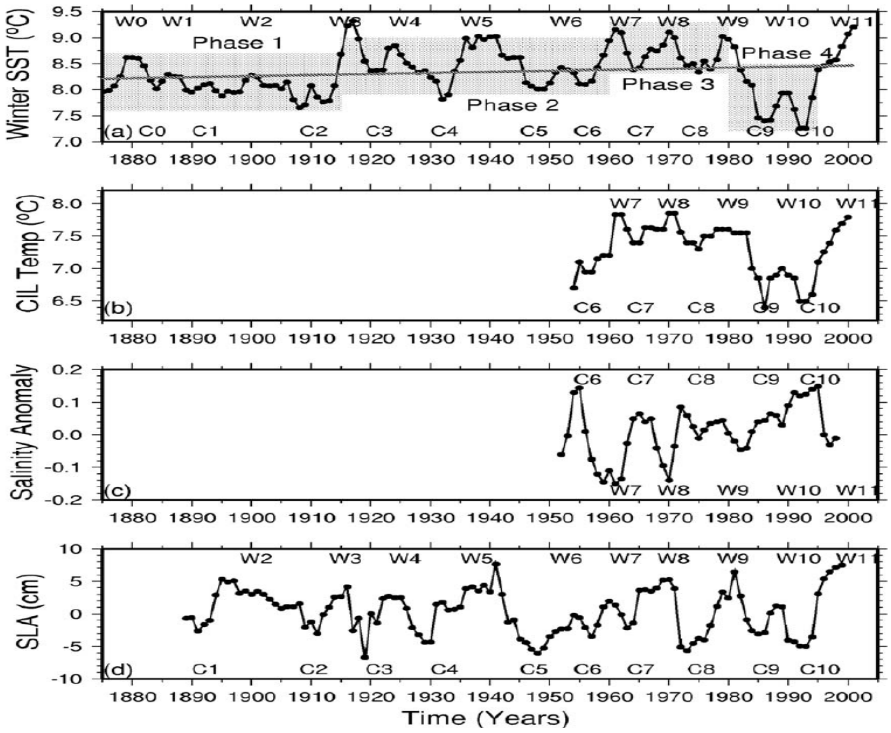


Figure 1.12. Three point moving average of long-term variations of a) winter (December–March) mean sea surface temperature (°C) averaged over the interior basin with depths greater than 1500 m, b)mean temperature (°C) of the Cold Intermediate Layer (May–November) , c) annual mean salinity anomaly of the upper 200 m layer, d) the detrended sea level anomaly (cm) (Oğuz *et.al*., 2006).

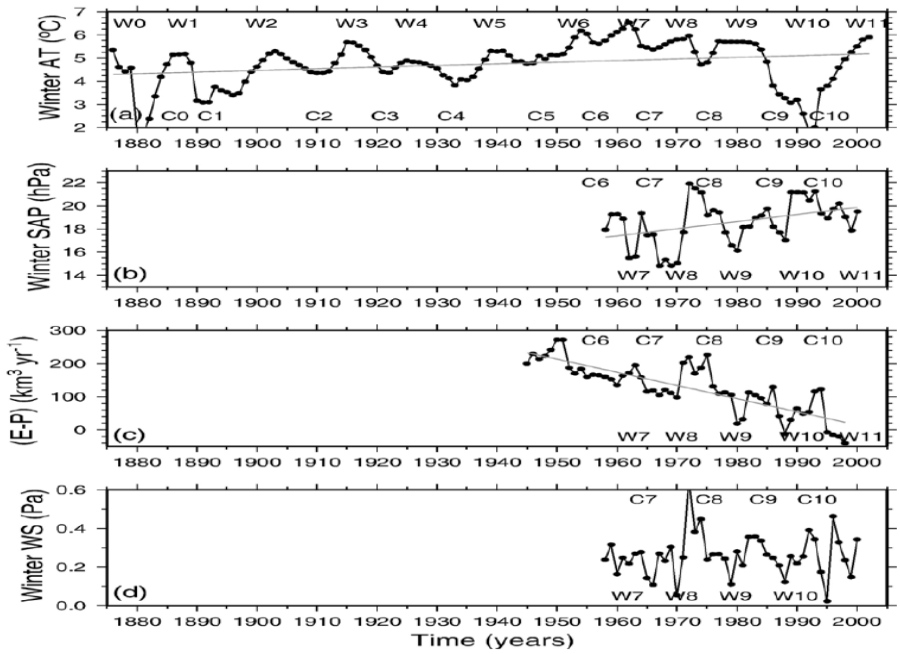


Figure 1.13. Three point moving average of Long-term variations of a) winter (December–March) mean air temperature (°C) , b) the winter (December–March) mean surface atmospheric pressure (hPa), c) winter (December–March) mean evaporation minus precipitation (km3 yr− 1), d) winter (January–March) mean wind stress magnitude averaged over the basin (Oğuz *et.al*., 2006).

Phosphate concentration increases gradually with depth up to values of 1 – 1.5 μM just above the denitrification zone, before decreasing to minimum values of 0.05 – 0.1 μM in the denitrification zone. With the appearance of sulfide around $\sigma_t$=16.2 kg $m^{-3}$, phosphate concentrations increase to peak concentrations of 5 – 8 μM (Oguz *et al*., 2005). Phosphate associated iron and manganese oxides can explain these high values (Shaffer, 1986; Codispoti *et al*., 1991). Silicate has a simple increasing trend with the depth such that, at around $\sigma_t$=16.2 kg $m^{-3}$ it has a value of nearly 70 – 75 μM and at around $\sigma_t$=16.8 kg $m^{-3}$ it has a value approximately 150 μM (Oguz *et al*., 2005).

In conclusion, temperature profiles recorded in the Black Sea exhibit a temperature minimum zone which is called the Cold Intermediate Layer (CIL; Figure 1.11 (a)) and around the lower boundary of this layer exists the upper boundary of the sub-oxic layer (Figure 1.11 (d) and (e)). The rate of change of temperature in z direction (Figure 1.11 (f)) shows a minimum that coincides with the upper boundary of the CIL and the rate of change of salinity in the z direction (Figure 1.11 (g)) exhibits two maximums; an upper maxima coincides with the seasonal pycnocline and a lower maxima coincides with the permanent pycnocline. The rate of change of density in the z direction (Figure 1.11 (h)), which is also a measure of stability, shows the same maximums with salinity and reflects the mixed layer depth and the base of CIL respectively.

## 1.3 Interannual and longer term variability in physical and biogeochemical characteristics

A linear trend fitted to the winter mean (December – March) sea surface temperature (SST) record of the Black Sea (Figure 1.12a) exhibit a 0.25 $^{o}$C warming trend over last century Oğuz *et al*. (2006). Oğuz *et.al*. consider that five different climatic phases can be defined based on the winter SST record defined as follows; the period between 1875 and 1915 was relatively cool with temperatures ranging from 7.6 $^{o}$C to 8.7 $^{o}$C. A second phase characterized by temperatures between 7.9 and 9.0 $^{o}$C lasted until 1960. Temperatures ranged between 8.3 and 9.3 $^{o}$C in phase 3 from 1960 to 1980. Phase 4 is identified as a cool period with temperatures range from 7.2 $^{o}$C to

8.0 $^{o}$C during the years 1980 - 1995. Finally, the period post-1995 (phase 5) is characterized by increasing temperatures (Figure 1.12(a); Oğuz *et al*., 2006). Changes in the May – November mean temperature of the cold intermediate layer (CIL) almost follow the SST variance showing the same cold and warm cycles with an ~3 year time lag since the 1950s (Figure 1.12(b); Oğuz *et al*., 2006; Belokopytov, 1998).

Annual mean salinity of the upper 200 m (Figure 1.12 (c)) shows an opposite pattern to the SST record, with fresher conditions observed during warmer periods and more saline conditions observed during cold years since the 1950s (Tsimplis and Rixen, 2003; Oğuz *et al*., 2006). The reason for the inverse relationship between SST and SSS records is said to be increased convective mixing and upwelling combined with increased evaporative loses during cold periods, and the reverse situation during warm years (Oğuz *et al*., 2006). Detrended sea level anomaly (SLA) of the last century (Figure 1.12d) shows a similar pattern of variability to SST. According to the original data presented by Reva (1997), SLA shows a ~0.18 cm year$^{-1}$ linear increasing trend while the warming trend of SST is around 0.0022 $^{o}$C year$^{-1}$. Since SLA is related to the changes in the surface atmospheric pressure, density changes with varying temperature and salinity and also evaporation, precipitation and river runoff, it reflects the response of the Black Sea to the atmospheric forcing well (Oğuz *et al*., 2006; Tsimplis *et al*., 2004; Stanev and Peneba 2002) on the other hand, since SLA depends on many inter related factors, it is convenient to analyze individual parameters throughout this thesis.

Winter air temperature (AT) near the Black Sea shows a warming trend of 0.9 $^{o}$C over the past hundred years with the same cold and warm cycles as the sea surface temperature record (Figure 1.13 (a)). Based on data from a meteorological station near the Kerch Strait, winter mean air temperature ranges from 1.5 $^{o}$C to 6.5 $^{o}$C. As can be seen in Figure 1.13 (b), basin mean winter surface atmospheric pressure (SAP) shows an inverse relation with air temperatures, with an increasing trend over the past 50 years. Winter mean evaporation minus precipitation (E-P) has an inverse relation with SST, with higher E-P during cold and dry winters, and lower E-P during mild and humid winters. E-P shows a decreasing trend from 250 km$^{3}$ year$^{-1}$ to zero

between 1945 and 2000, and after 1995 it is clear that precipitation exceeds evaporation because of the decreasing evaporation and increasing precipitation associated with the increasing trend of atmospheric temperature (Figure 1.13 (a) and (c)). Finally in Figure 1.13 (d), it can be seen that periods of stronger winds coincided with colder and drier winters while weaker winds accompanied the warmer and wet winters during the last 40 years (Oğuz *et al*., 2006).

Interannual variability in the vertical water column structure since the 1960s is evident in the T-S diagram in Figure 1.14. The temperature of the cold intermediate layer (CIL) and upper sulfide limit has decreased between 1960 and 1995 according to Figure 1.14 (Konovalov and Murray, 2001; Ivanov *et al*., 1998a and 1998b). The response of the deeper waters to the climatic variations seen in surface waters can be seen in Figure 1.15. Deeper waters respond to the surface changes with a time lag of 2 – 3 years for the upper suboxic zone (salinity ~20.0 – 20.5) and 4 – 6 years for the sulfide onset (salinity ~21) (Buesseler e*t al*., 1991; Konovalov and Murray, 2001).

During the last 50 years the Black Sea has also experienced some changes in the vertical chemical distribution, associated with the changing physical and ecological environment. In Figure 1.16, interannual variations in the vertical profile of oxygen and sulfide concentrations in the Black Sea are presented. The sub-oxic zone is defined as a layer with sulfide concentrations less than 5 μM and, for detection purposes, oxygen concentrations lower than 20 μM. The upper boundary of this transition zone has risen from $\sigma_t$~15.9 to $\sigma_t$~15.4 between 1960 and 1986 while the lower boundary showed little change. As a result the sub-oxic zone has thickened during the same period of time. After 1986 the suboxic zone seems to narrow slightly due to deepening of the upper boundary. Since the data collection method changed around 1985, changes in the sulfide concentration are discussed over two different time scales. From 1960 – 1985 there was a decreasing trend in the concentration of sulfide at the $\sigma_t$=16.4 and $\sigma_t$=17.1 density levels. After 1985 observation reveals a deepening trend for the same density surfaces extending to greater depths (1000 m and 2000 m; Konovalov and Murray, 2001).

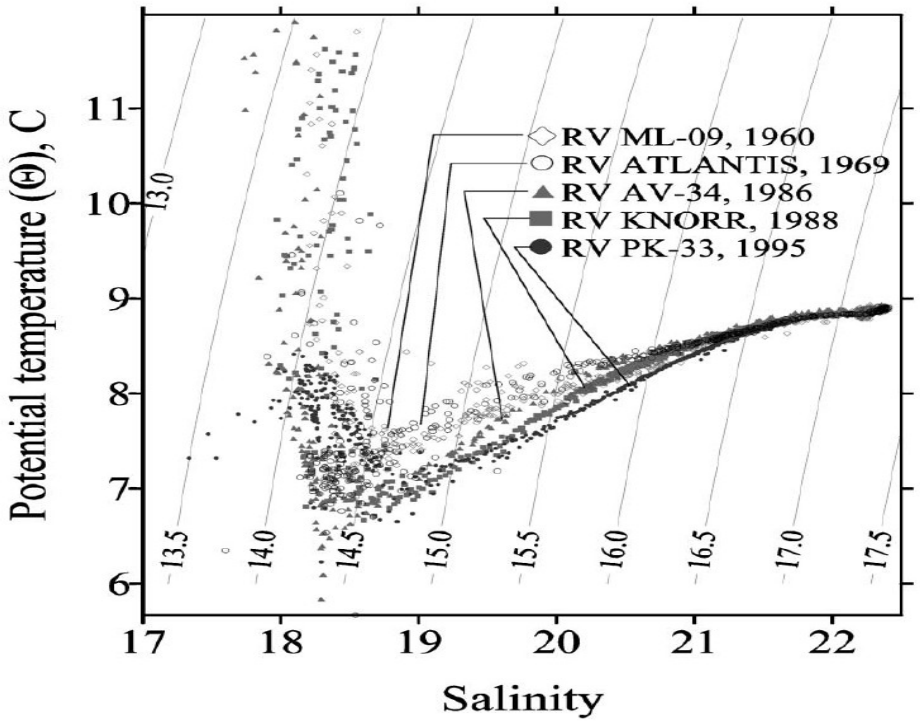


Figure 1.14. T-S diagram of the Black Sea derived from different cruises (Konovalov and Murray, 2001).

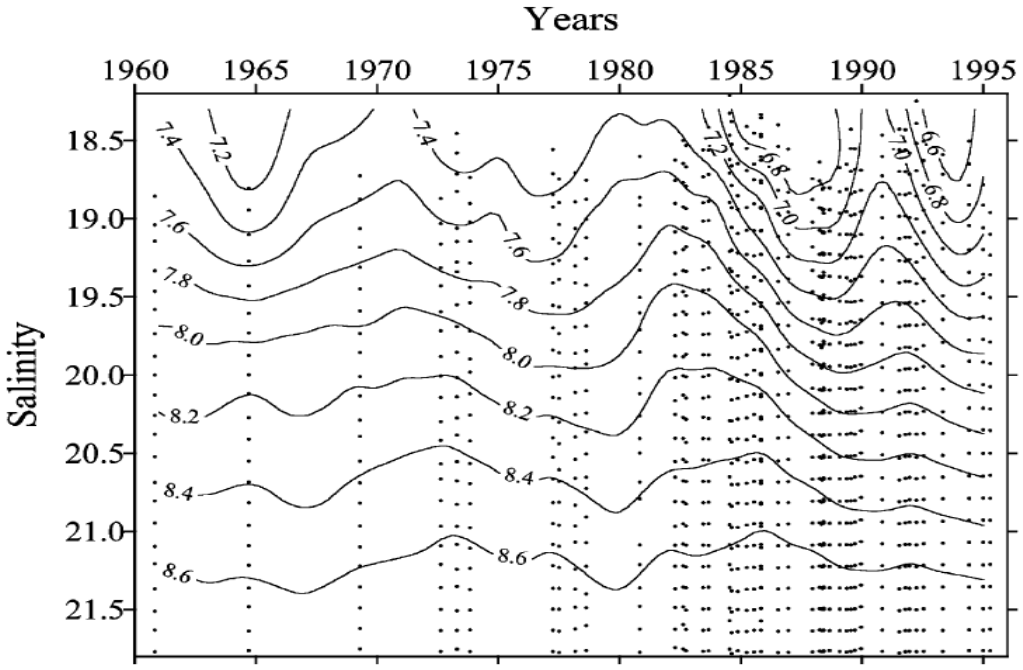


Figure 1.15. Interannual variability of temperature (°C) versus salinity (Konovalov and Murray, 2001).

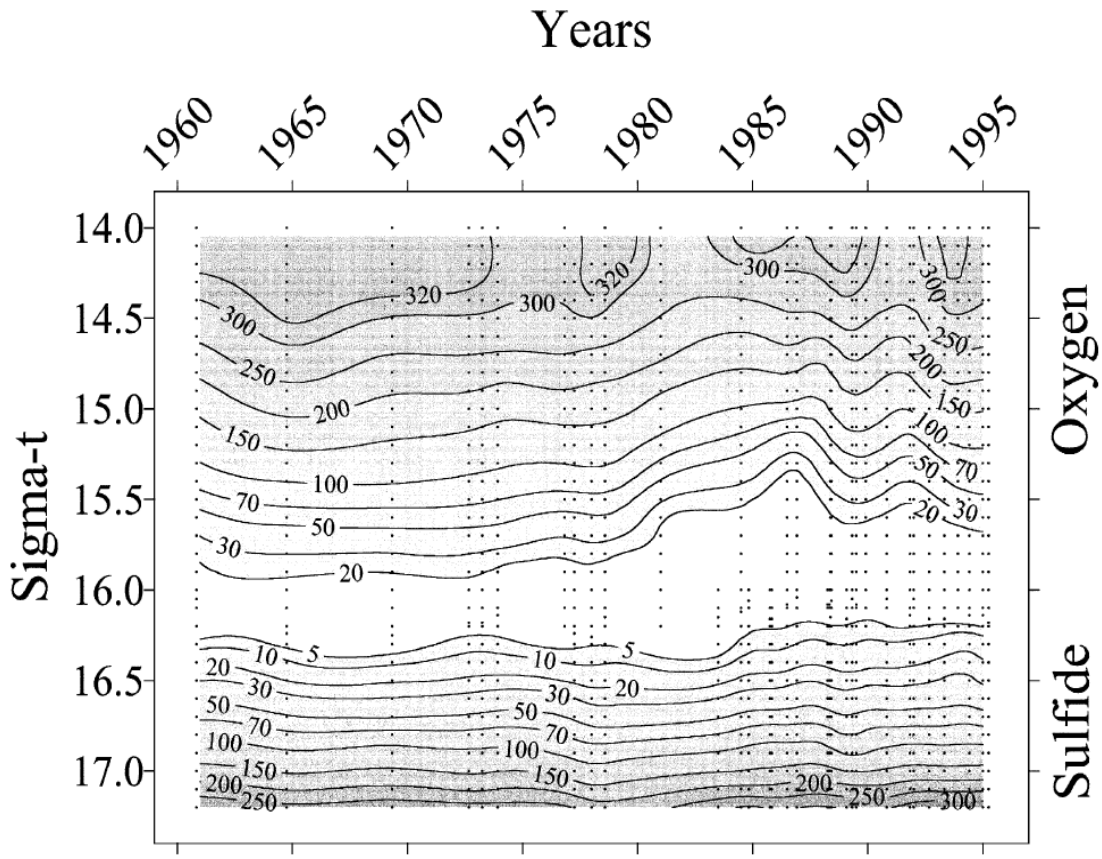


Figure 1.16. Interannual variations in the distribution of oxygen and sulfide (μM) versus sigma-t in the Black Sea (Konovalov and Murray, 2001).

Time series of nutrient concentrations in the Black Sea between 1970 and 1999 from Konovalov and Murray (2001) are presented in Figure 1.17. As the data is relatively sparse between 1969 and 1990 to have comments, only data between 1990 and 1996 can be analyzed for trends and short term variability properly (Figure 1.17). The concentration of nitrate at the nitrate maximum increases from ~2 μM to ~6 μM between 1969 and 1990s while the position of nitrate maximum ascended from $\sigma_t$~15.7-15.9 to $\sigma_t$~15.3-15.5, while after 1990 there seems no obvious trend (Figure 1.17 (a)). The average concentration of ammonia seems decreased from ~0.5 μM to ~0.2 μM in the upper oxic layers between 1969 and 1990s but after 1990 ammonia concentrations remained stable. As can be seen in Figures 1.16 (b) and (c), changes in the phosphate concentrations at $\sigma_t$~15.7 and $\sigma_t$~16.4 shows no change greater than 10 – 20 % from 1969 to 1990s. In Figures 1.16 (d) and (e), it can be seen that silicate concentration at $\sigma_t$~14.0 (oxic region) decreased while the $\sigma_t$~16.4 (anoxic region) shows an increase between 1970s and 1990. After 1990 silicate concentrations shows

no big change. (Konovalov and Murray, 2001; Tuğrul *et al*., 1992). Although there are small changes, the chemical structure of the Black Sea showed no obvious trend for any of the nutrients mentioned above between 1970 and 1999. However, because of the large interannual variability, data is still not sufficient to see the full picture between 1969 and 1990s.

During the last 50 years the Black Sea experienced several distinct shifts in ecological state associated with degradation of the marine environment. Eutrophication is one of many environmental pressures that influenced such changes. The effects of eutrophication can be seen in the annual phytoplankton cycle which was characterized by spring and autumn blooms during the pre-eutrophication period. During post-eutrophication the bloom cycle has been shifted to include several blooms, with the summer bloom being the most prominent. The species composition of the blooms has also changed from diatom dominated to *dinoflagellate* and *coccolithophore* dominated. This is linked to the decreased dissolved silicate and increased nitrogen since the 1970s (Mikaelyan, 1997; Moncheva and Krastev, 1997; Uysal *et al*., 1998; Oğuz *et al*., 2004). Mean phytoplankton biomass increased between the 1960s and the 1990s with a corresponding decrease in secchi disc depth (Figure 1.18 (a) and (b)), indicating a reduction in water transparency (Oğuz *et al*., 2004; Oğuz and Gilbert, 2006). As a consequence of increased primary production, mesozooplankton and fish stocks increased between the 1970s and the 1980s. In the late 1980s opportunistic species such as *Mnemiopsis leidyi, Aurelia aurita, Noctulica scintillans* and *Pleurobrachia rhodopis* increased in abundance (Figures 1.17 (c) and (e)), decreasing the biomass of mesozooplankton through predation (Porumb, 1989; Kovalev *et al*., 1998; Shiganova, 1998; Shuskina *et al*., 1998; Kideys and Romanova 2001; Oğuz *et al*., 2004).

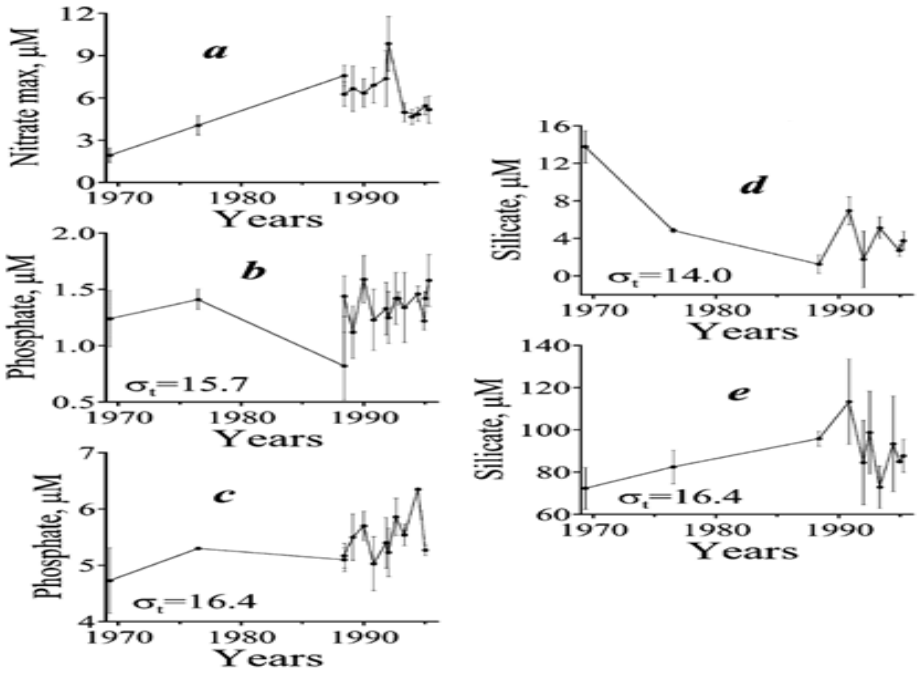


Figure 1.17. Interannual variability of a) nitrate maximum b) phosphate at $\sigma_t$~15.7 and c) $\sigma_t$~16.4 d) silicate at $\sigma_t$~14.0 and e) $\sigma_t$~16.4 (Konovalov and Murray, 2001).

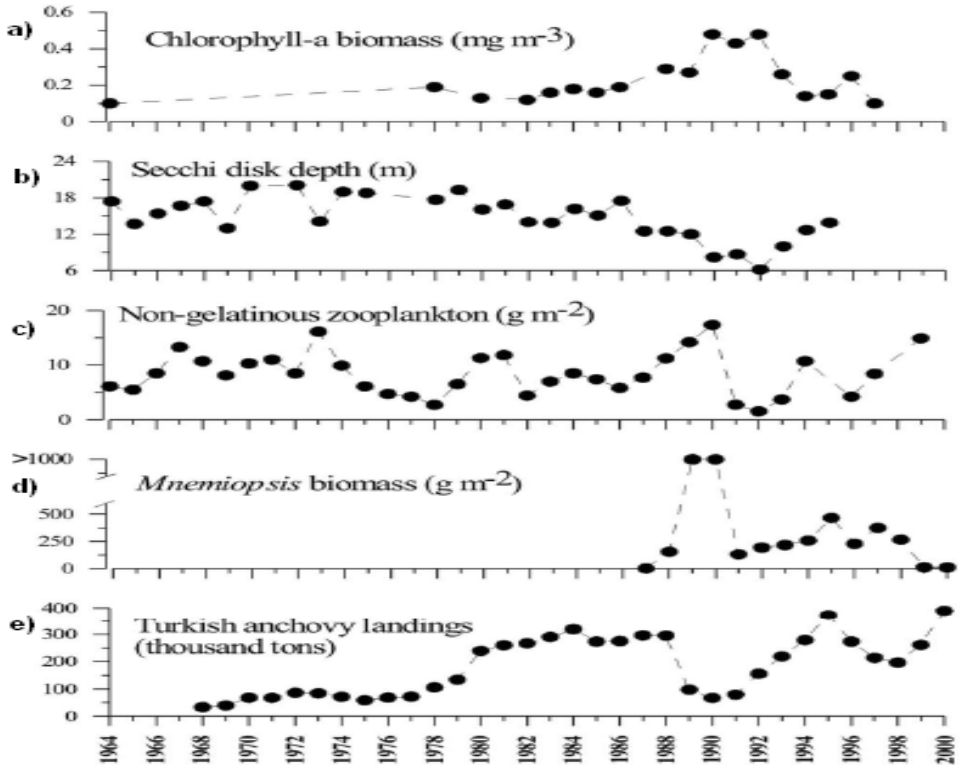


Figure 1.18. Interannual changes in a) chlorophyll concentration (mg m-3), b) secchi disk depth (m), c) non-gelatinous mesozooplankton biomass (g m-2), d) Mnemiopsis biomass (g m-2), e) Turkish anchovy landings (ktons) (Oğuz *et.al.*, 2004).

When considering predation influences on zooplankton, the period between the early 1970s and the late 1990s, can be divided into four phases. From the mid-1970s until 1987 *Aurelia aurita* was a dominant predator of mesozooplankton. During this period *Aurelia aurita* fed on mesozooplankton in competition with small pelagic fishes like anchovy and during the summer season small pelagic biomass increased with a decrease in *Aurelia aurita* biomass. Second phase is the *Mnemiopsis Leidyi* dominated one during 1989 and 1991, *Mnemiopsis leidyi* accidentally entered the Black Sea during the early 1980s with ballast waters, and came to dominate the ecosystem in the absence of its predators between 1989 and 1991 (Figures 1.17 (c), (d) and (e)). During this period, *Mnemiopsis leidyi* outcompeted *Aurelia aurita* as a dominant bloom organism and began to compete with small pelagic fishes for mesozooplankton in addition to consuming fish egg and larvae. Due to the combined influences of fishing pressure and grazing there was a collapse of small pelagic fish stocks during this *Mnemiopsis leidyi* dominated period (Rass 1992; Shuskina *et al*., 1998; Gücü 2002; Oğuz *et al*., 2004; Oğuz and Gilbert, 2006).

A decrease in *Mnemiopsis leidyi* biomass between 1992 and 1993 (Figure 1.18e) was caused by the intense winter cooling which is unfavorable for *Mnemiopsis leidyi*. During this period the biomass of *Mnemiopsis leidyi* reduced to values comparable to the biomass of *Aurelia aurita.* After 1993 gelatinous species have not reached such critical values to compete with pelagic fish stocks so that 1993 – 1995 showed a recovery in fish stocks and the mesozooplankton community (Kideys and Romanova, 2001; Oğuz *et al*., 2004, Oğuz and Gilbert, 2006). The last period, post-1995 represents a climate induced warming period with weaker turbulent mixing and increased stratification leading to reduced upward nutrient fluxes. Nutrient limitation limited primary production and as a consequence of this, the biomass of higher trophic levels was reduced. After 1998 *Beroe ovata* was introduced into the Black Sea and started to consume *Mnemiopsis leidyi* especially in shelf and coastal regions. During this period, mesozooplankton biomass increased together with anchovy biomass in Turkish coasts. Some authors have attributed this to the reduced grazing pressure by *Mnemiopsis leidyi* exerted on mesozooplankton (Kideys, 2002; Oğuz *et al*., 2003; Oğuz *et al*., 2004; Oğuz and Gilbert, 2006).

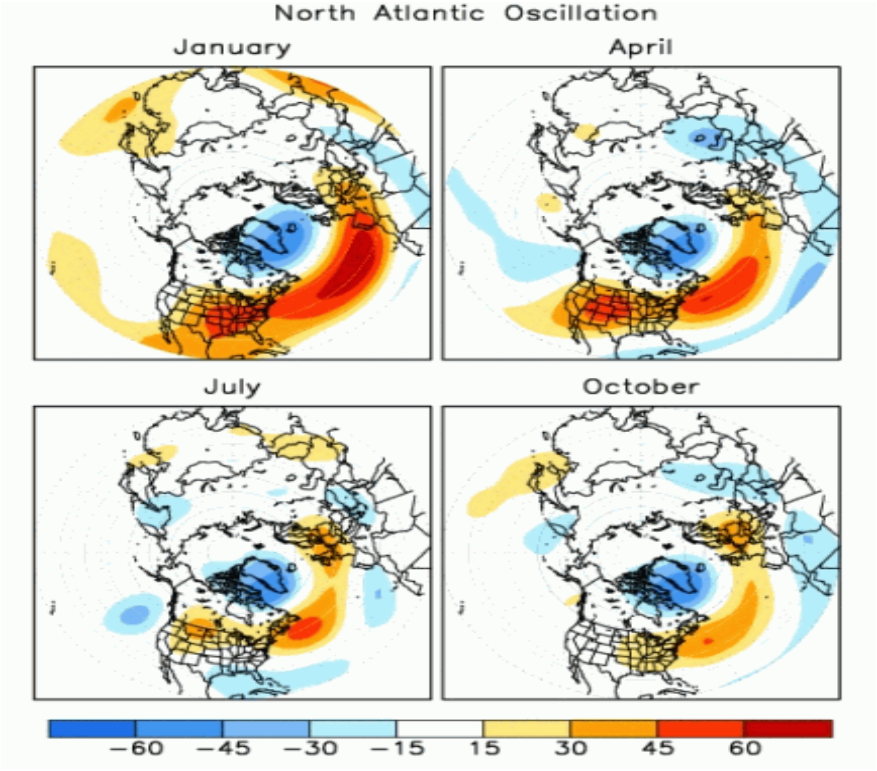


Figure 1.19. Spatial Distribution of Positive Phase of NAO (retrieved from http://www.cpc.ncep.noaa.gov/data/teledoc/nao_map.shtml).

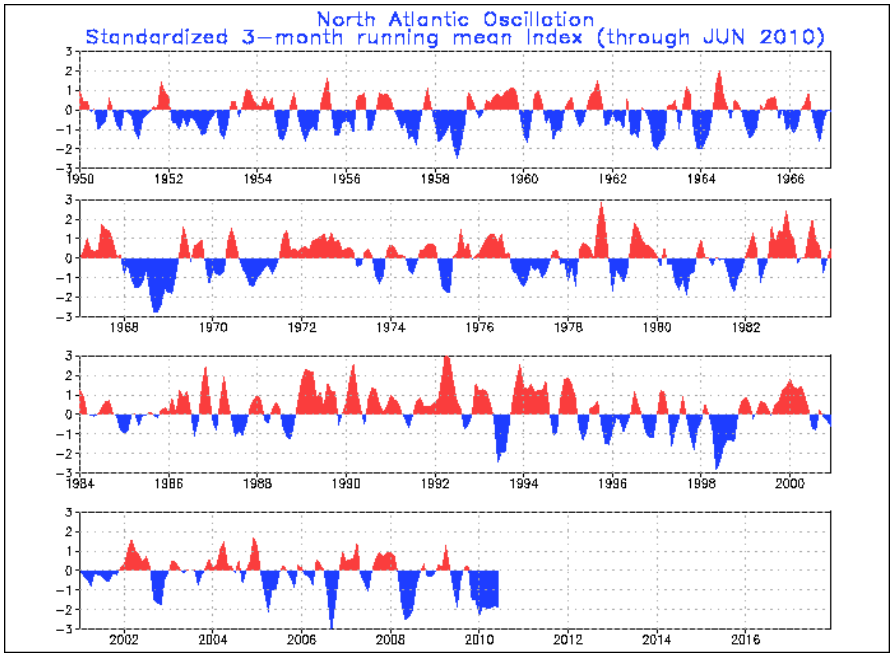


Figure 1.20. 3-month running mean value of the NAO index (retrieved from http://www.cpc.ncep.noaa.gov/data/teledoc/nao_ts.shtml).

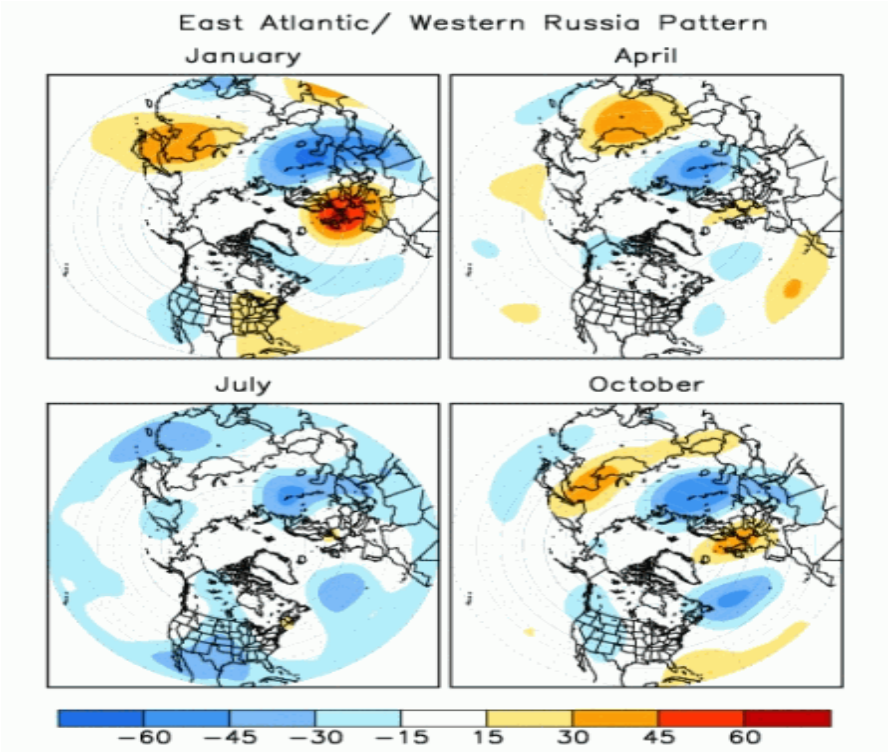


Figure 1.21. Spatial Distribution of Positive Phase of EA/WR Pattern (retrieved from http://www.cpc.ncep.noaa.gov/data/teledoc/eawruss_map.shtml).

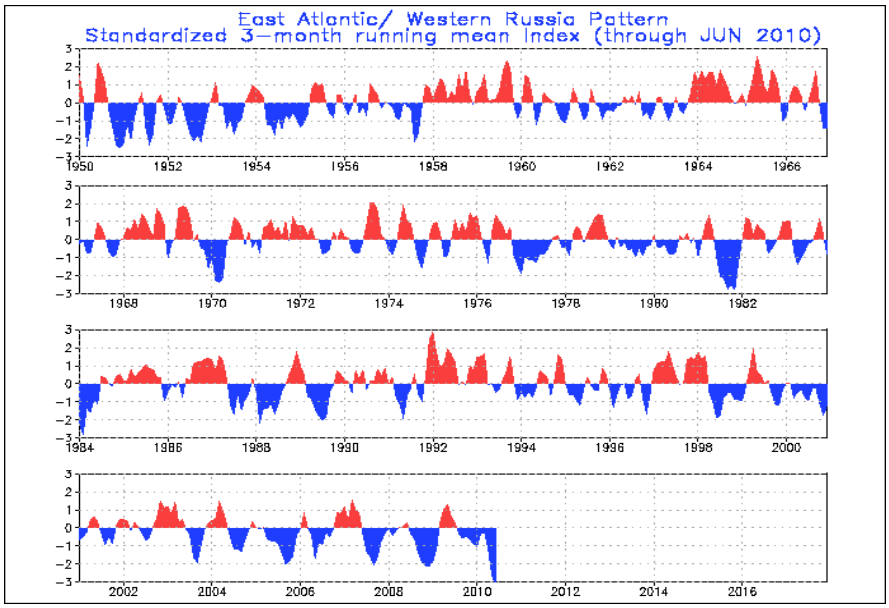


Figure 1.22. 3-month running mean value of the EA/WR index (retrieved from http://www.cpc.ncep.noaa.gov/data/teledoc/eawruss_ts.shtml).

Dramatic changes in ecosystem functioning including changes in bloom timing, species composition, and number of blooms are often referred to as 'Regime Shifts'. The reasons for regime shifts in the Black Sea are still matters of discussion (Oğuz and Gilbert, 2006). Anthropogenic effects like fishing pressure (Gücü, 2002), dam construction (Humborg *et al*., 1997) and ballast waters (Shushkina *et al*., 1998) are all factors, in addition to climate induced warming, increased stratification and decreased upward nutrient supply (Oğuz *et al*., 2003).

## 1.4 Climate

### 1.4.1 Description of Climate

Briefly, climate refers to a mean state, strictly defined by the the World Meteorological Organization as a 30 year average of temperature, precipitation, winds and other physical and chemical parameters of the atmosphere. (http://www.wmo.int/pages/themes/climate/understanding_climate.php). This thesis considers both *climate variability* and *climate change*. The distinction between the two is discussed in the next sections.

#### 1.4.1.1 Climate Variability

According to IPCC (International Panel on Climate Change) fourth assessment report, variations around the mean state, including frequencies of extremes, standard deviations of the mean etc. of the climate both spatially and temporally are called climate variability (Solomon *et.al*, 2007). This variability results in weather patterns and changes in atmospheric pressure systems and atmospheric circulation systems from time scales of a few days to several centuries. In order to understand this variability, large scale recurring patterns of atmospheric circulation and pressure systems have been identified. Because these patterns connect atmospheric anomalies in different regions, they are typically referred to as 'Atmospheric Teleconnection Patterns'. These patterns may be identified using the "rotated principal component analysis" (RPCA) method, applied to atmospheric pressure maps. RPCA is a statistical tool used to isolate the spatial and temporal anomalies of the weather in a

chosen area. This method will be explained in more detail in the 'Material & Methods' section. For the Northern Hemisphere, there are ten teleconnection patterns calculated by the Climate Prediction Center of National Weather Service of USA (http://www. cpc.ncep.noaa.gov/data/teledoc/ teleintro.shtml). According to Oğuz *et al.* (2006), the Black Sea is affected primarily by the 'North Atlantic Oscillation' (NAO) and the 'East Atlantic/West Russia' (EA/WR) patterns. For this reason, only these two ATPs will be discussed in more detail.

The North Atlantic Oscillation (NAO) is one of the most marked teleconnection patterns in the North Hemisphere (http://www.cpc.ncep.noaa.gov/data/ teledoc/nao.shtml). The NAO has two main centers with opposite pressure anomalies. A strong low pressure center is located over Greenland and a high pressure center is located over the central North Atlantic, East America and West Europe. Another weaker center of high pressure is located over East Asia. There is a strong gradient in atmospheric pressure between the North and South centers (Barnston and Livezey, 1987). The positive phase of the NAO can be seen in Figure 1.19. The NAO index describes the relative strengths of the high and low pressure centers. When the NAO is in a positive phase, the North center has a low pressure anomaly while the South center has a high pressure anomaly relative to the local mean state. The strength of the positive and negative phases is reflected by the index values shown in Figure 1.20 for the period from 1950 to 2010. The shift between negative and positive phases of the NAO affects temperature, precipitation and wind patterns throughout the North Hemisphere. These effects will be discussed in the following sections.

The East Atlantic/West Russia (EA/WR) pattern is the second most dominant teleconnection pattern influencing the Black Sea (Oğuz *et al.*, 2006). The EA/WR pattern has been named Eurasian 2 pattern by Barnston and Livezey (1987). The EA/WR pattern has four main anomaly centers with east-west polarities. One of the high pressure centers is located over Europe with a second weaker high located over northeast China. The stronger low pressure center is over the north-northeast of the Caspian Sea and a second weaker low pressure center is located over the central

North Atlantic (Figure 1.21). There is a strong gradient between the Europe center and the Caspian center over the Black Sea. The temporal change between positive and negative phases and the relative strength of the patterns can be identified by the index values in Figure 1.22. During the positive phase, the centers of negative values show lower pressure while the positive centers show higher pressure values relative to the mean state. The EA/WR pattern can be identified in all months of the year except in February, when the EA/WR pattern is mixed with the NAO (Barnston and Livezey, 1987; http://www.cpc.ncep.noaa.gov/data/teledoc/eawruss.shtml). Links between the EA/WR pattern and local climate will be discussed in the next sections.

#### 1.4.1.2 Climate change

According to the IPCC fourth assessment report, climate change is the change in the state of the climate (including mean temperature) and/or natural frequencies of the variability of the climate, due to anthropogenic and/or natural forcing. Beside this wide definition, according to IPCC Fourth Assessment Report, in the Framework Convention on climate Change (UNFCC) climate change refers to only the change in the climate altered by direct or indirect anthropogenic effects in addition to natural variability (Solomon *et.al,* 2007). In order to be consistent, the former definition of climate change is used in this thesis work (i.e. climate change is used to refer to a change in the 30 year mean state or 30 year mean variability of a climate variable, regardless of the forcing). In the next sections, two important concepts relating to the understanding of climate change, paleoclimatology and global warming (cooling), will be explained in detail.

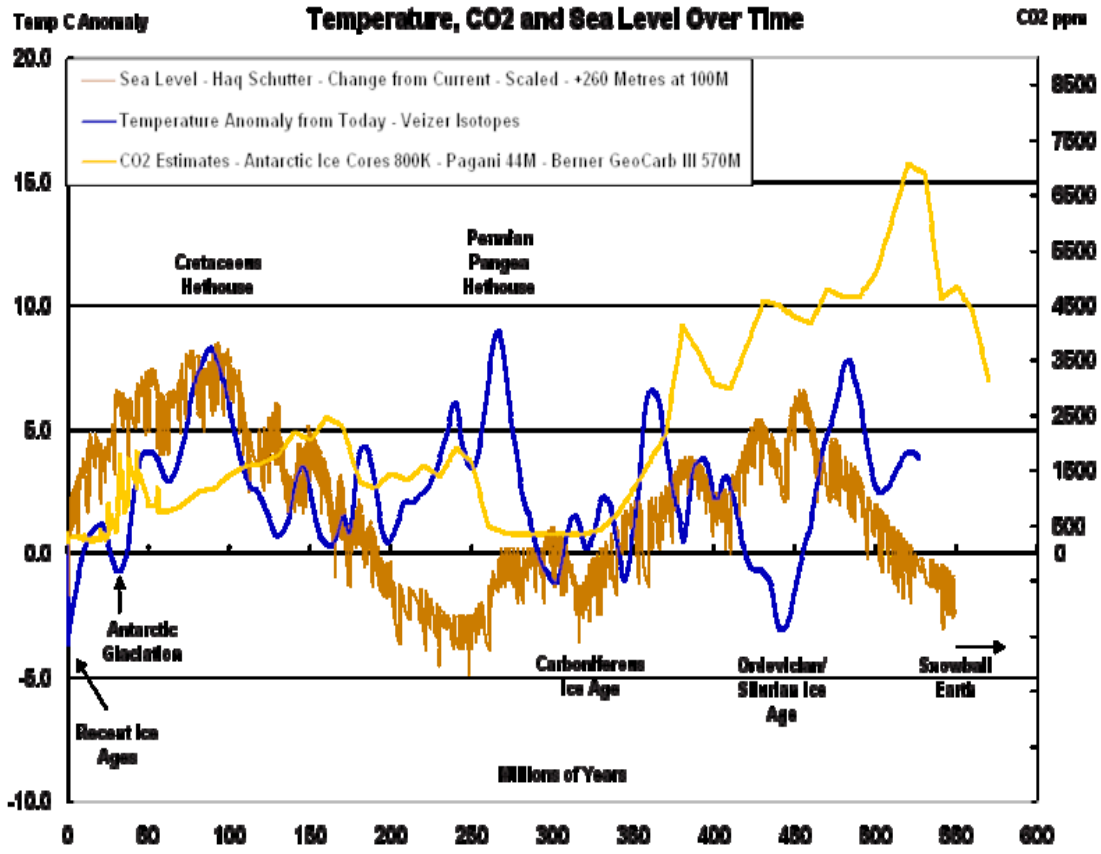


Figure 1.23. Atmospheric $CO_2$ Concentration, Temperature Anomaly and Sea Level Change with some important time periods over last 550 million years (Ward, 2007).

Paleoclimatology is a branch of science that studies past climates over time scale of millions of years, using data collected from ice cores, tree rings, coral reefs sediments, rocks and shells. Since Paleoclimatology considers time intervals before human activity, paleoclimate data can be used to determine the natural climate changes that have occurred on Earth. There is evidence of many global changes in the mean state of temperature, carbon dioxide and sea level during the past 550 million years (as indicated by the paleoclimate records presented in Figure 1.23). The frequencies of these global scale changes range from thousands to millions of years. An explanation for a large part of the low frequency variability has been provided by Milutin Milankovitch (1879-1958) who suggested a relation between climate and the periodic cycles of the Earth's orbit (Letcher, 2009). 'Milankovitch cycles' were named in his honour. Yet changes in climate cannot be explained by this theory alone, so change in cosmic radiation due to the changes of sun's orbit around the

centre of the galaxy (Shaviv and Veizer, 2003), plate tectonics and volcanic eruptions must also be considered (Hardy, 2003). There are also non periodic changes like the reduction of atmospheric carbon dioxide by the first development of photosynthetic organisms more than one billion years ago (Hardy, 2003).

Global warming (cooling) describes an increase (decrease) in the mean surface temperature of the Earth relative to long term averages. Since global warming (cooling) leads to climate change, the term global warming can be used to refer to climate change in the literature. Although there are several warming events in the Earth's history the term "global warming" typically referres to recent climate change mostly caused by the increased anthropogenic release of greenhouse gases (Philander 2008; Dawson and Spannagle, 2008). As can be seen in Figures 1.23 and 1.24, recent observations reveal that there has been an increase of about 0.76 ºC in the mean global atmospheric temperature record from 1850 to 2005, with an increase in atmospheric $CO_2$ equivalent of more than 40 % since 1750 (Dawson and Spannagle, 2008).

### 1.4.2 Impact of Climate on Marine Systems

#### 1.4.2.1 Impact of NAO on Marine Systems

Being the second most important mode of climatic variability after El-Nino/Southern Oscillation (ENSO), the NAO affects weather conditions in Europe, North America and North Africa as well as the strength of westerly winds over the North Atlantic especially in winter. When the NAO is in a positive phase, westerly winds which carry warm and moist air blow over North Europe and as a result air temperature and precipitation is higher than normal in North Europe, North Asia, the Greenland Sea and the Barent Sea. During positive NAO phases, sea ice declines over the Barent Sea due to warmer air and sea surface temperatures. On the other hand, the Labrador Sea receives the cold air mass that come from the North and experiences decreased air and water temperature with extended sea ice coverage compared to normal. At the same time, central and southern Europe, North Africa, the Middle East and Turkey

experience dry and cold air, while the eastern US experiences opposite conditions due to the stronger air flow around the subtropical high. For the negative phase of the NAO, reverse conditions occur (Dawson and Spannagle, 2008; Goosse *et al*., 2009).

The NAO not only affects weather conditions but also the physical and ecological properties of the North Atlantic Ocean and the Mediterranean Sea. During the positive phase of the winter NAO index, evaporation exceeds precipitation over the Mediterranean and around Greenland, while the opposite occurs in the North European seas. The sea surface temperature (SST) anomaly has a positive correlation with air temperature anomaly and the NAO in the North Atlantic. Mixed layer depths are shallower than usual in the northern North Atlantic and deeper in the southern North Atlantic during the positive phase of the NAO. Since mixed layer depth influences the available nutrients and sunlight for phytoplankton production, the NAO also has important effects on marine life from phytoplankton to sea birds (Ottersen *et al*., 2001; Stenseth *et al*., 2005; Hurrell and Deser, 2009).

The Black sea region is also affected by the fluctuations of the NAO (Ozsoy, 1999; Tsimplis and Josey, 2001; Stanev and Peneva, 2002). The NAO affects the Danube discharge (Rimbu *et al.*, 2004) and when the NAO is in a positive phase the Black Sea experiences high atmospheric pressure, colder and drier air, colder SST, higher evaporation minus precipitation and stronger wind stress (Oğuz *et al*., 2006).

#### 1.4.2.2 Impact of EA/WR on Marine Systems

Another important climate variation affecting the Black Sea is the East Atlantic/West Russian Pattern (Oguz, 2005). When the EA/WR pattern is in a positive phase, the Black Sea experiences cold and dry air from the North and vice versa. In order to explain the changes in meteorological conditions that the Black Sea experiences, both the NAO and the EA/WR patterns should be considered. When both are positive, the Black sea experiences dry and cold air with strong winds coming from the Northeast and the Northwest. When the NAO is negative while the EA/WR is positive, again the Black sea is exposed to the cold and dry air coming from the

North but if the Azores high pressure system is strong enough then warm and mild conditions may occur. In the opposite case, when the NAO is positive and the EA/WR pattern is negative, either condition may affect the Black Sea depending on the relative strengths of the patterns. When both are negative warm and mild air coming from southwest and southeast influence the Black Sea (Oguz *et al*., 2006).

To describe the variations in the ecosystem of the Black Sea Oğuz (2005) introduced an Ecosystem index (ECOI) constructed from secchi disk depth variations, phytoplankton and mesozooplankton biomass, surface chlorophyll concentration and hydrogen sulphite concentration at 150 m. This index shows a significant negative correlation (~0.59) with the modified NAO (Mod_NAOI) which is created by replacing the NAO values with the EA/WR values for the early 60s when NAO < 0 and EAWR > 0 (Hardy, 2003).

#### 1.4.2.3 Impact of Climate Change on Marine Systems

Throughout the history of Earth, there have been several extinction events that can be linked to climate change like the Permian extinction which wiped out 90% of all species and 97% of all living things. During the Permian extinction, 96% of marine species became extince during a period when mean sea temperatures decreased by about 5$^{o}$C (Ward, 2007). Beside this kind of mass extinction event in the past, there are many studies that investigate the effects of recent global warming on marine systems.

Any increase in the temperature of the lower atmosphere is reflected in the oceans with a time lag because of the heat content of the oceans. It has been recorded that there has been an increase in the mean temperature of all the oceans of about 0.06 $^{o}$C since 1950. Because the deeper part of the ocean reacts to atmospheric warming very slowly, sea surface temperature values reflect the warming trend more clearly. The global SST record exhibits a mean warming trend of 0.5 $^{o}$C since 1950 (Figure 1.24). Also Polar Regions have been affected by the recent warming trend much more than equatorial regions. For example, SSTs of the North Sea (sub polar region) warmed by

approximately 2 $^{o}$C over the past few decades (Dawson and Spannagle, 2008).

Due to the increasing temperature of the lower atmosphere and the surface waters of the oceans, there will be an increase in melting of polar land ice, glaciers and sea ice, which together with thermal expansion, results in a rise in the sea level globally. Observations show that there has been an increase of about 2.4 mm per year in the sea level for the last 100 years (Hardy, 2003). According to the IPCC scenario projections there will be an increase in sea level of between 0.2 and 0.7 m during the current century (Solomon *et.al*., 2007).

It is expected that the ocean currents and circulation systems will be affected by global warming. Since the warming in the Polar Regions is greater than in the equatorial regions, temperature difference between latitudes may decrease and as a result of this, temperature driven currents may be weakened. On the other hand, in the coastal regions, the temperature difference between land and ocean may increase creating stronger winds which may drive stronger coastal currents. Also it is expected that the intensity and frequency of ENSO will increase (Hardy, 2003). Another possible change is the slowing or even stopping the thermohaline circulation. Such an event would create strong thermal stratification in the North Atlantic which would prevent the vertical mixing of deeper and surface waters of the ocean (Dawson and Spannagle, 2008). An important consequence of the slowing of the thermohaline circulation would be a reduction in the pumping of oxygen to the deep ocean. In the absence of oxygen pumping, eventually the deeper parts of the ocean will become anoxic and aerobic life forms will be replaced by anaerobic sulphate reducing creatures. These creatures will produce hydrogen sulphide that consumes an important nutrient, iron (Dawson and Spannagle, 2008). If the thermohaline circulation slowed down due to decreased salinity caused by the melting of polar sea ice, warm water transportation to the Northern West Atlantic would slow down resulting in a decrease of SST and lower atmospheric temperature in this region. Furthermore, changing ocean and atmosphere currents will change the evaporation/precipitation ratio all over the world, together with the river discharge volumes which in return will change the surface salinity distribution, another driver

of the ocean currents (Hardy, 2003).

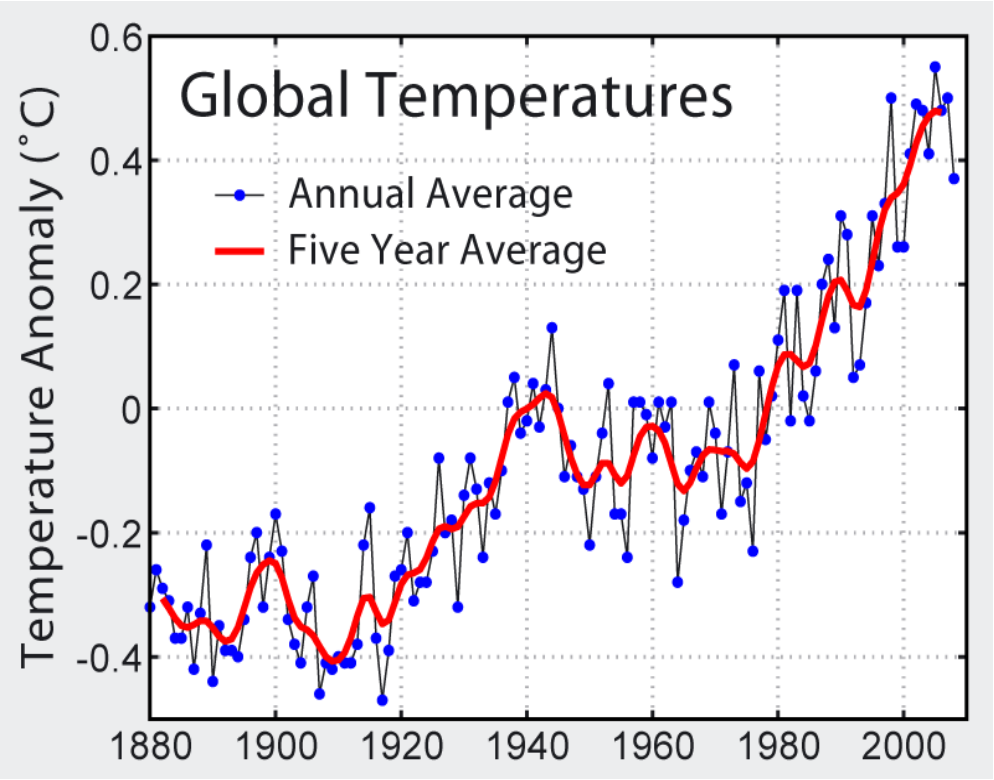


Figure 1.24. Global air temperature anomaly during the last 120 years (Hansen *et al*., 2006).

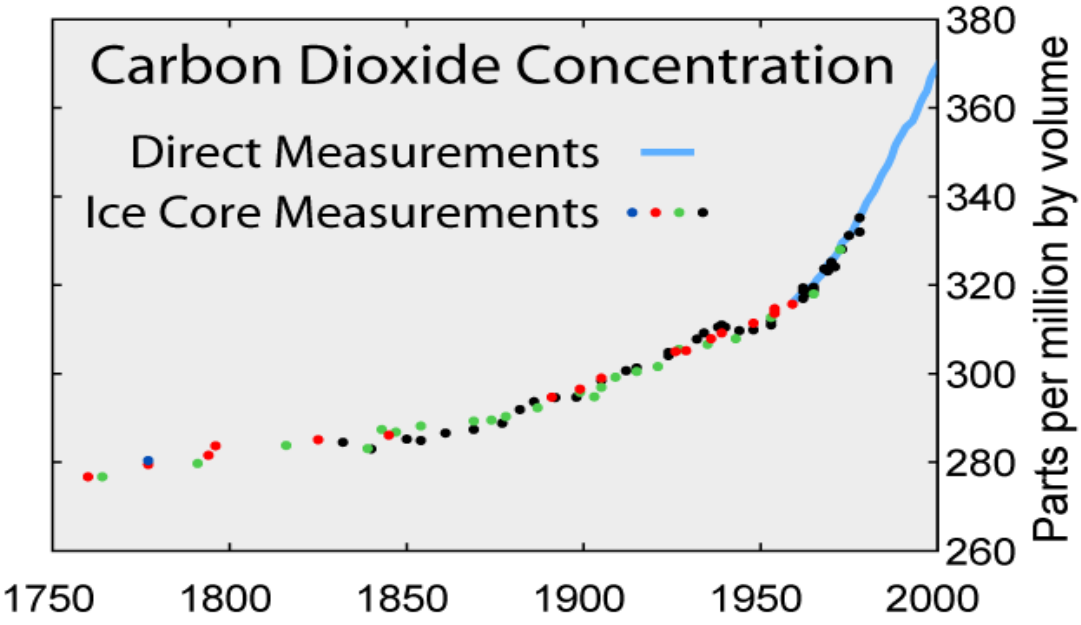


Figure 1.25. Global atmospheric CO2 concentrations of the last 250 years (Robert, 2007).

Changes in the physical structure of the ocean as a consequence of global warming modify the biogeochemical environment with consequences for ecosystem functioning. Increased atmospheric $CO_2$ values (Figure 1.25) directly influence the $CO_2$ concentration in the ocean waters. The ocean absorbs $CO_2$ in the form of carbonic acid through complex mechanisms. With the increased carbon uptake by the oceans, more carbonic acid is forming and increasing the acidity of the oceans. Observations reveal that there has been a pH decrease in the oceans from 8.2 to 8.1 during the last century. According to IPCC, there will be a further decline in pH during the current century of between 0.14 and 0.35 and pH may drop to a value of 7 over the next three centuries (Dawson and Spannagle, 2008).

As a result of increased stratification which prevents vertical mixing, the upward transfer of essential nutrients for photosynthetic life forms such as phytoplankton will be precluded. In other words the vertical nutrient distribution will change to a worse state for photosynthesis (Dawson and Spannagle, 2008).

Physical and biological changes to the condition of the oceans resulting from global warming have biological consequences across all trophic levels. Increasing stratification has implications for nutrient availability, primary production and phytoplankton species composition. Furthermore, zooplankton, a consumer of phytoplankton, will be affected with feedback to the pelagic fish population that consumes zooplankton. The rest of the ecosystem from piscivore fishes to sea mammals and sea birds will also be affected. Many plankton and fish species have temperature sensitive metabolisms so that the increasing temperature will cause them to migrate to colder waters or even kill them. Corals are very sensitive to temperature and acidity of the water. Increasing temperature and acidification will damage the corals with all the life they support (Hardy, 2003; Casper, 2010; Philander, 2008; Letcher, 2009). In conclusion, biodiversity and ecosystem dynamics will be affected by the current global warming phase, as has happened before in the history of Earth.

# CHAPTER 2
# MATERIAL and METHODS

## 2.1 Description of data sets utilised

### 2.1.1 Description of Model Output

The two model reanalysis utilised in this study were performed on behalf of the Black Sea commission by colleagues at the Ukranian Marine Hydrophysical Institute (MHI). This thesis contributes towards a collaborative effort between scientists at MHI and IMS-METU towards fulfilling the goals of the EU projects MEECE (Marine Ecosystem Evolution in a Changing Environment; http://www.meece.eu/) and SESAME (Southern European Seas: Assessing and Modelling Ecosystem changes; http://www.sesame-ip.eu/index.php). Two model reanalyses were performed spanning the period from 1971-2001. Due to data limitations, two separate model runs with different data assimilation procedures were conducted as follows: The first model run spans 23 years between 1971 and 1993 and assimilates gridded CTD data. In preparing the CTD data for assimilation deviations in the measurements from the climatic mean were fitted to the model grid using an optimal interpolation scheme, at monthly intervals. The second model run spans a 10 year period from 1992 to 2001 and assimilates satellite altimeter data as temperature and salinity.

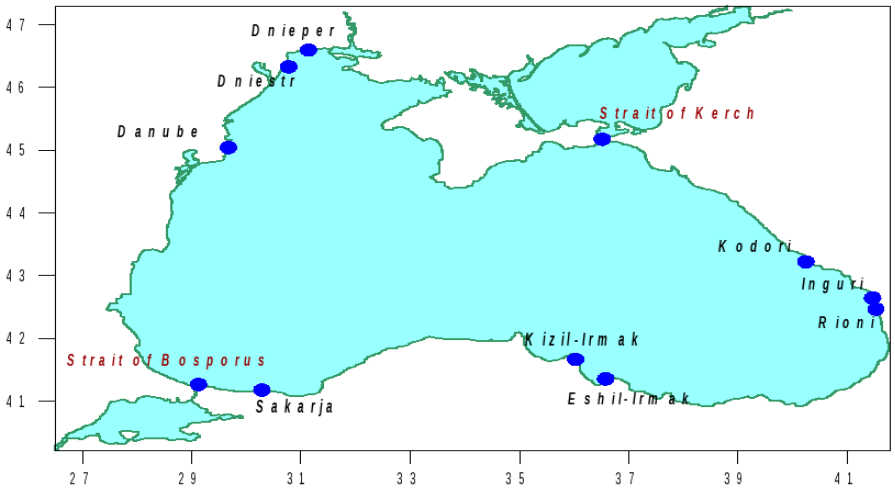


Figure 2.1. Rivers and Straits included in the model obtained from http://www.meece.eu/

The model used for the two simulations was The Princeton Ocean Model (POM; Blumburg and Mellor, 1987) POM is a sigma coordinate, free surface, finite difference ocean model. The governing equations of the model are the primitive hydrostatic equations and the continuity equation for an incompressible fluid. The model domain consisted of a 5 km resolution, Arakawa C, horizontal grid and 26 level, sigma coordinate vertical grid with maximum depth of 2200 m. The model time steps were 5 seconds for the barotropic mode and 5 minutes for the baroclinic mode. The model was forced by ERA 40 atmospheric forcing at 6 hourly intervals (see section 2.1.5 for further details). Both model runs were spun up for 5 years from initial conditions produced from climatological temperature and salinity obtained from World Ocean Atlas 2005 (http://www.nodc.noaa.gov/OC5/WOA05/pr_woa05.html).

Although there are no open boundaries, monthly mean climatologies of rivers and straits are included as in Figure 2.1. The Sea of Azov was not included in the model simulations. For the purpose of this thesis, model output is interpolated onto 35 z-levels which are concentrated towards the surface. In order to conserve file size data are stored at 5 daily intervals.

### 2.1.2 HadSST2 data set

HadSST2 is a data product containing SST measurements for the years 1850 to 2010. HadSST2 is produced using *in situ* data collected by ships and buoys. Measurements which fail quality checks are ignored. The Resulting anomalies are averaged on a $5^{o}$ by $5^{o}$ monthly grid. (Rayner *et al*., 2005). This data set is used to validate interannual variability of modeled basin averaged annual mean SST.

### 2.1.3 AVHRR data set

The Advanced Very-High-Resolution Radiometer **AVHRR** data set is a global data set of remotely sensed SST with spatial resolution of 4 km grids and various temporal resolutions from daily to annual spanning the time interval from 1981 to

2009. SST data is taken from the 5-channel AVHRRs on the NOAA-7, 9, 11, 14, 16 and 17 polar orbiting satellites and prepared by National Oceanographic Data Center and the University of Miami's Rosenstiel School of Marine and Atmospheric Sciences (http://podaac.jpl. nasa.gov/PRODUCTS/p216.html). This data set is used to validate modelled basin averaged annual mean SST for years 1986 – 2001.

### 2.1.4 Climate indices

The monthly Northern Hemisphere teleconnection indices relevant to the Black Sea region are used. These indices are calculated by the use of RPCA (Rotated Principle Component Analysis) method by the National Weather Service Climate Prediction Center (http://www.cpc.ncep.noaa.gov/data/teledoc/ teleindcalc.shtml). For all months, primary teleconnection patterns are isolated with this method in order to construct time series. The method is used between 20°N – 90°N and from 1950 to 2000 on the monthly mean standardized 500-mb height anomalies obtained from the CDAS by the National Weather Service Climate Prediction Center. As stated in the introduction section, NAO and EA/WR teleconnection patterns are used to help understand variability in climatic forcing of the Black Sea.

### 2.1.5 ERA 40 data set

The atmospheric forcing of the model is produced from the ECMWF - ERA 40 daily fields the ERA40 reanalysis extends from September 1957 to August 2002 and covers various fields from wind speed to soil temperature (http://data-portal.ecmwf.int/data/d/era40_daily/). For the purpose of this thesis work, evaporation, surface solar radiation downwards, surface thermal radiation, surface sensible heat flux and sea surface temperature are used as well as 10 m wind speeds from which wind stress is calculated.

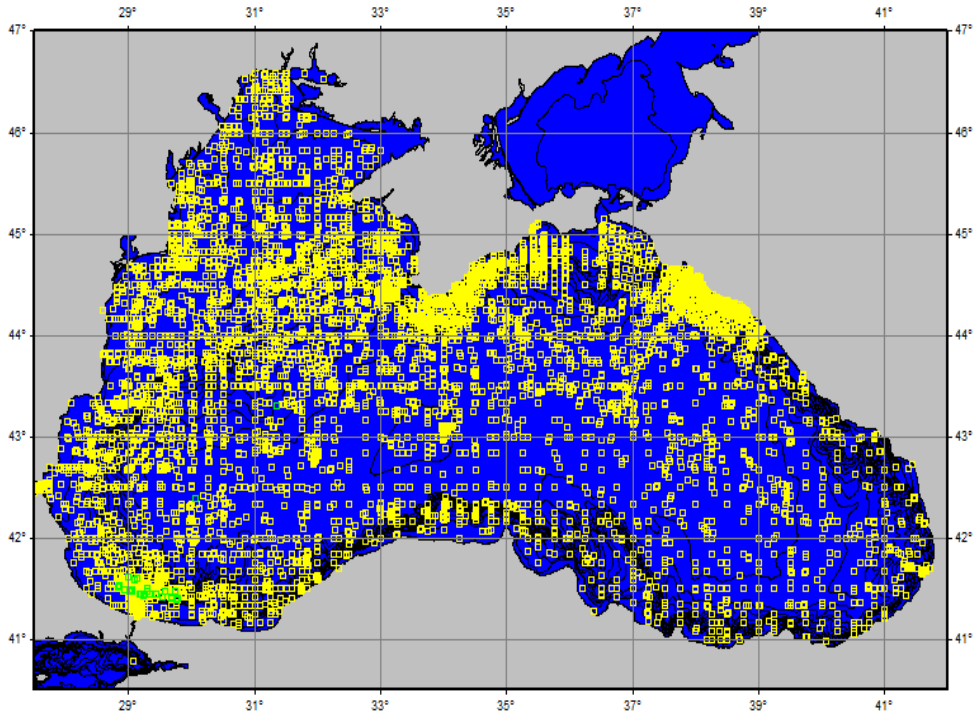


Figure 2.2 Spatial distribution of temperature, salinity and density stations (1971-1993) from Black Sea Database (15415 stations; http://sfp1.ims.metu.edu.tr/)

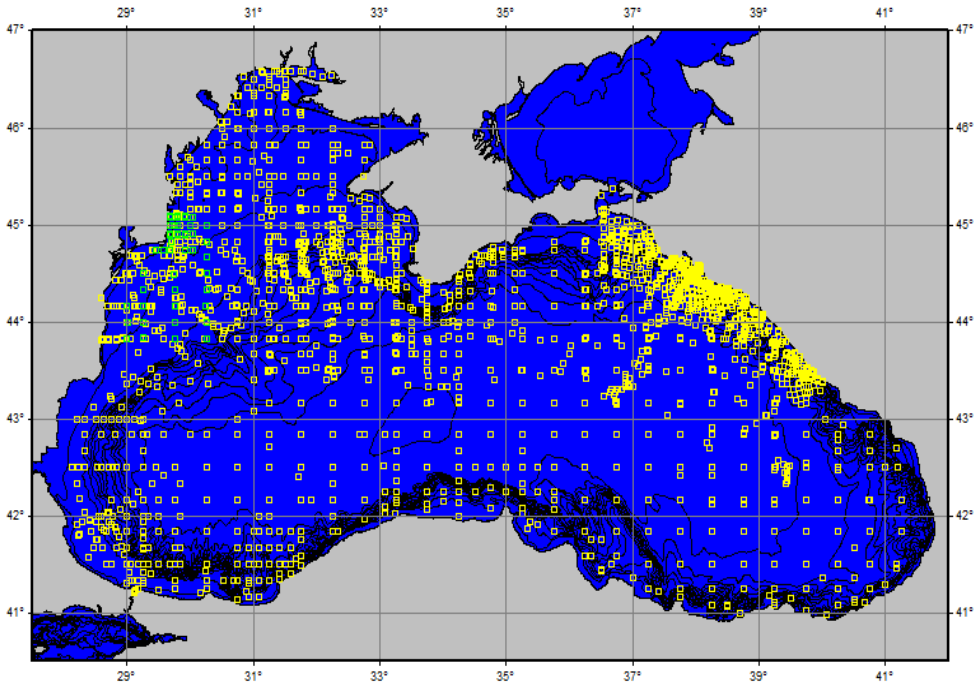


Figure 2.3 Spatial distribution of temperature, salinity and density stations (1992-1996) from Black Sea Database (3776 stations; http://sfp1.ims.metu.edu.tr/)

### 2.1.6 Black Sea Database

CTD data used for the purpose of model validation were extracted from the Black Sea database. The Black Sea Database was released after the NATO SfP ODBMS Black Sea project and consists of various physical, chemical and biological observations from 1959 to 1996. CTD observations of temperature, salinity and density from 15415 stations for the first model run and 3776 stations for the second model run are used to validate model outputs. The Spatial distribution of the stations can be seen in Figure 2.2 and 2.3 (http://sfp1.ims.metu.edu.tr/).

## 2.2 METHODS

### 2.2.1 Validation of model

#### Interannual variability

In order to see how well the model solves interannual variability of surface temperature, basin averaged annual mean SST from the first and second model periods were compared with annual mean SSTs from AVHRR and HadSST2. Anomalies were then calculated relative to the 1971 – 1993 mean.

#### Accuracy and model stability

To determine model accuracy and stability model results were compared with *in situ* data taken from the Black Sea data base. First, difference of modelled and observed data (Surface temperature and salinity, mixed layer depth, cold intermediate layer (CIL) upper and lower limits, CIL thickness and CIL mean temperature) were calculated individually. All first period (1971 – 1993) observations were compared with first model run period (1971-1993) and all second period (1992 – 1996) observations were compared with second model run period (1992 – 2001). Then, mean differences between observations and model results were mapped and spatially and temporally averaged mean differences were plotted seasonal and annual time

series. Finally, Taylor diagrams (Taylor, 2001) were used to show correlation coefficients, RMS errors and standard deviations between modelled and observed data.

**Vertical water column structure**

To show how well the model solved the vertical structure of the Black Sea, basin averages of temperature, salinity; density and stability profiles (see section 2.2.6) were calculated up to the first 200 m for each of the model runs. Then differences between model runs and observations were checked visually for any obvious difference. Also differences between the first and second model runs were inspected.

**General circulation structure**

Annually averaged and 1971 – 1993 averaged currents for first model period were calculated in order to assess whether the model is able to reproduce the general circulation features of the Black Sea. Annually averaged currents were overlain on to annually averaged surface densities while all time period average was overlain onto current strengths.

### 2.2.2 Annual Mean SST, Surface Salinity and Surface Density anomaly time series

In order to eliminate seasonal signals and to emphasise inter – multi annual variability and trends, annual mean anomalies were used. Since the first model period (1971 – 1993) is longer than the second model period (1992 – 2001), anomalies are calculated relative to the first model run. Also anomalies presented in this thesis work are generally (unless otherwise is stated) annual means. First, annual mean time series of basin averaged SST, surface salinity and surface density were calculated from the first and second model run output. The same procedure was applied to stability, mixed layer depth, cold intermediate layer mean and core temperatures and CIL lower and upper boundaries and CIL thickness, buoyancy flux,

vertical convective velocity, net het flux and wind stress. Since net heat flux and wind stress have a continuous time series, their anomalies were calculated relative to 1971 – 2001 mean. The resultant time series were analyzed using linear regression to investigate the existence of any trends and correlations of these linear regression curves with annual mean anomalies were calculated to check the significance of trends. Resultant time series of SST and surface salinity were compared to climate indices (the NAO and the EA/WR).

### 2.2.3 Annual Mean CIL Thickness Anomaly

By definition, as described in the background section, the CIL of Black Sea is the depth interval where the water temperature is below 8 $^{o}$C. Using this definition, the depths of the CIL upper limit and lower limit were determined from the modelled temperature fields. The distance between the upper and lower boundaries of the CIL were then used to calculated CIL thickness. If there was not any temperature value below 8 $^{o}$C at a particular location CIL thickness was assigned to zero. Annual mean time series of basin averaged CIL upper limit, lower limit and thickness were calculated as in the previous section. Again, time series are presented as anomalies in order to emphasise interannual variability.

### 2.2.4 MLD anomaly

In order to find the thickness of the surface layer which interacts with atmosphere directly, mixed layer depth was calculated. Density fields were interpolated onto a 1 m horizontal grid and the density change between every 1 m depth interval below the surface was calculated at every horizontal grid points at 5 day intervals throughout the duration of simulations. The first depth below the surface where the density change was greater or equal to the value 0.0125 kg m$^{-4}$ was used to define the lower limit of the mixed layer, following the methods of Montegut *et al*. (2004) and Suga *et.al*. (2004). This method was chosen after some experimentation with different methods. Threshold methods which use averaged profiles and temperature difference were omitted because of their inability to find individual mixed layer depths

properly. Different threshold values presented in Montegut *et al*. (2004) were tried and the method of Suga *et.al*. (2004) worked better than others for the Black Sea for all seasons and locations. The distance from the surface to the lower limit of the mixed layer was called mixed layer depth (MLD). If there was no change greater than or equal to the value 0.0125 kg $m^{-4}$ then MLD was assigned to the depth of the water column and if there was a change greater or equal to the value 0.0125 kg $m^{-4}$ in the first 5 meters below the surface then MLD was assigned to zero because of the maximum vertical resolution of the model. Finally, anomalies of annual mean time series of basin averaged MLD were calculated as in the previous sections.

### 2.2.5 Heat accumulation

Annual mean time series of surface forcing parameters were constructed in order to aid understanding of the trends and variability observed in the hydrographical data sets. Surface fluxes and 10 m wind speed data were extracted from the ERA40 data product as discussed previously. Then the net surface heat flux $H_{net}$ was estimated as the sum of the individual components as follows:

$$H_{net} = H_s + H_L - H_o - H_e - H_c \ (W\ m^{-2}) \quad (2.1)$$

where $H_s$ is incident shortwave radiation, $H_L$ is incident long-wave radiation, $H_o$ is outgoing long-wave radiative flux, $H_e$ is evaporative heat flux and $H_c$ is sensible heat flux.

$H_s$ and $H_c$ were directly extracted from the ERA 40 data base as was ($H_L - H_o$) which is equivalent to the net surface thermal radiation and $H_e$ was calculated as follows:

$$H_e = \rho L_v E \ (W\ m^{-2}) \quad (2.2)$$

where ρ is density, $L_v$ is latent heat of vaporization and E (kg $m^{-2}$ $s^{-1}$) is evaporation which was taken from ERA 40. For the density, model output was used and $L_v$ was calculated as recommended by Henderson-Sellers (1984; following Cannaby, 2005):

$$L_v = 1.91846 \times 10^6 (T/(T - 33.91))^2 \quad (2.3)$$

where T ($^oC$) is sea surface temperature of the water, taken from ERA 40.

After calculating net heat flux at every grid point at 5 day intervals throughout the two model periods, the basin scale annual averages were calculated. Finally the net atmosphere to ocean heat accumulation between 1970 and 2001 was calculated. Annual averages of the individual heat flux components and surface wind stress fields were also calculated.

### 2.2.6 Brunt–Väisälä frequency

The Brunt–Väisälä frequency N is a measure of vertical static stability of a liquid. In order to measure interannual and multiannual variations of stability of the Black Sea, BVF is calculated from modelled data. For sea water the calculation of BVF is as follows:

$$N^2 \equiv gE \ (s^{-2}) \quad (2.4)$$

and

$$E \approx -\frac{1}{\rho}\frac{d\rho}{dz} \ (m^{-1}) \quad (2.5)$$

where g is gravitational acceleration, ρ is density, z is vertical distance and E is stability of the water column. Stability can be interpreted as follows:

E > 0 Stable
E = 0 Neutral Stability
E < 0 Unstable

where higher values of E indicate a more stable water column and vice versa for instability (Robert, 2005).

Because we only consider relative changes in the stability of the water column in this thesis, stability was calculated instead of a full calculation of the Brunt–Väisälä frequency.

### 2.2.7 Buoyancy Flux and Penetrative Convection Velocity

Buoyancy flux is a measure of the rate of buoyancy and heat exchange at the surface and positive values of the buoyancy flux mean buoyancy loss. In order to compare interannual and multiannual variations of mixed layer depth with its internal properties like buoyancy and vertical convective velocity, the buoyancy flux B can be calculated as follows

$$B = \frac{-g\alpha H}{C_{pw}\rho} \ (m^2 s^{-3}) \tag{2.6}$$

where g is gravitational acceleration, $C_{pw}$ is the specific heat of water, ρ is density of water and α is the thermal expansion coefficient for sea water (Chen and Millero, 1986; see appendix A).

Penetrative convection velocity (w) provides an indication of the mechanical energy introduction to the water column by surface cooling and is calculated as follows

$$w = (B h_m)^{1/3} \ (ms^{-1}) \tag{2.7}$$

where B is buoyancy flux and $h_m$ is the mixed layer depth (Imberger and Parker, 1985).

### 2.2.8 EOF analysis

EOF (Empirical Orthogonal Functions) analysis is a statistical tool used to decompose a time series of spatial data into a series of recurring spatial modes. EOF analysis can for example, be used to isolate temporal and spatial modes of variance in a mapped data field such as atmospheric pressure and temperature. The resultant

functions are orthogonal and represent different modes of variability but may or may not be physically meaningful. Every EOF has a corresponding principle component (PC) which shows no trend because any existing temporal trend is removed from the data. When PC shows a negative value, EOF shows an opposite pattern and vice versa. Also absolute value of PC shows the strength of difference between negative and positive anomaly centres.

In this thesis work EOF analysis was used to investigate the existence of any recurring modes of variability in the sea surface temperature and sea surface salinity fields obtained from the model output. Results were then compared to model forcing fields and climate indices. In order to calculate EOFs the data was first arranged such that each row represents a time step and each column represents a spatial coordinate as can be seen below:

$$X = \begin{bmatrix} x_{11} & x_{12} & \cdots & x_{1p} \\ x_{21} & x_{22} & \cdots & x_{2p} \\ \vdots & \vdots & \ddots & \vdots \\ x_{n1} & x_{n2} & \cdots & x_{np} \end{bmatrix} \tag{2.8}$$

where X is the data matrix, $x_{ij}$ is the individual data where $t_i$ represents time and $s_j$ represents spatial coordinates for i=1,…,n and j=1,…,p. Then the time average matrix $\bar{x} = (\overline{x_{.1}}, \ldots, \overline{x_{.p}})$ is calculated by this formula:

$$\overline{x_{.j}} = \frac{1}{n} \sum_{k=1}^{n} x_{kj} \tag{2.9}$$

Then the anomaly field matrix X' will be:

$$x'_{ts} = x_{ts} - \bar{x}_{.s} \tag{2.10}$$

After calculating the anomaly field matrix X', the covariance matrix is calculated by this formula:

$$\Sigma = \frac{1}{n-1} X'^{T} X' \tag{2.11}$$

In order to find a direction $\boldsymbol{a} = (a_1, \ldots, a_p)^T$ such that X'**a** has maximum variability:

$$var\left(X'\boldsymbol{a}\right) = \boldsymbol{a}^T \Sigma \boldsymbol{a} \tag{2.12}$$

The vector **a** should be unitary to make the problem bounded and the problem becomes:

$$\max_{\boldsymbol{a}} (\boldsymbol{a}^T \Sigma \boldsymbol{a}) \tag{2.13}$$

such that $\mathbf{a}^T\mathbf{a}=1$. The solution to equation (6) is this eigenvalue problem:

$$\Sigma \boldsymbol{a} = \lambda \boldsymbol{a} \tag{2.14}$$

After solving this eigenvalue problem, eigenvalues λ and corresponding eigenvectors **a** are sorted in decreasing order so that the explained variance in percentage of the $k^{th}$ EOF $\mathbf{a}_k$ becomes:

$$\frac{100\lambda_k}{\sum_{k=1}^{p} \lambda_k} \% \tag{2.15}$$

Finally projection of the anomaly field X' onto the $k^{th}$ EOF $\mathbf{a}_k$ is:

$$c_k(t) = \sum_{s=1}^{p} x'(t,s) a_k(s) \tag{2.16}$$

which is the $k^{th}$ principle component (PC) (Hannachi 2004, Lorenz 1956).

In conclusion, EOF analysis give three important results; first one is EOF map which shows spatial distribution of anomaly centers, second one is corresponding PC which shows interannual and multiannual modes of variability and third one is explained variance which shows how much of the total variance can be explained by each corresponding EOF and PC.

# CHAPTER 3
# RESULTS

## 3.1 Model validation

### 3.1.1 Interannual variability in the SST record

To assess the models ability to represent interannual scale variability we begin by comparing annual mean SST records from the model simulations to the available observational time series. The two observational time series used are the remotely sensed data product (AVHRR; http://podaac.jpl.nasa.gov/PRODUCTS/p216.html) and the *in situ* data product (HadSST2; http://badc.nerc.ac.uk/data/hadsst2/). In Figure 3.1, basin averaged annual mean SST anomalies from the first (1971-1993) and second (1992-2001) model periods and from AVHRR (1986-2001) and HadSST2 (1971-2001) are overlain on the same bar plot. For each time series anomalies are calculated relative to the mean of the first model period (i.e. relative to a value of 14.5 $^{o}$C). This approach was taken in order to compare time series spanning different periods but has the disadvantage that the resultant time series of anomalies may not be centred on zero. Although SST anomalies are persistently higher in the HadSST2 data set compared to the other data sets, interannual variations in SST are similar in each of the data sets. A quantitative comparison of each of the SST records was performed through calculation of correlation coefficients, standard deviations and root mean square differences. The results are presented on a normalized Taylor diagram in Figure 3.2. Each of the SST time series are significantly correlated with a correlation coefficient (r) value of >0.9 and a root mean square difference lower than 1.2. From this analysis we conclude that the model does a good job of representing interannual variability and multidecadal trends in the SST record.

### 3.1.2 Vertical water column structure

Simulated vertical distributions of temperature and salinity within the upper 200 m of the water column, averaged over both model periods, (Figure 3.3 (a) and (b)) exhibit similar distributions to observed profiles (e.g. see Figures 1.3 and 1.4). However, there is a divergence of the modelled salinity profiles between 30 m and 190 m depth, with the second model run having relatively higher salinities within this depth range compared to the first model run (despite having lower surface salinities). The divergence in the simulated salinity profiles at intermediate depths is reflected in the density profiles (Figure 3.3 (d)). While the second model simulation shows lower density values within the upper 20 m of the water column compared to the first simulation, densities between 40 m and 150 m depth are higher. The significance of these differences is most clearly illustrated by comparing vertical profiles of stability, which is related to the vertical density change per meter (Figure 3.3 (e)).

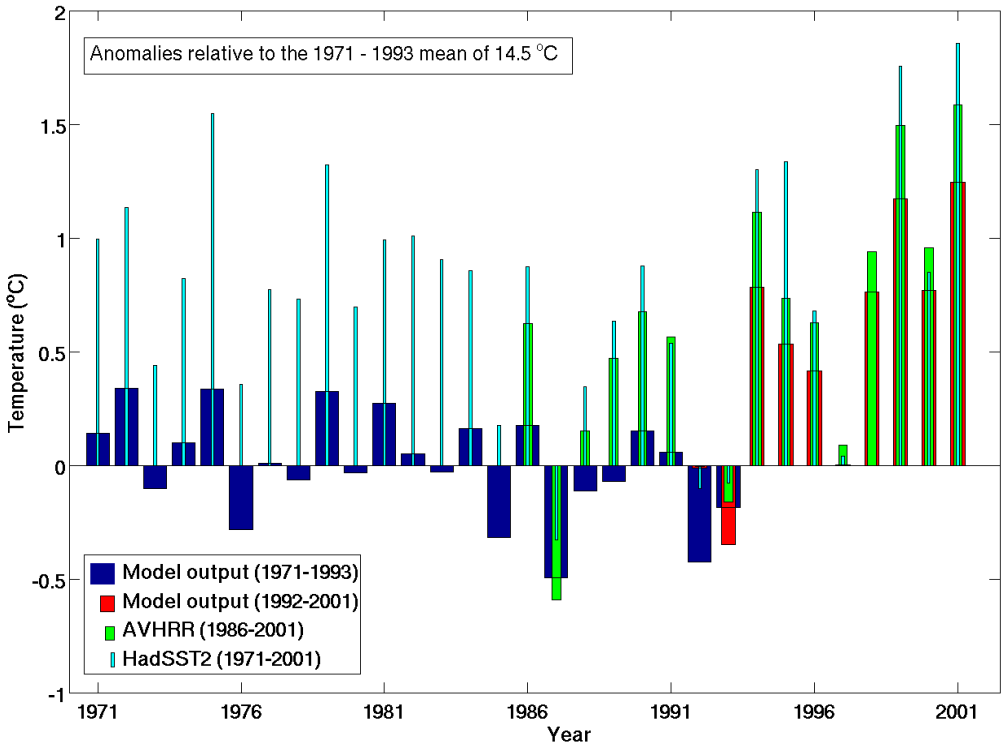


Figure 3.1 Annual mean SST anomalies from the first (1971 – 1993) and second (1992 – 2001) model periods (blue and red respectively), derived from AVHRR observations (1986 – 2001; green), and extracted from the HadSST2 data set (1971 – 2001; cyan).

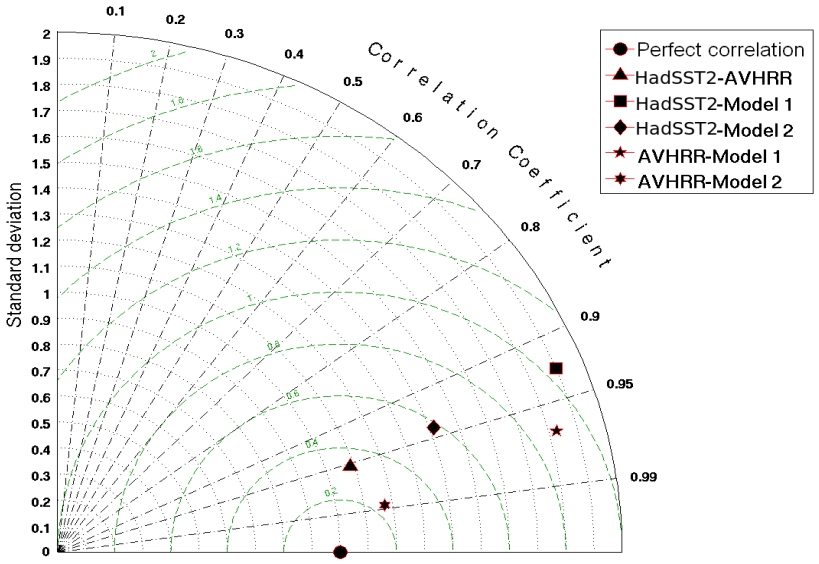


Figure 3.2 Taylor diagram showing the relationship between each of the SST time series presented in Figure 3.1 over the following periods: HadSST2 and AVHRR; 1986 – 2001, HadSST2 and first model run; 1971 – 1993, HadSST2 and second model run; 1992 – 2001, AVHRR and first model run; 1986 – 1993, AVHRR and second model run; 1992 – 2001. The green axis represents root mean square values.

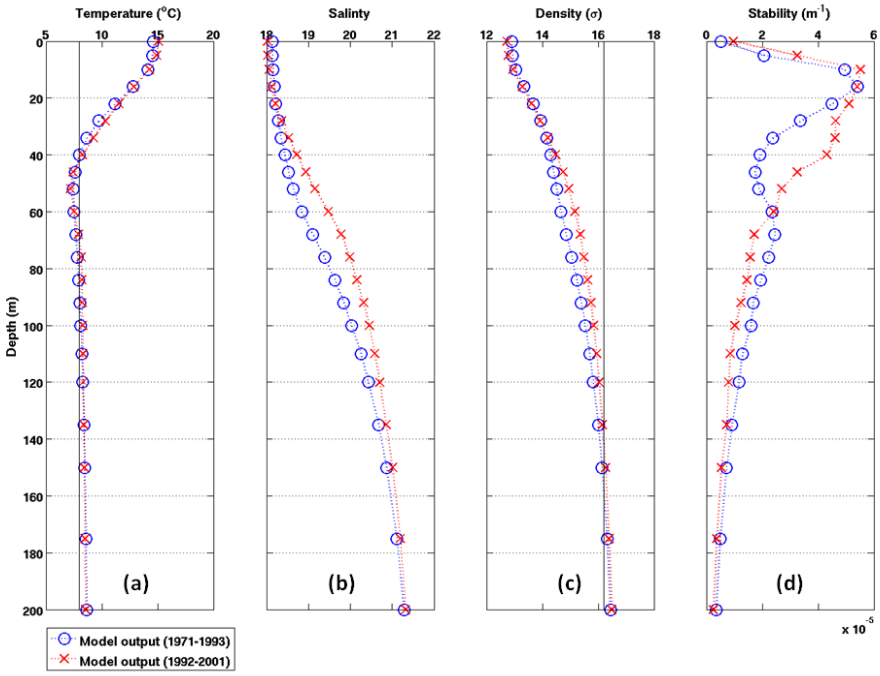


Figure 3.3 Mean vertical distribution of (a) temperature ($^{o}$C), (b) salinity, (c) density (kg m$^{-3}$) and (d) stability (m $^{-1}$) of first 200 m. Blue 'o' represents first model period and red 'x' represents second model period means.

The mean stability profile of first model run has two distinct maxima, one of which coincides with the bottom of the mixed layer at around 20 m and the other of which coincides with the bottom of the CIL at around 70 m (Figure 3.3 (d)). The mean stability profile obtained from the second model simulation, on the other hand, shows a gradual decrease in stability between ~20 m and ~120 m depth, with only one maxima around 20 m. Comparison of the simulated density and stability profiles to those derived from observations reveals that the first model simulation closely resembles the observed water column structure of the Black Sea whilst the second is unrealistic. In conclusion, both models exhibit realistic temperature, salinity and density properties within the depth range of the surface mixed layer and seasonal thermocline. The second model simulation, however, is not able to simulate realistic conditions between the depths of the seasonal thermocline and permanent pycnocline, suggesting that CIL formation is not properly represented by the second model. As the only difference between the two model runs is the assimilation procedure it appears that the altimetry assimilation process introduces errors into the model (without data assimilation model accuracy is reduced but salinity, density and stability profiles resemble those of the first model run presented here). Since the intermediate water column structure of the second model run does not look physically meaningful, data from the second model run were excluded when analysing properties of the CIL throughout this thesis work.

### 3.1.3 Model accuracy (comparison to discrete measurements)

To assess model accuracy, direct comparisons were made between discreet observations and the corresponding modelled variable at the nearest point in space and time. For this purpose all available *in-situ* (CTD) observations overlapping the two model periods were extracted from the Black Sea Database (http://sfp1.ims.metu.edu.tr/ODBMSDB/ODBMSDB.dll/querydb). Values of SST, SSS, MLD, depth of the CIL upper and lower boundaries, CIL thickness and CIL mean temperature were obtained from each available CTD cast, and differences between observed values and the corresponding modelled values were calculated. In

Figures 3.4 (a) and (b) differences between modelled and observed surface temperatures during the both of the simulation periods are presented in the form of an error map. It should be noted when considering Figure 3.4 that the error maps contain data spanning the entire model period in one figure and that the distribution of observations is irregular both in space and time. Also in all Figures errors are presented as a modelled value minus an observed value. Except for a small number of outliers, SST errors lie within the range ±2 $^{o}$C during both model periods. As a crude test for model drift, annually averaged errors were calculated and the resultant time series were checked for any trend. Annually averaged SST errors range between ±1 $^{o}$C and show no trend for either of the model runs (see appendix B).

Differences between modelled and observed salinity values during the first and second model periods can be seen in Figures 3.4 (c) and (d). Salinity errors typically fall within the range ±0.2 except within the Danube discharge area. The model tends to overestimate salinity in the immediate vicinity of the Danube discharge and underestimate salinity in the surrounding regions. Salinity errors near river discharges are not unexpected as the model uses monthly averaged climatological river fluxes. Interannual and smaller scale variability in the fresh water budget is introduced to the model primarily through the data assimilation procedure which tends to smooth signals over a wider area. The spatial distribution of salinity errors is the same for the second period; however, salinity errors are a factor of ~4 larger for the second model period. On the other hand, time series of annually averaged salinity differences range between ±1 for the first period and ±0.5 for the second period and show no trend. Most of the CTD observations were limited to the North-western Shelf before 1981 meaning the data available for assimilation was limited. Salinity error decreases to nearly zero after 1981 for the remainder of the first simulation period (see appendix B), when more data was available for assimilation.

Differences between modelled and observed mixed layer depths during the first (Figure 3.4 (e)) and second (Figure 3.4 (f)) model periods show no concentration of error in any one region. Even though the models underestimate MLD at some

stations by as much as 40 m, errors are typically within the range ±10 m. Annually averaged mixed layer depth errors fall within the range ±5 m, which is the maximum vertical resolution of model, and show no trend (see appendix B). The sporadic occurrence of large differences between observed and modeled mixed layer depths may be at least in part due to temporary upwelling or downwelling of the thermocline due to the passing of eddy systems.

Errors in the depth of the CIL upper boundary for the first and second model periods (Figures 3.4 (g) and (h)) are typically within the range ±6 m, which is approximately equal to the vertical resolution at the mean depth of the CIL upper boundary (~30 m). Maximum errors are, however, are as large as ±50 m for both time periods. Errors in annually averaged CIL upper boundary depth range between -20 m and 0 m before 1985 and are within the range of ±5 m after 1985 and throughout the second model period and shows no distinct trend (see appendix B).

The first model simulation typically underestimates the depth of the CIL lower boundary near the 200 m depth contour. Away from the 200 m depth contour, differences between modelled and observed CIL bottom boundary are within the range ±10 m (Figure 3.4 (i)). Time series of annually averaged CIL bottom boundary error show a persistent mean error of approximately -10 m (see appendix B). Due to the sparse distribution of data during the second model period (Figure 3.4 (j)), it is difficult to assess how errors are distributed. Annual mean errors during the second model period are approximately -20 m (see appendix B).

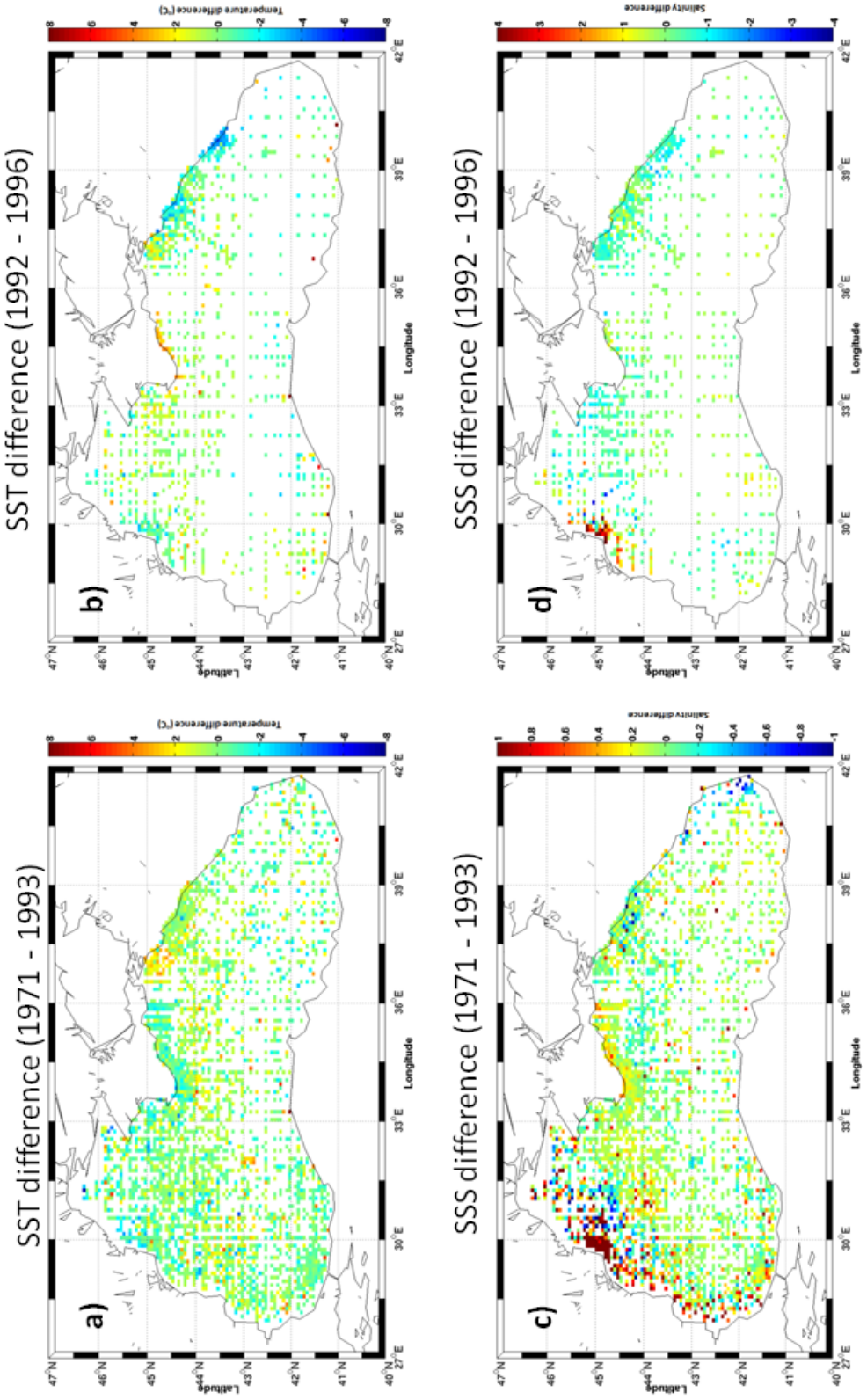
SST difference (1971 - 1993)
SST difference (1992 - 1996)
SSS difference (1971 - 1993)
SSS difference (1992 - 1996)
a)
b)
c)
d)
Temperature difference (°C)
Salinity difference
Latitude
Longitude

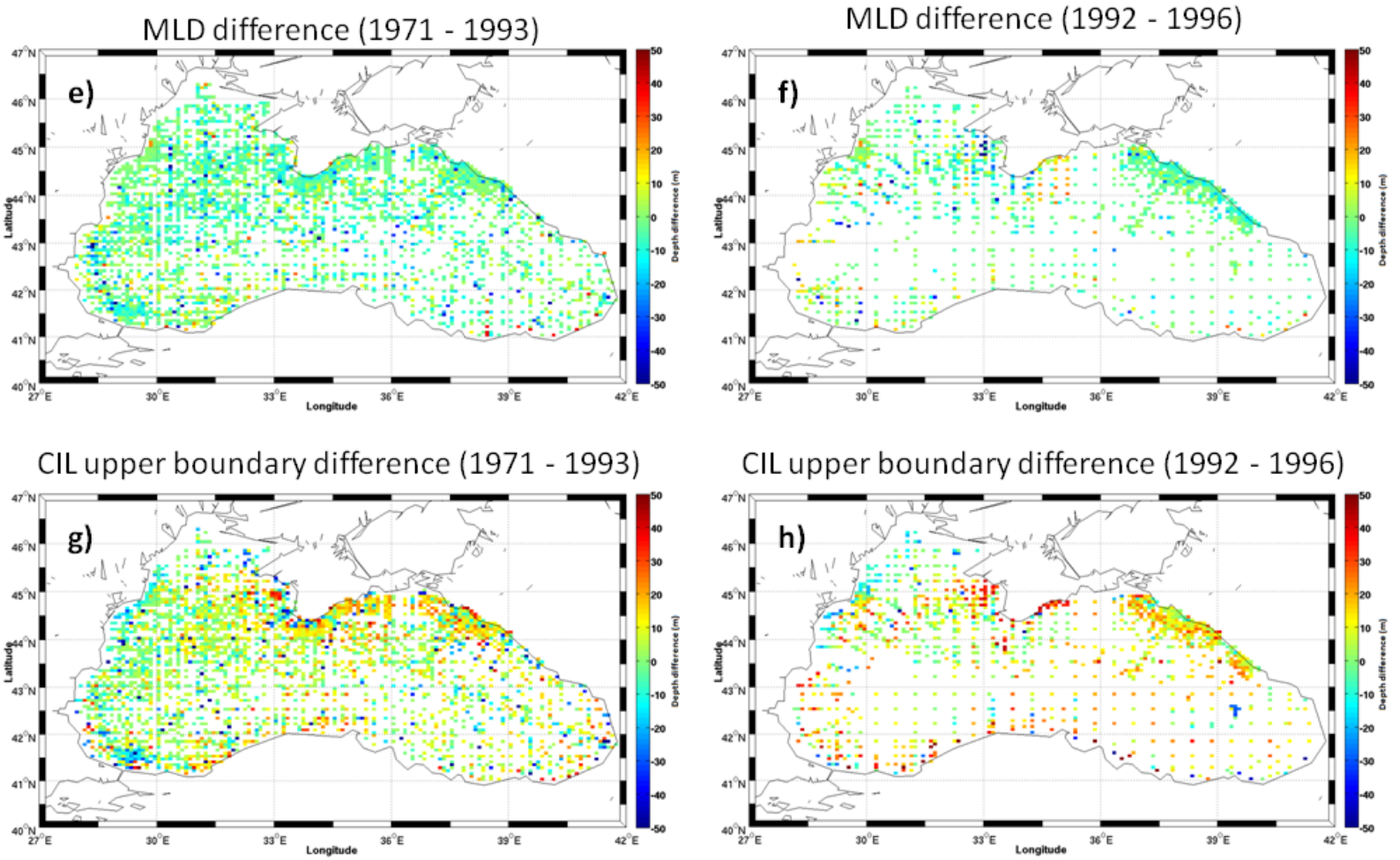
MLD difference (1971 - 1993)
e)
MLD difference (1992 - 1996)
f)
CIL upper boundary difference (1971 - 1993)
g)
CIL upper boundary difference (1992 - 1996)
h)
Latitude
Longitude
Depth difference (m)

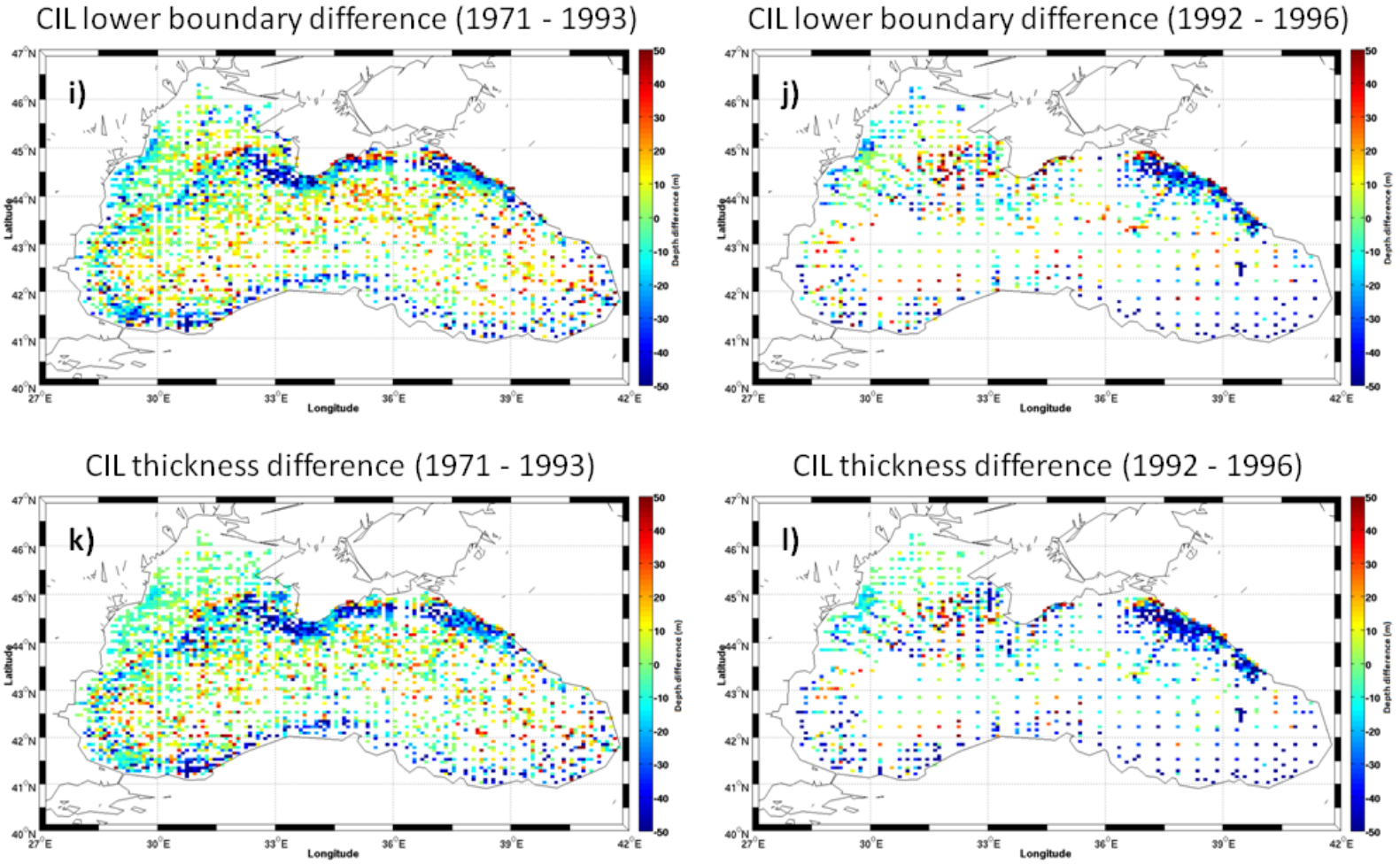
CIL lower boundary difference (1971 - 1993)
i)
CIL lower boundary difference (1992 - 1996)
j)
CIL thickness difference (1971 - 1993)
k)
CIL thickness difference (1992 - 1996)
l)
Latitude
Longitude
Depth difference (m)
47°N
46°N
45°N
44°N
43°N
42°N
41°N
40°N
27°E
30°E
33°E
36°E
39°E
42°E
50
40
30
20
10
0
-10
-20
-30
-40
-50

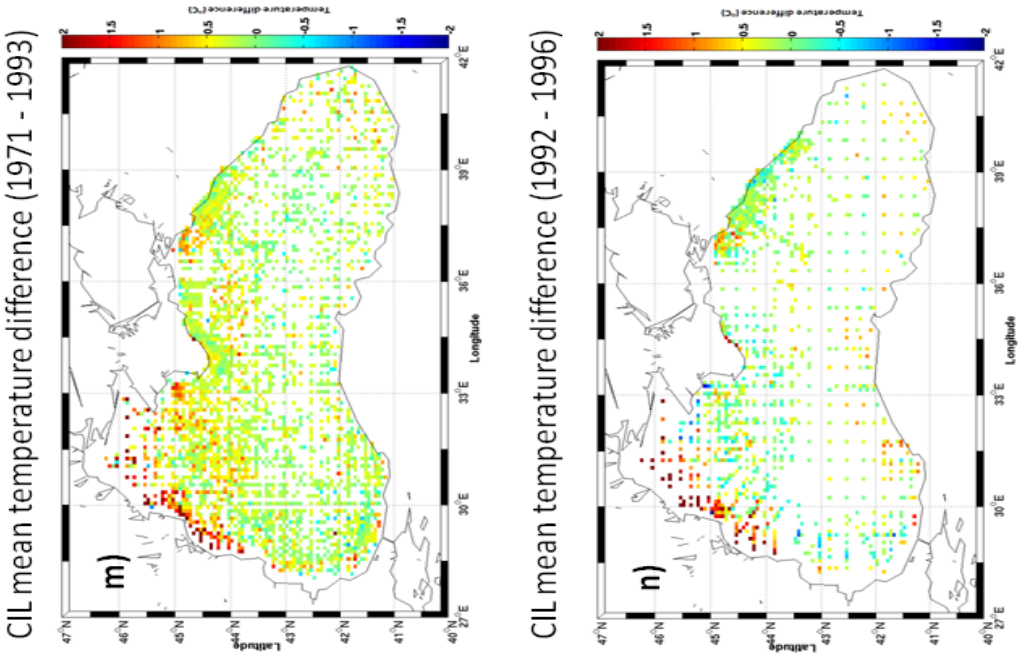


Figure 3.4 Difference between modelled and observed variables (model result minus observation) (a) SST (1971 – 1993), (b) SST (1992 – 2001), (c) SSS (1971 – 1993), (d) SSS (1992 – 2001), (e) MLD (1971 – 1993), (f) MLD (1992 – 2001), (g) CIL upper boundary (1971 – 1993), (h) CIL upper boundary (1992 – 2001), (i) CIL lower boundary (1971 – 1993), (j) CIL lower boundary (1992 – 2001), (k) CIL thickness (1971 – 1993) (l) CIL thickness (1992 – 2001), (m) CIL mean temperature (1971 – 1993) and (n) CIL mean temperature (1992 – 2001). The number of stations and total number of observations included in each of the maps can be seen in table 3.1.

Table 3.1 Number of CTD stations and individual observations included in the maps in Figure 3.4.

| | Observations | Stations |
|---|---|---|
| **a** | 14783 | 2778 |
| **b** | 3769 | 987 |
| **c** | 14616 | 2752 |
| **d** | 3658 | 990 |
| **e** | 13412 | 2877 |
| **f** | 2903 | 1147 |
| **g** | 13782 | 2797 |
| **h** | 3118 | 1131 |
| **i** | 13782 | 2797 |
| **j** | 3118 | 1131 |
| **k** | 13782 | 2797 |
| **l** | 3118 | 1131 |
| **m** | 13782 | 2797 |
| **n** | 3118 | 1131 |

As the model error in CIL lower boundary is larger than the error in CIL upper boundary, errors in CIL thickness show nearly the same spatial distribution as the errors in the bottom boundary (Figures 3.4 (k) and (l)). Annual mean errors in CIL thickness are within the range ±10 m before 1985, increasing to -20 m after 1993 with an increasing trend for the first simulation period. Annually averaged errors in CIL thickness from the second mode model simulation are approximately -20 m, meaning the modeled CIL thickness is on average 20 m thinner than the observed CIL thickness throughout the second simulation period (see appendix B)).

Both models overestimate CIL mean temperature by about 2 $^{o}$C near river discharges in the North-western Shelf. Difference between modeled and observed CIL mean temperature are within the range between ±0.5 $^{o}$C throughout the rest of the basin for both model runs (Figure 3.4 (m) and (n)). Time series of annually averaged CIL mean temperature shows an overestimation fluctuating between 0 $^{o}$C and 1 $^{o}$C for first model run and between 0 $^{o}$C and 0.5 $^{o}$C for second model run (see appendix B).

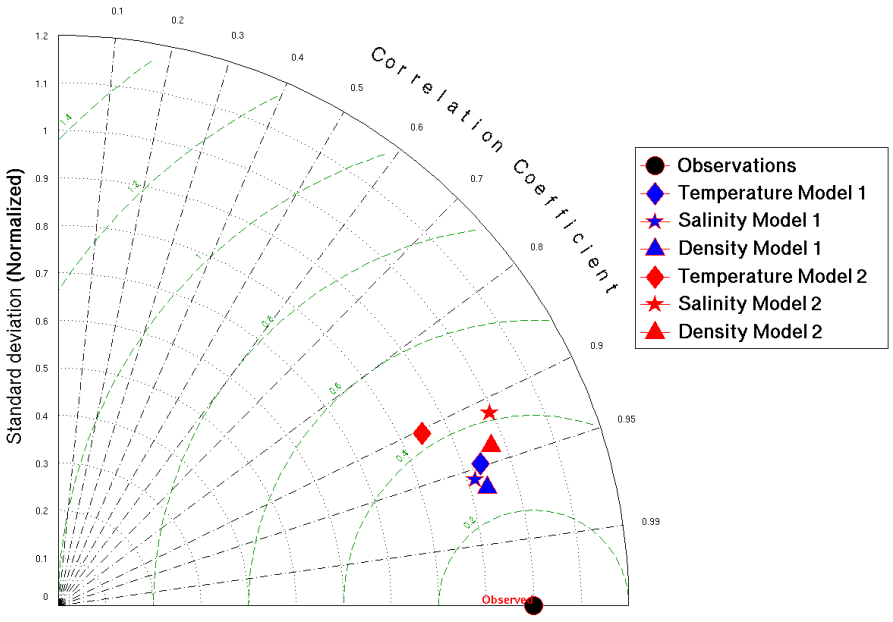


Figure 3.5 Taylor diagram showing the relationship between CTD observations and modelled temperature, salinity and density. Model 1 (blue) covers the period from 1971 to 1993 and model 2 (red) covers the period from 1992 to 2001. The green axis represents root mean square values.

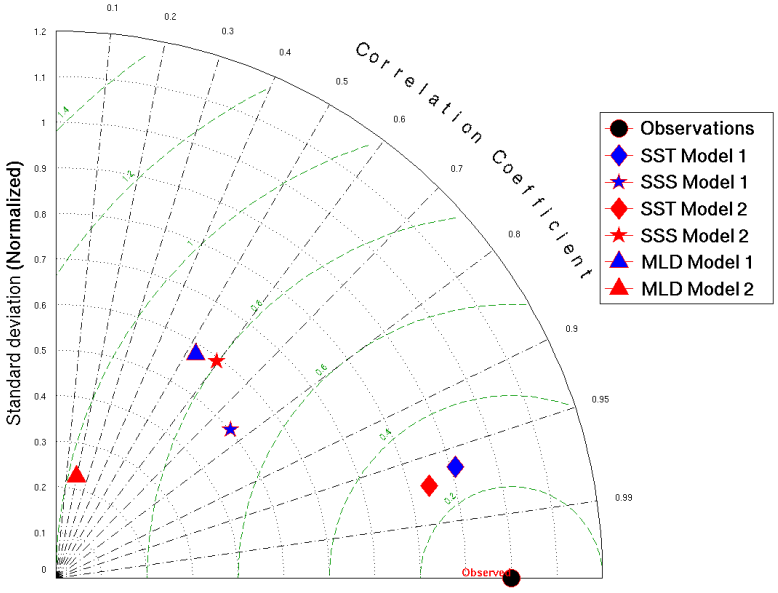


Figure 3.6 Taylor diagram showing the relationship between CTD observations and modelled SST, SSS and MLD. . Model 1 (blue) covers the period from 1971 to 1993 and model 2 (red) covers the period from 1992 to 2001. The green axis represents root mean square values.

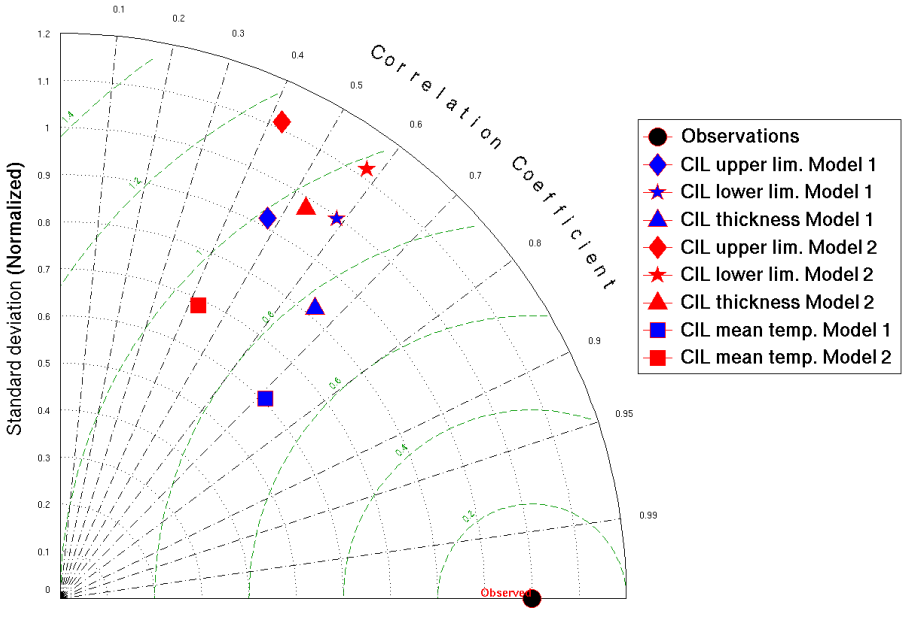


Figure 3.7 Taylor diagram showing the relationship between CTD observations and modelled CIL upper and lower boundaries, CIL thickness and CIL mean temperature. . Model 1 (blue) covers the period from 1971 to 1993 and model 2 (red) covers the period from 1992 to 2001. The green axis represents root mean square values.

The relationships between modeled and observed temperature, salinity and density values (using all available observations between the surface and bottom) are summarized in the form of a Taylor diagram in Figure 3.5. For each variable and for both model runs there is a significant correlation between modeled and observed data sets ($r > 0.9$) and normalized standard deviations are between 0.9 and 1. The high correlations presented in Figure 3.5 are partly due to the inclusion of data from below the permanent pycnocline where temperature and salinity characteristics are stable in time. For all variables the first model simulation is more accurate than the second. In Figure 3.6, comparison of modeled and observed sea surface temperature (SST), sea surface salinity (SSS) and mixed layer depth (MLD) are presented. SST data sets from both models are significantly correlated to observations with r values of >0.95 and root mean square errors between 0.2 and 0.4. SSS values also compare well to observations with correlation coefficients of 0.6 and 0.8 and root mean squares errors of 0.6 and 0.8 for the first and second model runs respectively. MLD are weakly correlated to observations ($r \sim 0.5$ and $\sim 0.2$ for the first and second model runs respectively) with normalized standard deviations of ~0.6 and ~0.2. As MLD is not expected to vary greatly with location, the poor correlations between modeled and observed values is not unexpected. Correlations between observed and modeled CIL upper boundary depth, lower boundary depth and thickness produce r values between 0.4 and 0.7 with normalized standard deviations between 0.8 and 1.2 while CIL mean temperature comparisons of first and second model have correlations ~0.7 and 0.4 with normalized standard deviations 0.6 and 0.7 respectively (Figure 3.7).

In conclusion, both model runs represent surface mixed layer characteristics (temperature and salinity and mixed layer depth) with an acceptable and stable degree of accuracy throughout the simulation periods. Since the number of observations and their locations are not consistent from season to season and year to year, comparing annual mean errors provides limited information. However as there are no obvious trends in the error time series of surface layer properties it is assumed

that interannual variability and trends in modeled variables reflects changes in the physical characteristics of the system rather than model error. Errors are typically larger for the second model run for all variables and this is especially true when considering CIL properties, which exhibit increasing error throughout the course of the model run.

### 3.1.4 Qualitative assessment of modelled circulation structure

Figure 3.8 shows a map of mean surface velocity averaged over the period from 1971-1993. The structure of the cyclonic rim current and the Eastern and Western gyres is clearly represented by the model. The Kerch, Sevastopol, Sakarya, Sinop, Kizilirmak, Danube and Batumi anticyclones are also represented by the model although the Batumi eddy is smaller and weaker than observed. Although the strength of surface rim current is lower than the literature value of 0.5 – 1 m/s (Oğuz *et al., 2005a*), the general circulation pattern of model compares well to the schematic diagram presented earlier (Figure 1.6) which is based on observations. The model is forced by ERA40 wind fields which are known to poorly represent the actual wind conditions of the region (Cannaby per. com.) which may provide one explanation for the lower than observed surface velocities. Maps showing annual mean surface currents from 1971 to 1993 (appendix C) demonstrate the stability of the surface circulation structure throughout the simulation period.

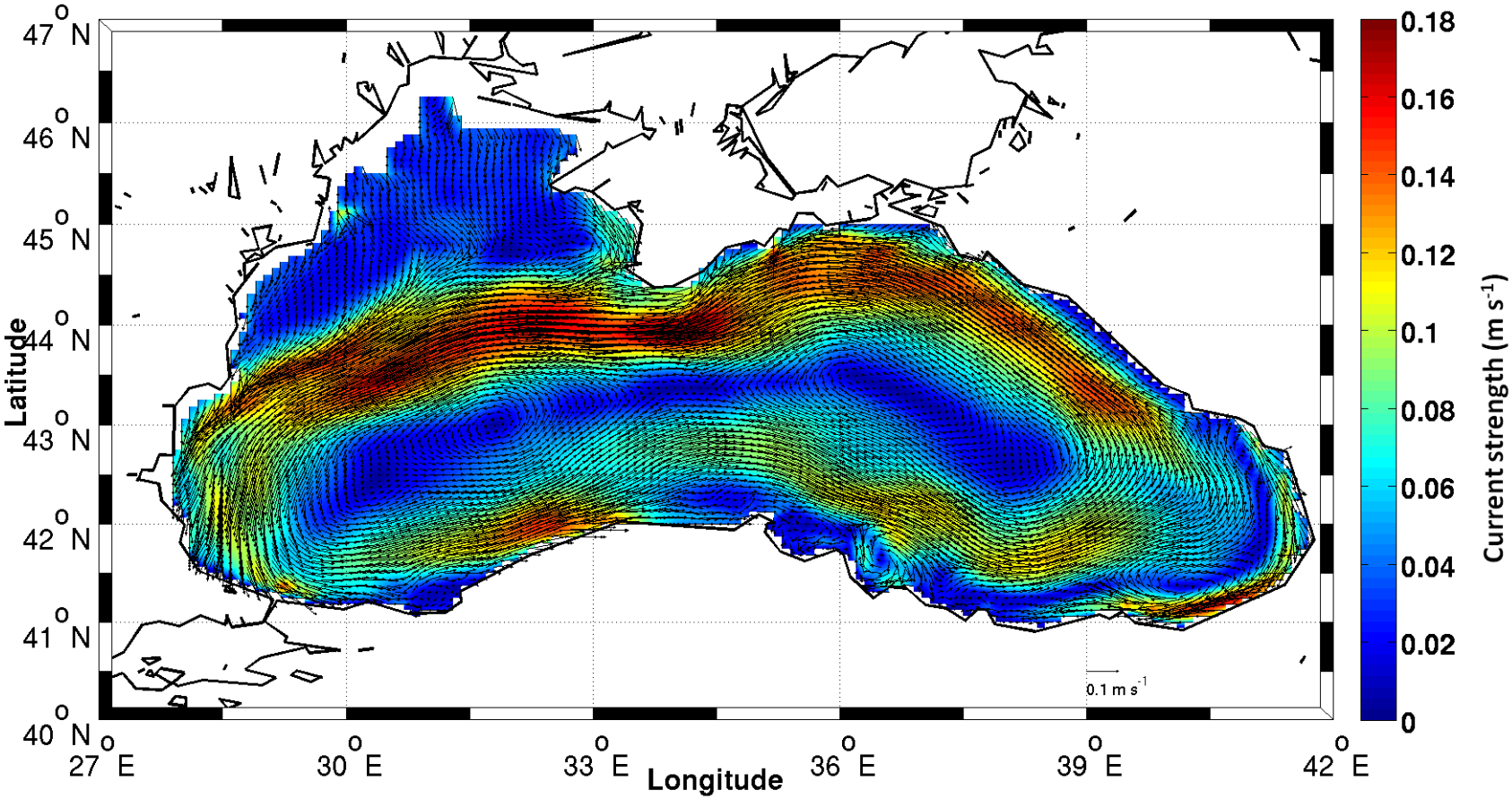


Figure 3.8 Mean surface currents and their strength of first model period (1971 – 1993)

## 3.2 Temporal variability in the water column structure

### 3.2.1 Summary of water column structure

Hovmöller plots showing the temperature, salinity and density evolution of the upper 200 m of the water column throughout the first and second model periods can be seen in Figures 3.9 – 3.14 respectively. The temperature plots illustrate inter-annual and intra-annual variations in CIL characteristics between 40 – 100 m as well as surface cooling during the first model period and surface warming over the course of the second model period. Salinity shows an increasing trend below 100 m during the first model period and a concurrent freshening trend above 100 m depth. For the second model period, salinity below 100 m and above 28 m shows a freshening trend while salinity between 28 – 100 m shows no observable change. Intra-annual variations in salinity are evident at all depths throughout the first model run, whilst the second model run exhibits little variability over sub-annual time scales. Seasonal and inter-annual variations in the density of the upper 40 m are evident during both model simulations (Figures 3.13 and 3.14). A declining trend in the density of the upper 40 m throughout the second model period is particularly evident during the winter months. For the first model period, density below 40 m shows non-seasonal intra-annual oscillations and an increasing trend between 1971 and 1993. Density below 40 m from the second model simulation shows a seasonal oscillation associated with the winter formation and summer erosion of the CIL. A declining trend in density between 40 and 80 m combined with a decline in the density of winter surface waters appears to indicate a reduction in the formation and renewal of CIL waters throughout the second model simulation.

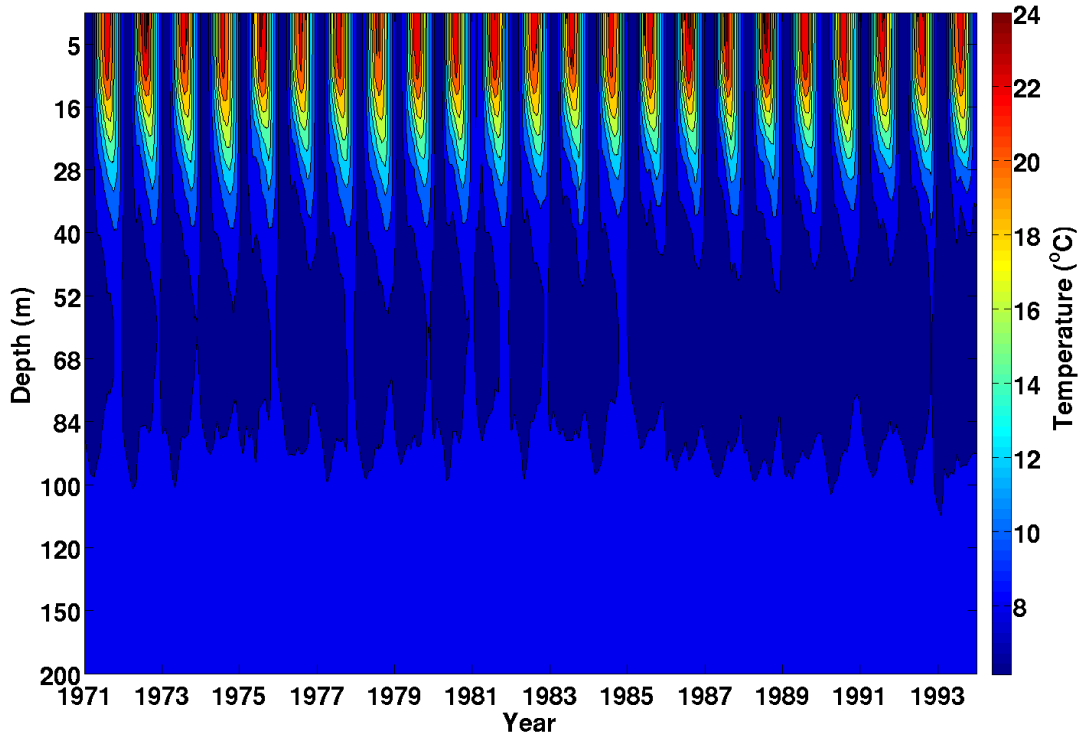


Figure 3.9 Basin mean temperature (0 – 200 m) of first model period (1971 – 1993)

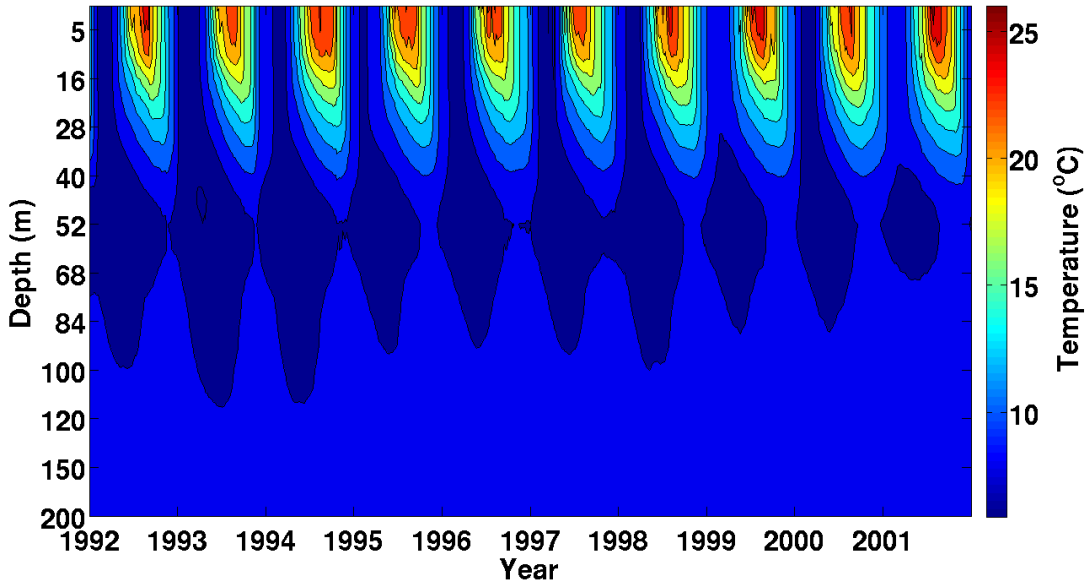


Figure 3.10 Basin mean temperature (0 – 200 m) of second model period (1992 – 2001)

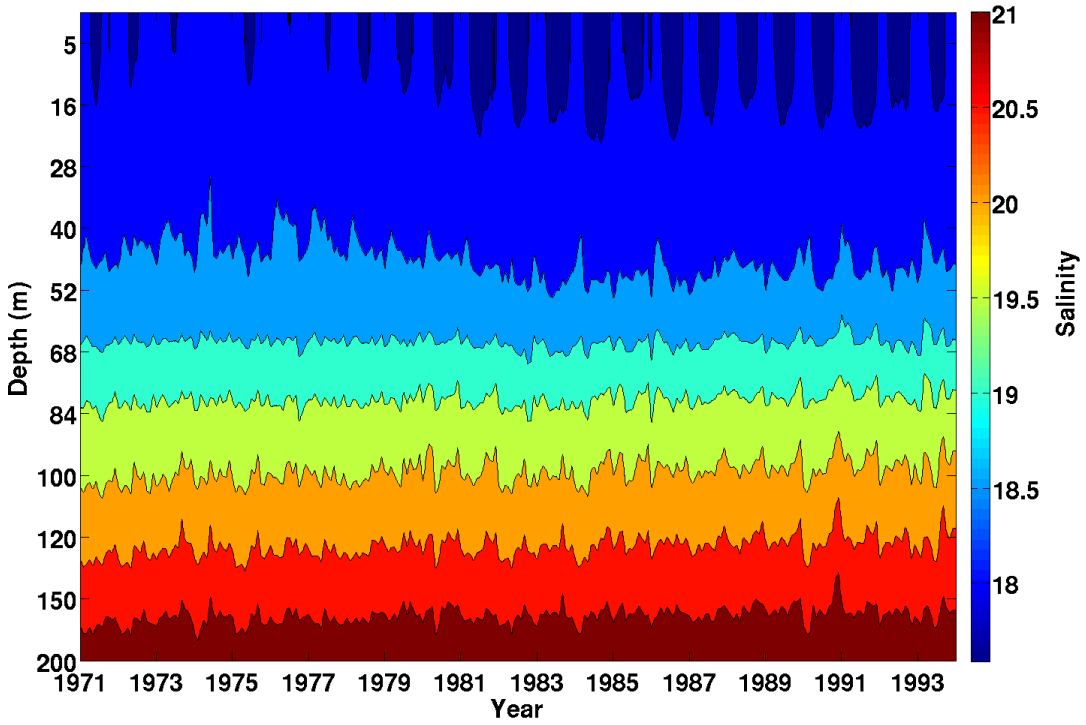


Figure 3.11 Basin mean salinity (0 – 200 m) of first model period (1971 – 1993)

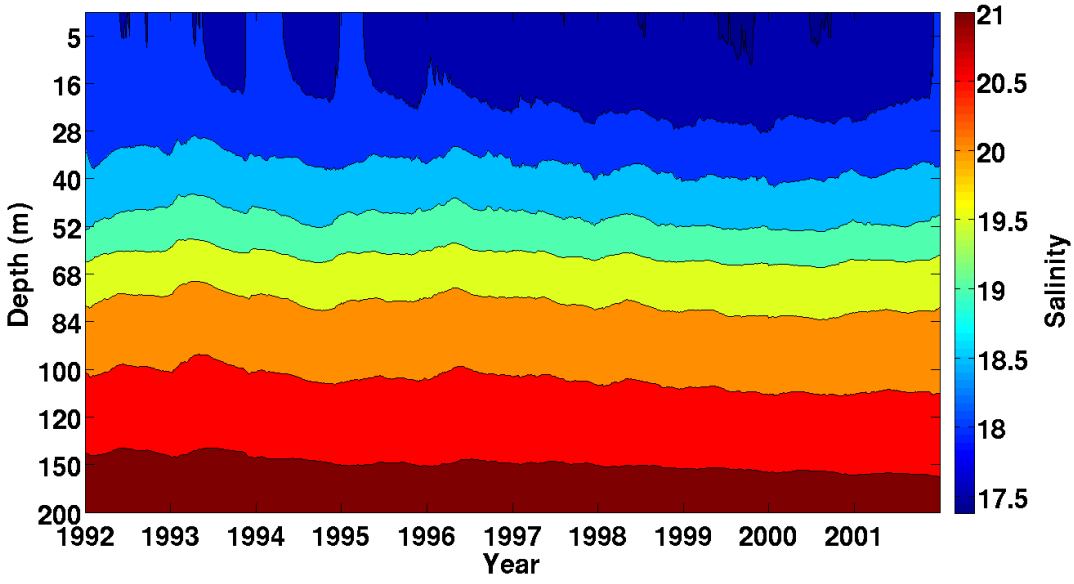


Figure 3.12 Basin mean salinity (0 – 200 m) of second model period (1992 – 2001)

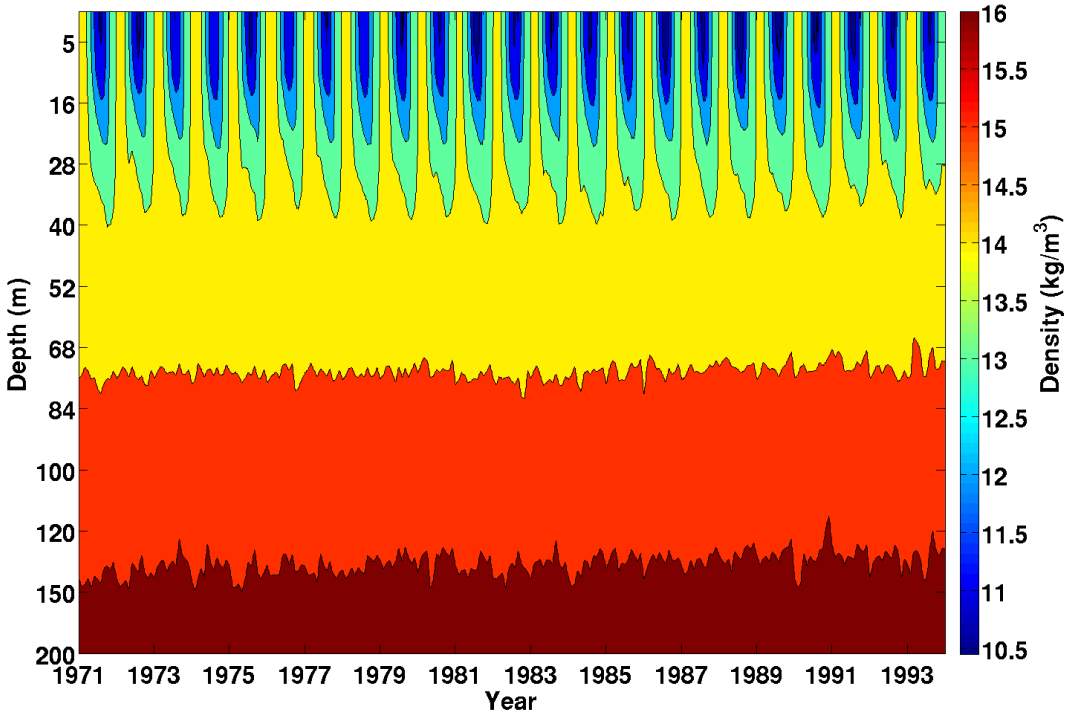


Figure 3.13 Basin mean density (0 – 200 m) of first model period (1971 – 1993)

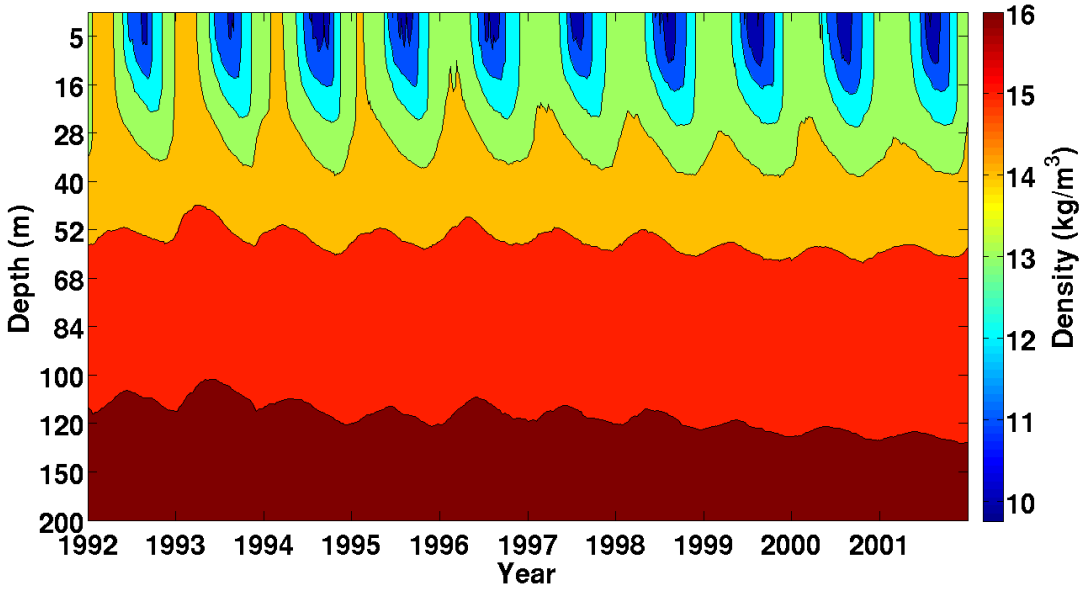


Figure 3.14 Basin mean density (0 – 200 m) of second model period (1992 – 2001)

### 3.2.2 Interannual variability and trends in mixed layer (ML) properties

Basin averaged annual mean and annual maximum SST time series, constructed by combining results from both model simulations, exhibit warming trends of 0.7 °C ($r^2$ = 0.21) and 1.7 °C ($r^2$ = 0.31) respectively, while the annual minimum SST time series shows no significant trend between 1971 and 2001 (Figures 3.15, 3.16 and 3.17). Each of the time series exhibits considerable interannual variability with interannual differences typically larger than the reported warming trends. The annual minimum SST record also exhibits considerable multiannual (approximately decadal) scale variability characterized by a relatively warm period between 1971 and 1981, a relatively cold period from 1982 to 1993, and a more defined warm period between 1994 and 2001. These periods can also be observed in the winter mean temperature record following Oğuz *et.al.* (2006) in Figure 1.11 (a) (Figure 3.17). However, distinguishing these three periods for annual mean SST is harder (Figure 3.15). The cool period between 1982 and 1993 cannot be identified in the annual maximum SST record (Figure 3.16). Annual mean and annual minimum SST records show correlations of -0.2 and -0.56 with the NAO and the EA/WR indices respectively, while the annual maximum SST record shows no significant correlation to these climate indices (Table 3.2). In summary, interannual variability in winter minimum conditions is linked to variability in atmospheric forcing, closely represented by the EA/WR index. As the atmospheric circulation is weaker during the summer months, oscillations in atmospheric circulation are generally less pronounced at this time. The increasing trend in summer maximum temperature does not appear to be related to the dominant modes of atmospheric variability, suggestive of an underlying global warming trend.

The first two EOF of annual mean SST (presented along with their principal components in Figures 3.18 (a), (b), (c) and (d)) explain 93.53 % of the total variance in the time series. The first EOF (Figure 3.18 (a)) explains 83.78 % of total variance alone. This EOF exhibits a dominant negative centre in the central north Black Sea and a weaker negative centre in the northern part of the North Western Shelf. There

are two positive centres in the southeast and southwest part of the Black Sea. The first PC (Figure 3.18 (b)), which describes the sign and relative magnitude of the pattern represented by the first EOF, is correlated to the NAO and EA/WR indices with r values of -0.31 and 0.34 respectively (Table 3.2). The second EOF of annual mean SSTs (Figure 3.18 (c)) explains 8.75 % of total variance and represents an east-west oscillation in the SST record. The corresponding PC (Figure 3.18 (d)) shows no significant correlation with the NAO or the EA/WR (Table 3.2). The existence of a significant correlation between annual mean and winter maximum SST, and PC of first EOF with the NAO and the EA/WR index, in addition to the positive North centre of first EOF, supports the hypothesis that interannual variations in the strength of northerly winds have a significant impact on the Black Sea SST record.

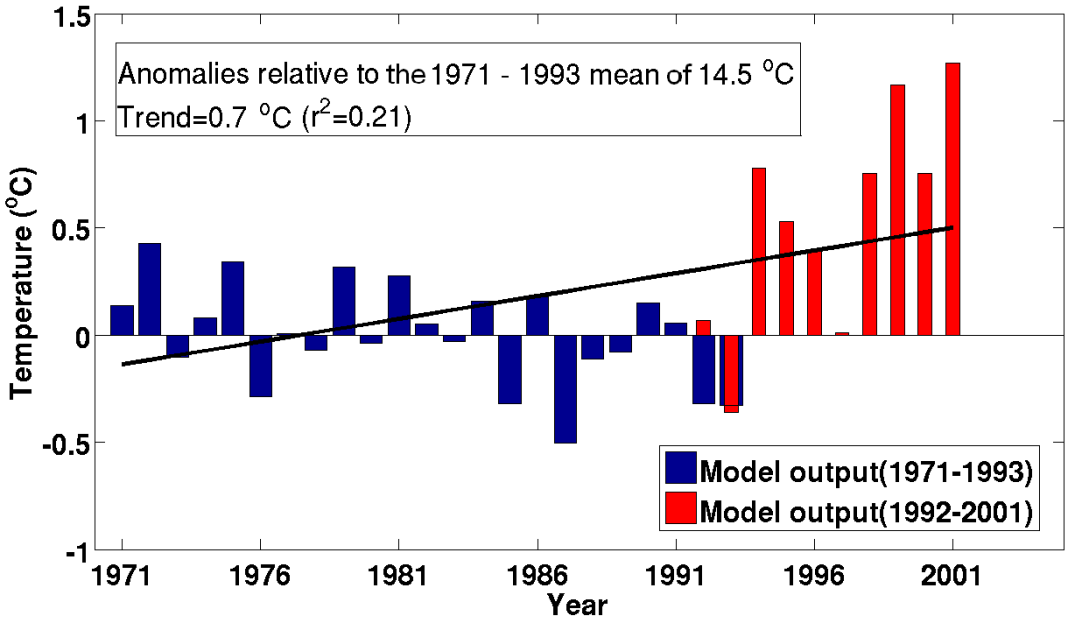


Figure 3.15 Basin averaged annual mean SST anomalies from the first model period (1971 – 1993; blue) and the second model period (1992 – 2001; red) relative to the 1971 – 1993 mean. The black line shows warming trend of 0.7 °C ($r^2$=0.21).

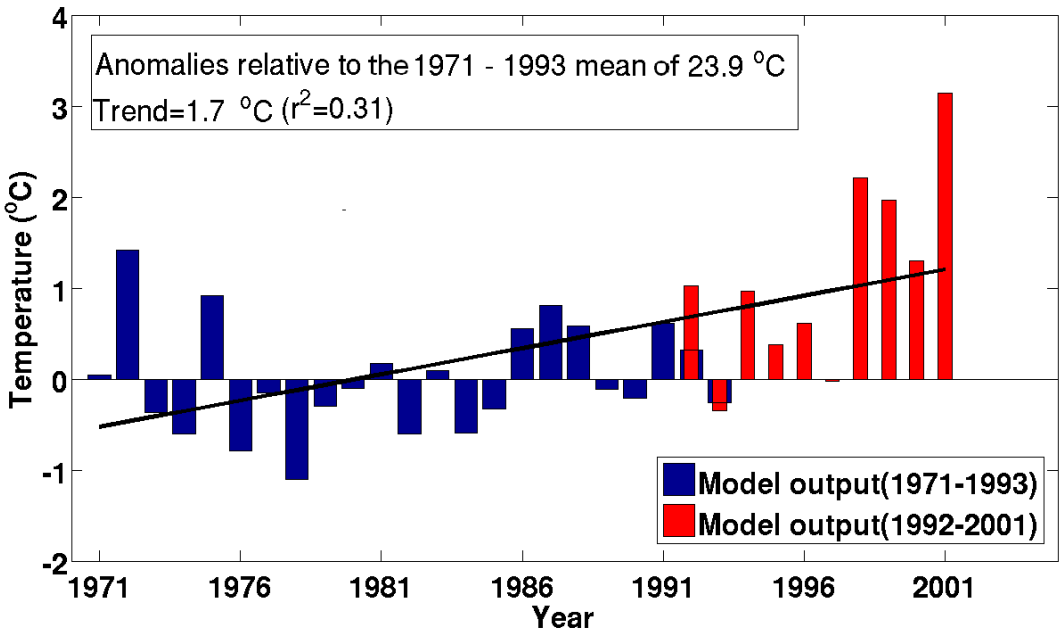


Figure 3.16 Basin averaged annual maximum SST anomalies from the first model period (1971 – 1993; blue) and the second model period (1992 – 2001; red) relative to the 1971 – 1993 mean. The black line shows warming trend of 1.7 °C ($r^2$=0.31).

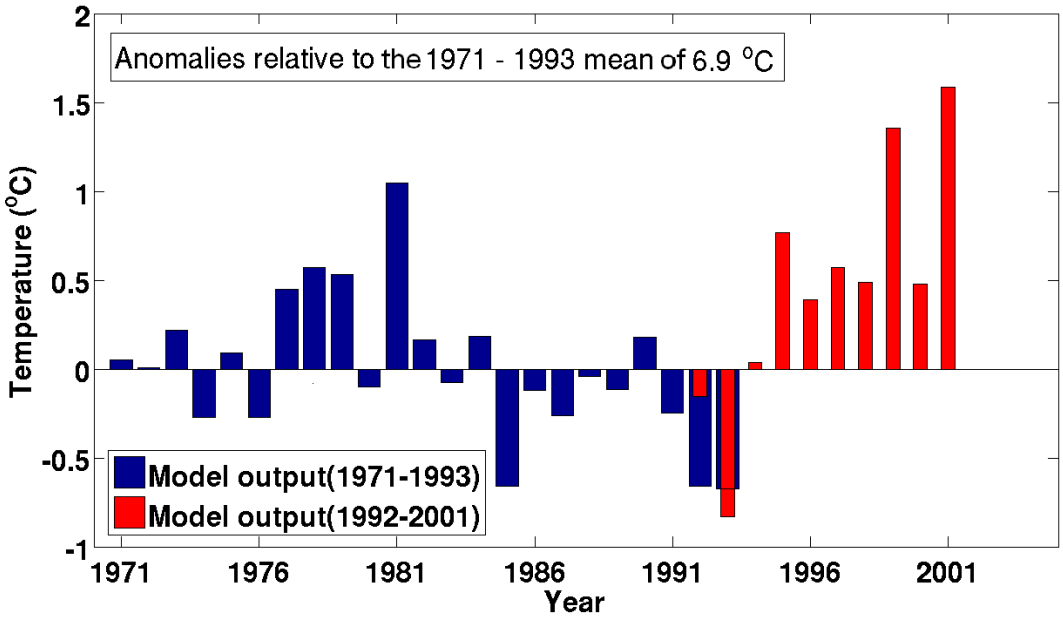


Figure 3.17 Basin averaged annual minimum SST anomalies from the first model period (1971 – 1993; blue) and the second model period (1992 – 2001; red) relative to the 1971 – 1993 mean.

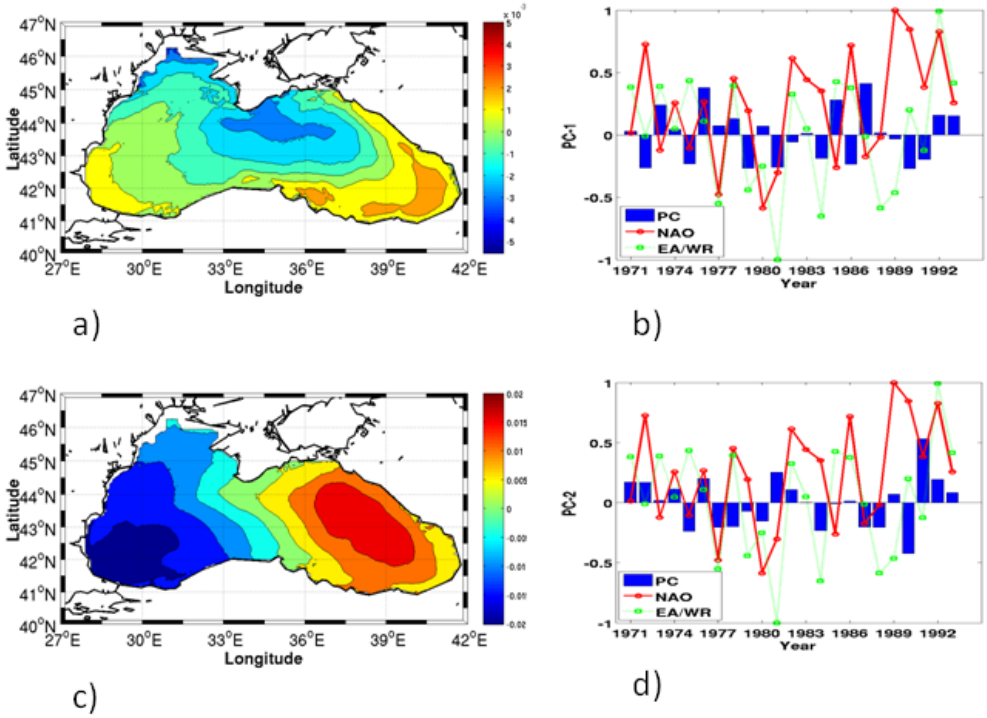


Figure 3.18 First EOF (a) and principle component (b) of annual mean SST with 83.78 % explained variance, second EOF (c) and principle component (d) of annual mean SST with 8.75 % explained variance. Red solid lines and green dotted lines show annual mean NAO and EA/WR indices respectively.

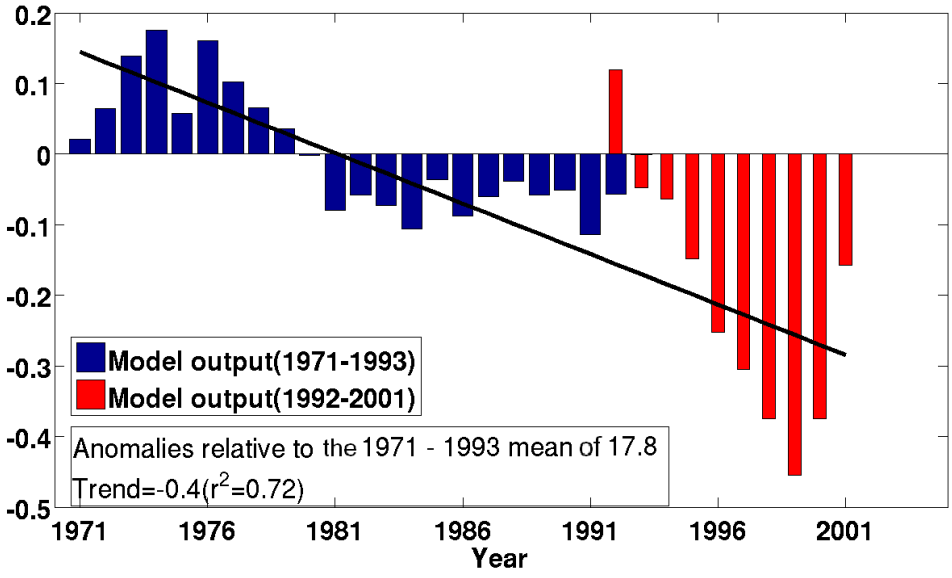


Figure 3.19 Basin averaged annual mean SSS anomalies from the first model period (1971 – 1993; blue) and the second model period (1992 – 2001; red) relative to the 1971 – 1993 mean. The black line shows a freshening trend of 0.4 ($r^2$=0.72).

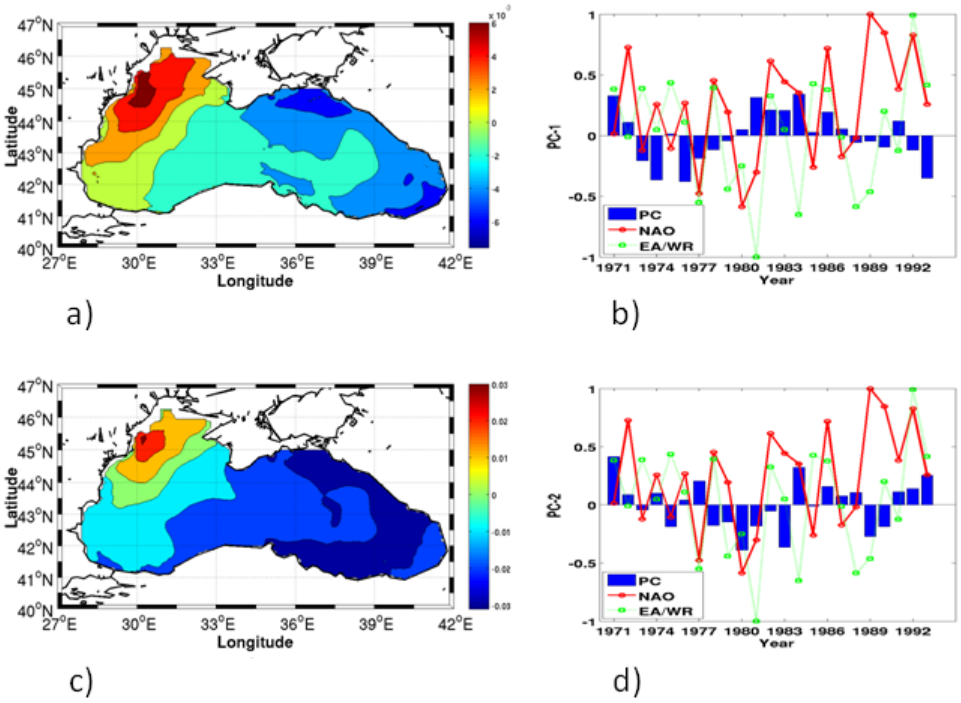


Figure 3.20 First EOF (e) and principle component (f) of annual mean SSS with 82.33 % explained variance, second EOF (g) and principle component (h) of annual mean SSS with 8.93 % explained variance. Red solid lines and green dotted lines show annual mean NAO and EA/WR indices respectively.

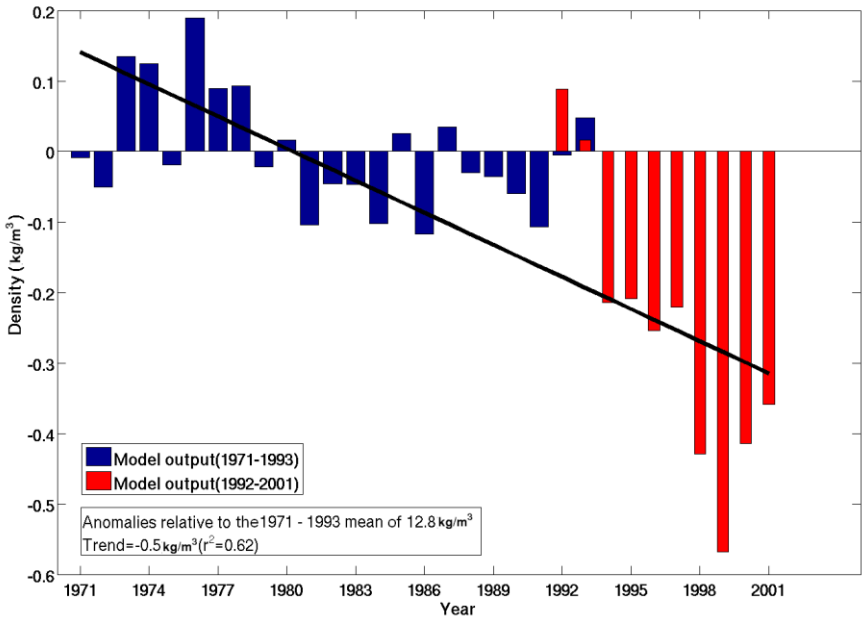


Figure 3.21 Basin averaged annual mean surface density anomalies from the first model period (1971 – 1993; blue) and the second model period (1992 – 2001; red) relative to the 1971 – 1993 mean. Black line shows decreasing trend of 0.5 kg $m^{-3}$ ($r^2$=0.62).

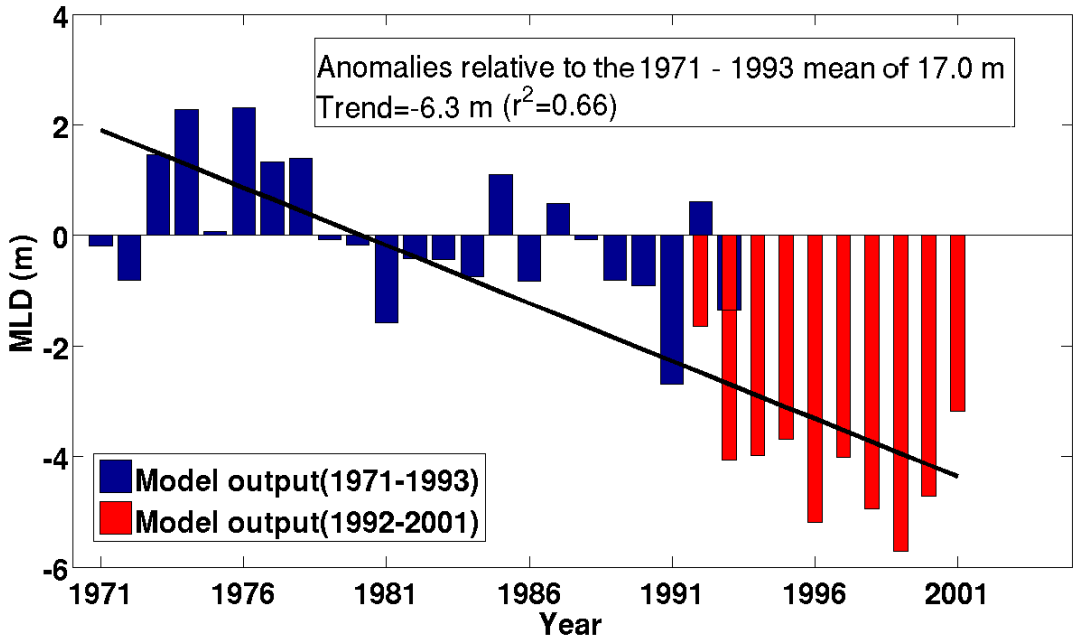


Figure 3.22 Basin averaged annual mean MLD anomalies from the first model period (1971 – 1993; blue) and the second model period (1992 – 2001; red) relative to the 1971 – 1993 mean. Black line shows shallowing trend of 6.3 m ($r^2$=0.66).

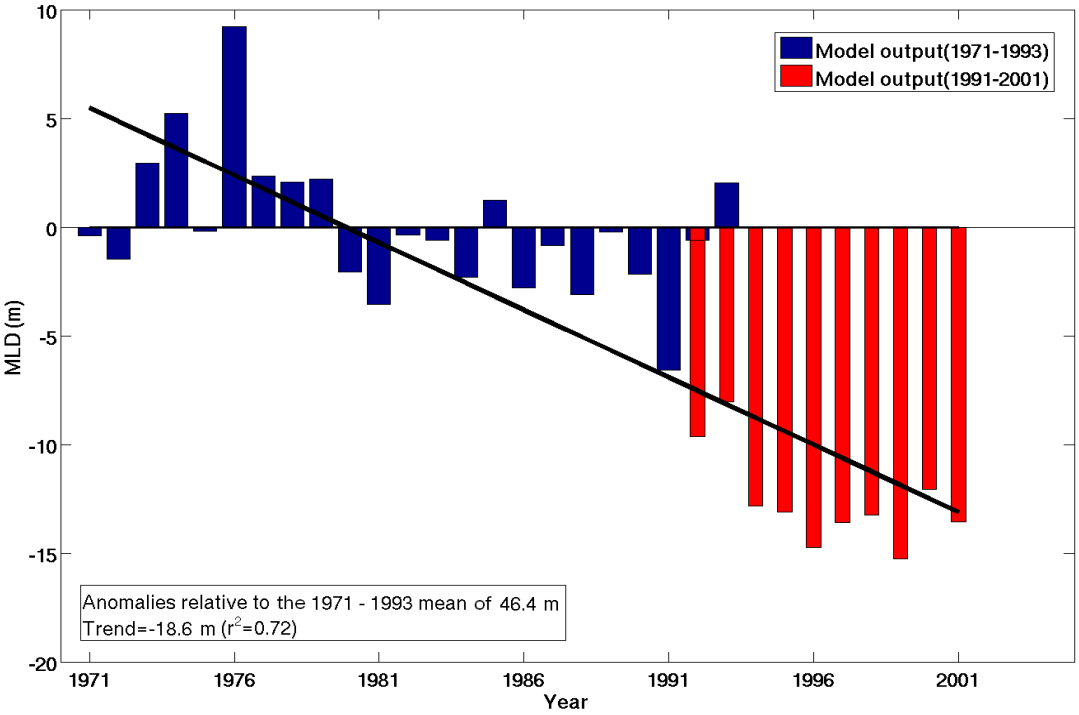


Figure 3.23 Basin averaged annual maximum MLD anomalies from the first model period (1971 – 1993; blue) and the second model period (1992 – 2001; red) relative to the 1971 – 1993 mean. Black line shows shallowing trend of 18.6 m ($r^2$=0.72).

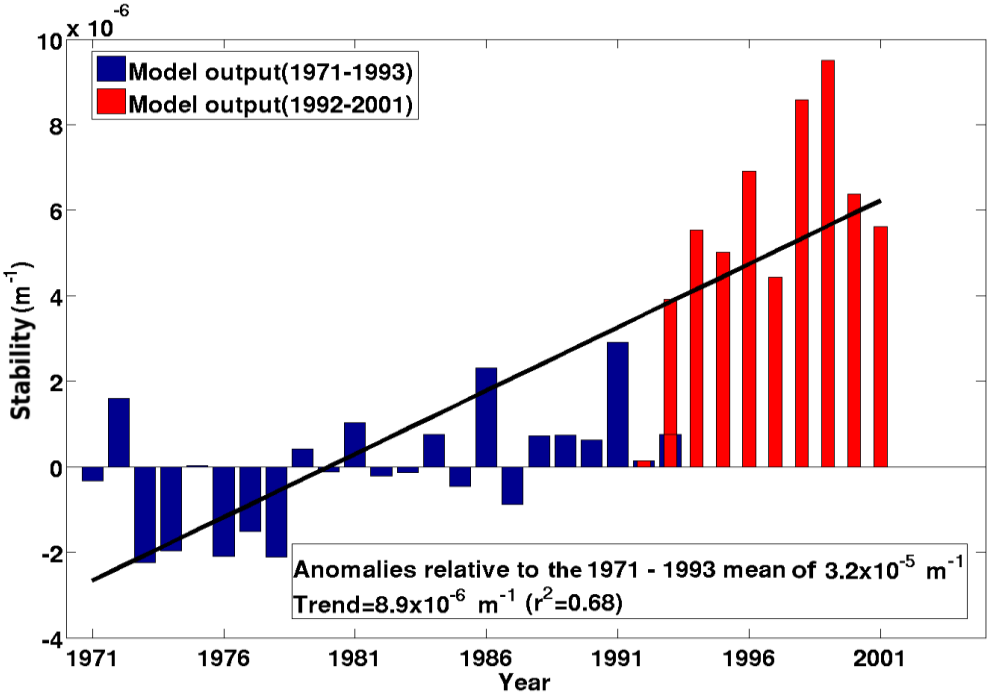


Figure 3.24 Basin averaged annual mean mixed layer stability (0 – 46 m) anomalies from the first model period (1971 – 1993; blue) and the second model period (1992 – 2001; red) relative to the 1971 – 1993 mean. Black line shows increasing trend of 8.9 x $^{10\text{-}6}$ m$^{-1}$ ($r^2$=0.68).

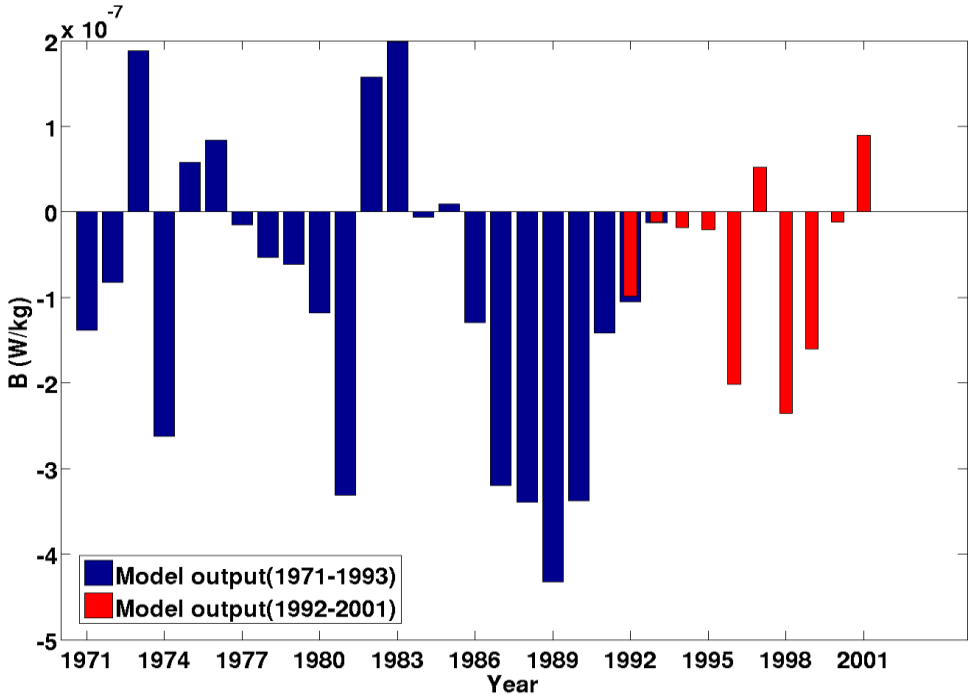


Figure 3.25 Basin averaged annual mean buoyancy flux (B) anomalies from the first model period (1971 – 1993; blue) and the second model period (1992 – 2001; red) relative to the 1971 – 1993 mean.

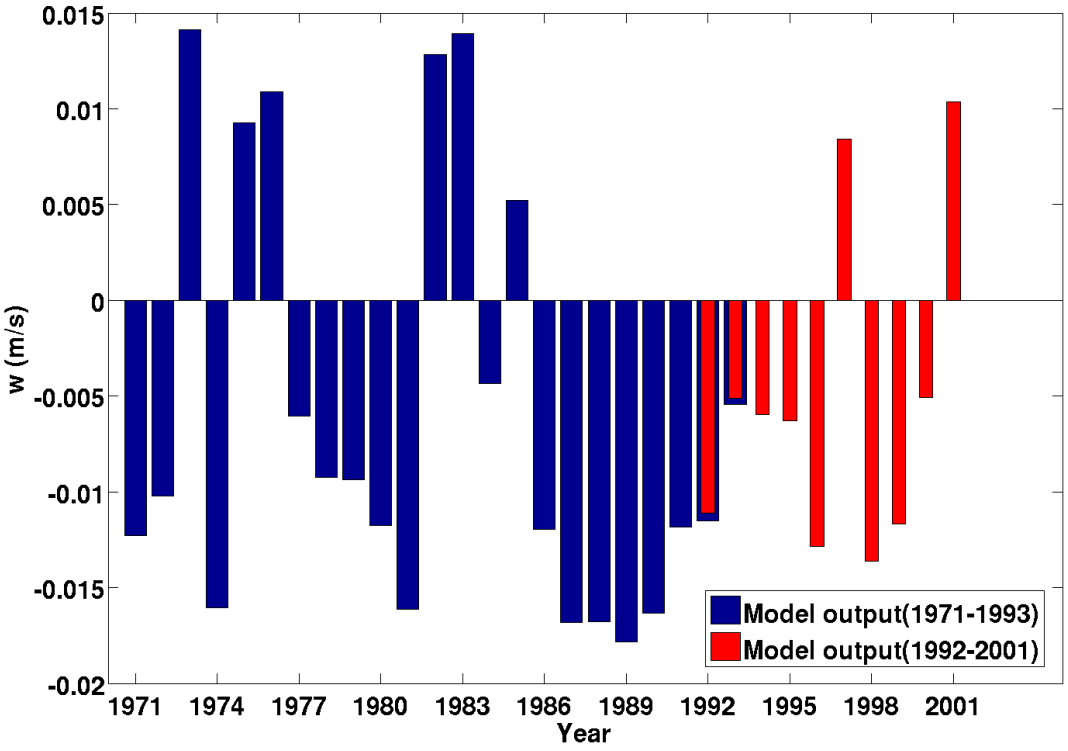


Figure 3.26 Basin averaged annual mean vertical convective velocity (w) anomalies from the first model period (1971 – 1993; blue) and the second model period (1992 – 2001; red) relative to the 1971 – 1993 mean.

Table 3.2 Correlation coefficient values of first and second PCs of SST and SSS, and maximum, minimum and annual mean of SST and annual mean of SSS from first model period with the NAO and the EA/WR indexes.

| | | | **NAO** | **EA/WR** |
|---|---|---|---|---|
| **Annual** | **SST** | **PC 1** | -0.31 | 0.34 |
| | | **PC 2** | 0.18 | 0.09 |
| | **SSS** | **PC 1** | 0.01 | -0.25 |
| | | **PC 2** | 0.01 | 0.14 |
| | | | | |
| **Annual** | **SST** | **Mean** | -0.20 | -0.56 |
| | | **Max.** | 0.01 | -0.03 |
| | | **Min** | -0.20 | -0.56 |
| | **SSS** | **Mean** | -0.26 | 0.16 |

Annual mean sea surface salinity shows a significant ($r^2$=0.72) freshening trend between 1971 and 2001 (Figure 3.18). Interannual variability is typically small compared to the overall freshening trend and as for the annual minimum temperature record, the SSS record appears to be divided into three phases. Between 1971 and 1980 surface waters are relatively saline. Between 1981 and 1993 salinities exhibit little temporal variability and after 1993 salinity decreases relatively rapidly until 1999 when the freshest conditions were observed. Between 1999 and 2001 salinity began to increase again.

The first two EOFs of SSS explain 91.26 % (82.33 % and 8.93 % respectively) of total variance. The first and second EOFs (Figure 3.20 (a) and (c)) are very similar and probably represent the same mode of variability. Both have a positive centre around Danube discharge region and a negative centre around the Kerch Strait. The corresponding PC of the first EOF (Figure 3.20 (b)) has a negative correlation coefficient (-0.25) with the EA/WR pattern while the second PC (Figure 3.20 (d)) shows no significant correlation to atmospheric indices (Table 3.2).

Sea surface density (SSD) shows a significant ($r^2$=0.62) decreasing trend between 1971 and 2001 due to the warming and freshening of surface waters (Figure 3.21). Interannual and multiannual variability in the surface density time series reflects that of the surface salinity time series.

Time series of annual mean and annual maximum mixed layer depths show shallowing trends of 6.3 m ($r^2$=0.66) and 18.6 m ($r^2$=0.72) relative to the first model means of 17.0 m and 46.4 m respectively (Figure 3.22 and 23). Moreover, the mean annual stability anomaly of the upper 46 m shows a significant increasing trend of $8.9 \times 10^{-6}$ $m^{-1}$ between 1971 and 2001 ($r^2$=0.68; Figure 3.24). Interannual variations in annual and maximum MLD mirror those in the salinity and density time series and the same ~decadal scale variability is evident in the MLD time series. During years associated with relatively saline surface conditions (most notably 1973-74 and 1976-1978) mixed-layer depths are deeper than average whilst during years associated

with relatively fresh surface conditions mixed layer depths are shallower than average.

Basin averaged annual mean buoyancy flux and vertical convective velocity show no significant trend between 1971 and 2001 (Figures 3.25 and 26). Multi annual changes of buoyancy flux and vertical convective velocity are similar to those in the SST record (i.e. buoyancy loss and increased vertical convective velocity during cold periods). Inter annual variations in buoyancy flux and vertical convective velocity mirror those in the annual net heat flux time series (Section 3.2.4; Figure 3.33).

### 3.2.3 Interannual variability in cold intermediate layer (CIL) properties

The mean depth of the upper boundary of the CIL shows a shallowing trend between 1971 and 1993. Inter annual variations in the depth of the CIL upper boundary show similar oscillations to the minimum SST record (Figures 3.17 and 27). Between 1970 and 1982 the upper boundary of the CIL is relatively shallow, while between 1983 and 1993 it resides at a relatively deep depth. The CIL lower boundary shows a deepening trend between 1971 and 1993 and again the time series suggest different conditions prevailed during the 1970s and early 80s as compared to the remainder of the 80s and early 90s. From 1971 to 1985 the lower boundary of the CIL was at a relatively shallow depth whilst from 1986 to 1993 the lower boundary was at a relatively deep depth (Figure 3.28). The divergence of the upper and lower boundaries of the CIL between 1971 and 1993 indicated a thickening of the CIL over this time period. CIL thickness show a statistically significant ($r^2$=0.45) increasing trend between 1971 and 1993, with a relatively thin CIL between 1971 and 1984 compared to the period between 1985 and 1993 (Figure 3.29). Interannual variations in the depth of the CIL lower boundary and CIL thickness show almost identical variability. Interannual changes in the depth of the CIL upper boundary are typically half the magnitude of the changes observed in the depth of the lower boundary.

Both CIL mean and core temperatures show a cooling trend from 1971 to 1993 (Figures 3.30 and 3.31) which reflects the trend in CIL thickness (between 1971 and 1984 the CIL was relatively warm and thin compared to the following period). Interannual variations of CIL mean and core temperature show almost the same pattern. Interannual variations in the bulk stability of the water column between 46 m and 200 m, which includes the CIL lower boundary, show no significant trend but much interannual and multiannual variability. The period between 1971 and 1980 can be considered as a less stable period relative to the period from 1984 – 1990. After 1990 stability again starts to decrease until 1993 (Figure 3.32).

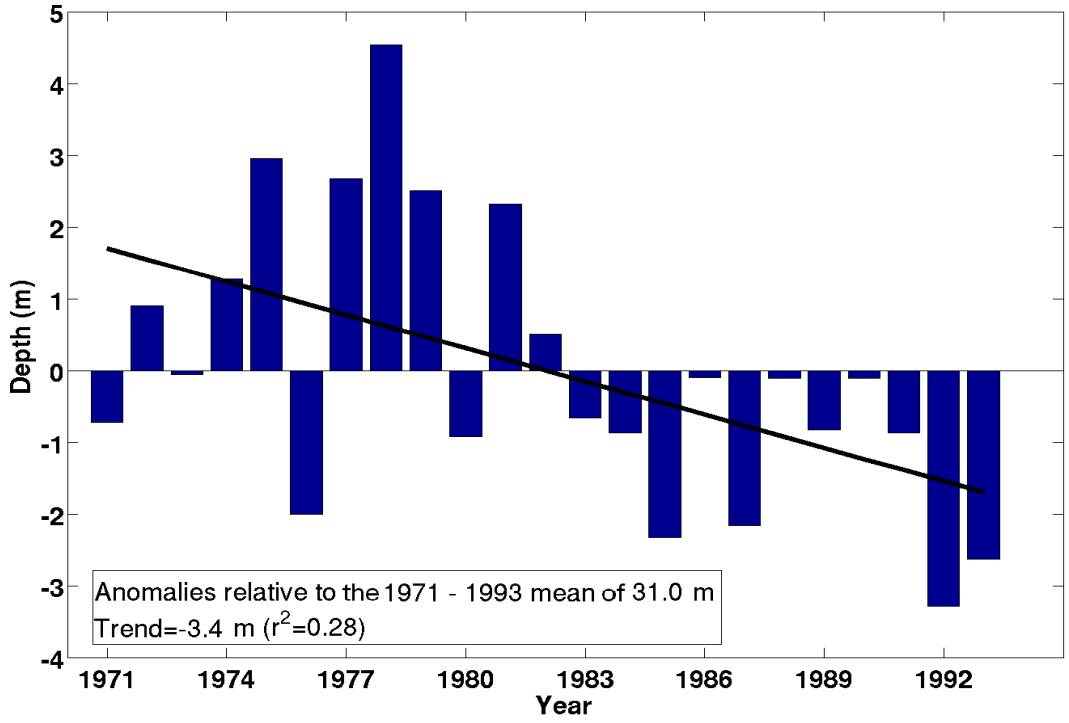


Figure 3.27 Basin averaged annual mean CIL upper limit anomalies from the first model period (1971 – 1993) relative to the 1971 – 1993 mean. Black line shows shallowing trend of 3.4 m ($r^2$=0.28).

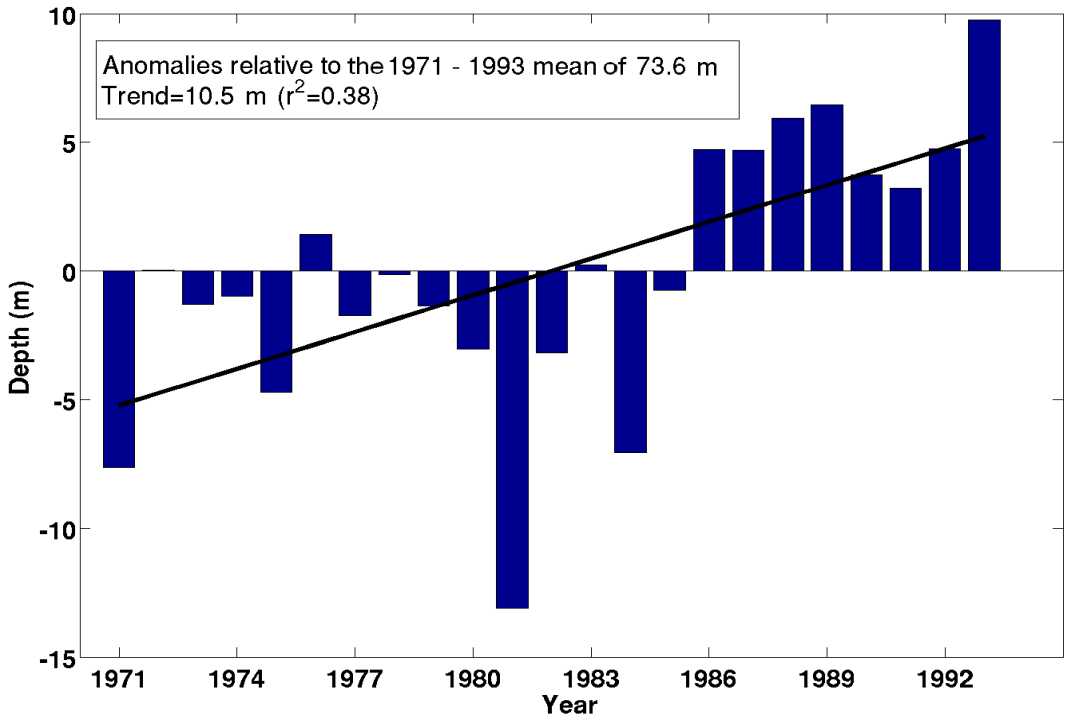


Figure 3.28 Basin averaged annual mean CIL lower limit anomalies from the first model period (1971 – 1993) relative to the 1971 – 1993 mean. Black line shows deepening trend of 10.5 m ($r^2$=0.38).

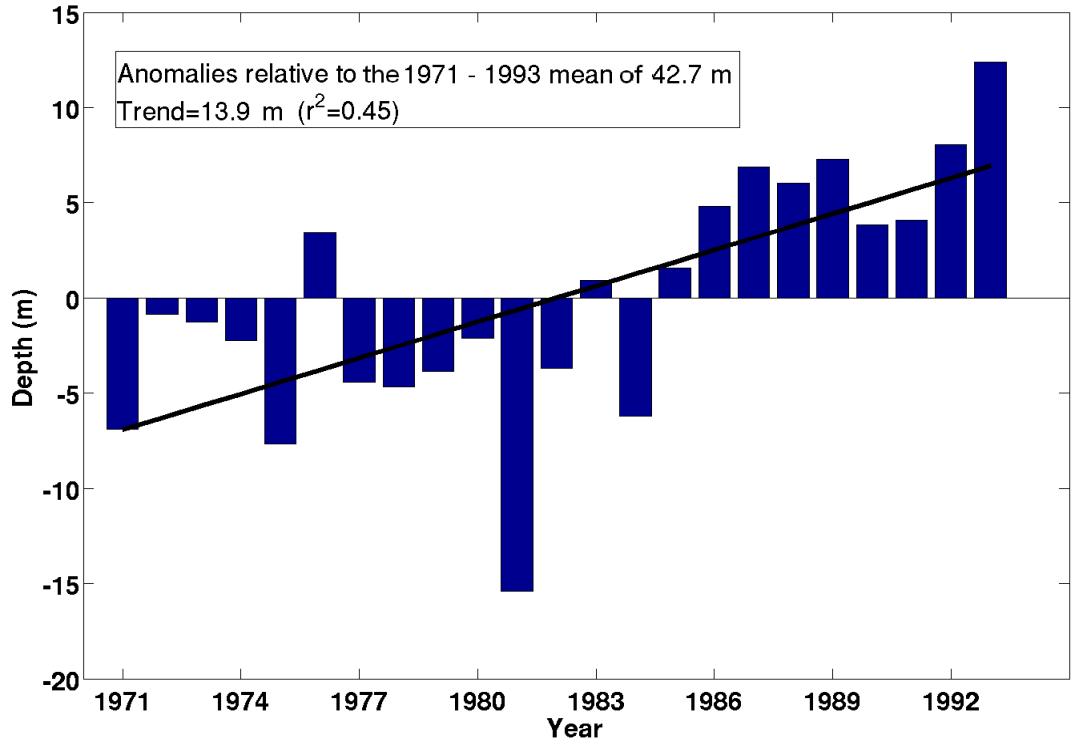


Figure 3.29 Basin averaged annual mean CIL thickness anomalies from the first model period (1971 – 1993) relative to the 1971 – 1993 mean. Black line shows shallowing trend of 13.9 m ($r^2$=0.45).

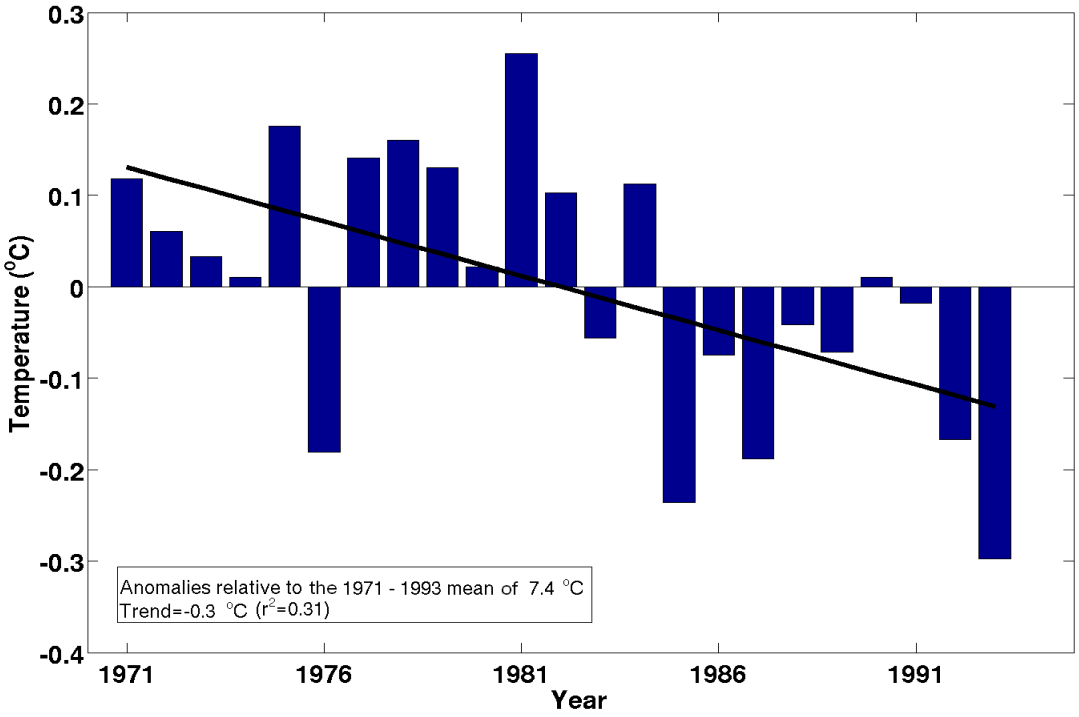


Figure 3.30 Basin averaged annual mean CIL mean temperature anomalies from the first model period (1971 – 1993) relative to the 1971 – 1993 mean. Black line shows cooling trend of 0.3 °C ($r^2$=0.31).

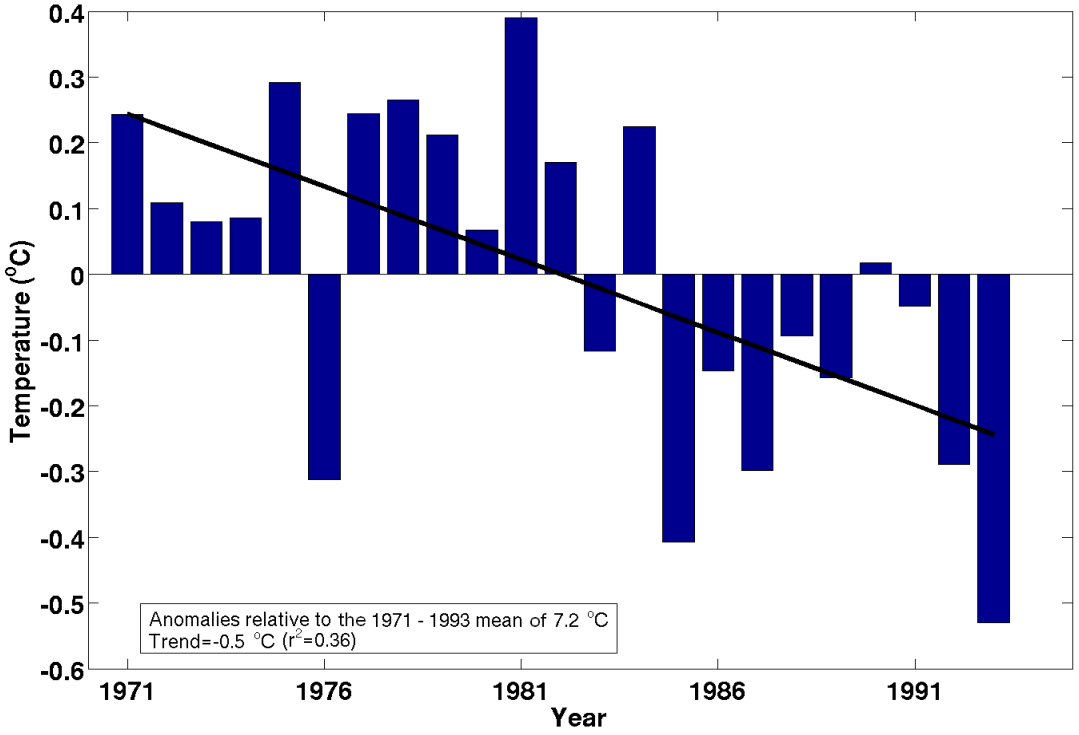


Figure 3.31 Basin averaged annual mean CIL core temperature anomalies from the first model period (1971 – 1993) relative to the 1971 – 1993 mean. Black line shows cooling trend of 0.5 °C ($r^2$=0.36).

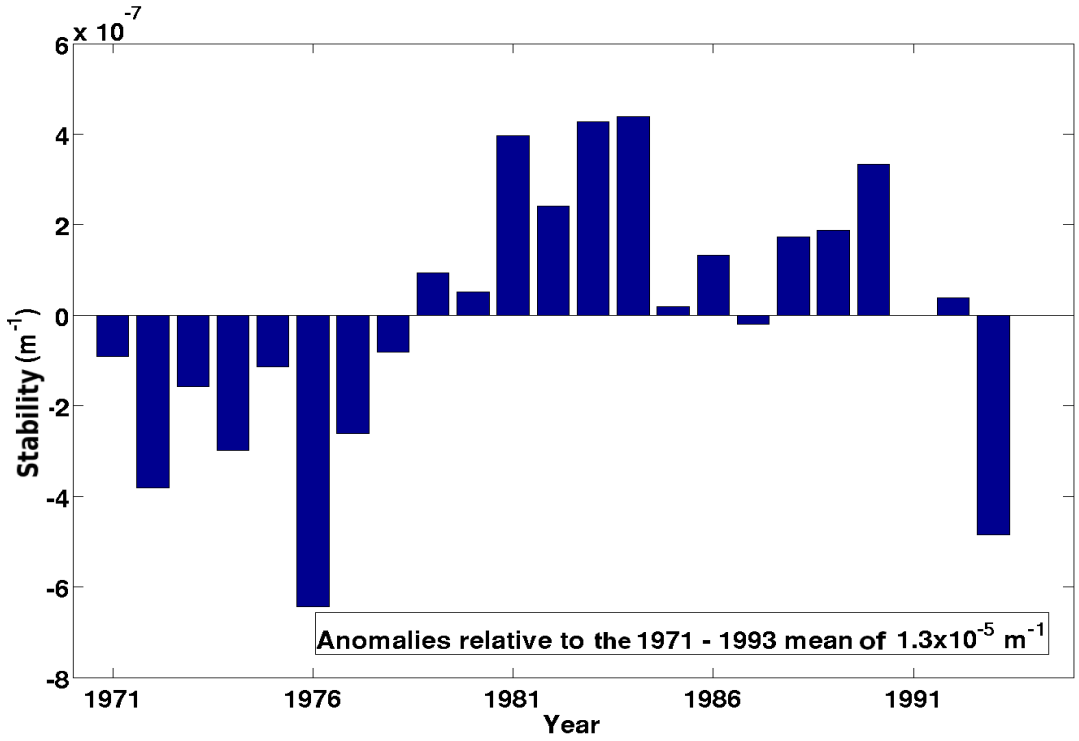


Figure 3.32 Basin averaged annual mean CIL stability (46 – 200 m) anomalies from the first model period (1971 – 1993) relative to the 1971 – 1993 mean.

### 3.2.4 Interannual variability in model forcing

To aid interpretation of interannual variability and trends in upper water column characteristics, interannual variability in surface fluxes are considered in the following section. Anomalies of annually averaged basin mean net heat flux (Figure 3.33) exhibit no statistically important trend between 1971 and 2001. However, there is a net influx of heat from the atmosphere to the ocean throughout this period, averaging 3.5 W $m^{-2}$. There are sustained periods of lower than average heat influx between 1975-1978 and 1982-1985, while there was a sustained period of higher than average heat influx between 1987 and 1993. Heat flux components are plotted alongside the net heat flux in Figure 3.34. The evaporative heat flux appears to contribute the largest component of interannual variability to the net heat flux. The positive mean heat flux throughout the simulation period results in an accumulation of heat within the water column, as illustrated in Figure 3.35. Between 1971 and

2001 there is a net heat accumulation of around 110 W $m^{-2}$. The most rapid heat accumulation occurs between 1985 and 1992 (Figure 3.35). Basin mean annual wind stress anomalies relative to the 1971 – 2001 mean of 2.8x$10^{-2}$ N $m^{-2}$ shows no significant trend although the frequency of lower wind stress years increases while the frequency of higher wind stress years decreases (Figure 3.36).

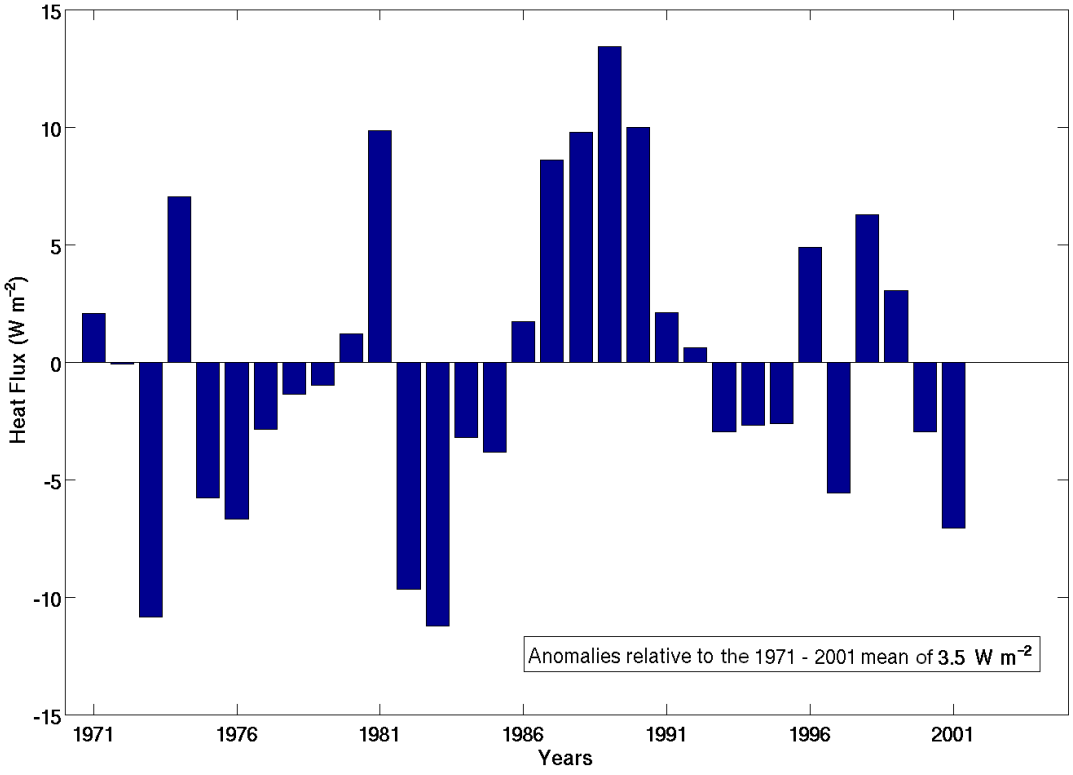


Figure 3.33 Basin averaged net heat flux anomaly relative to the 1971 – 2001 mean.

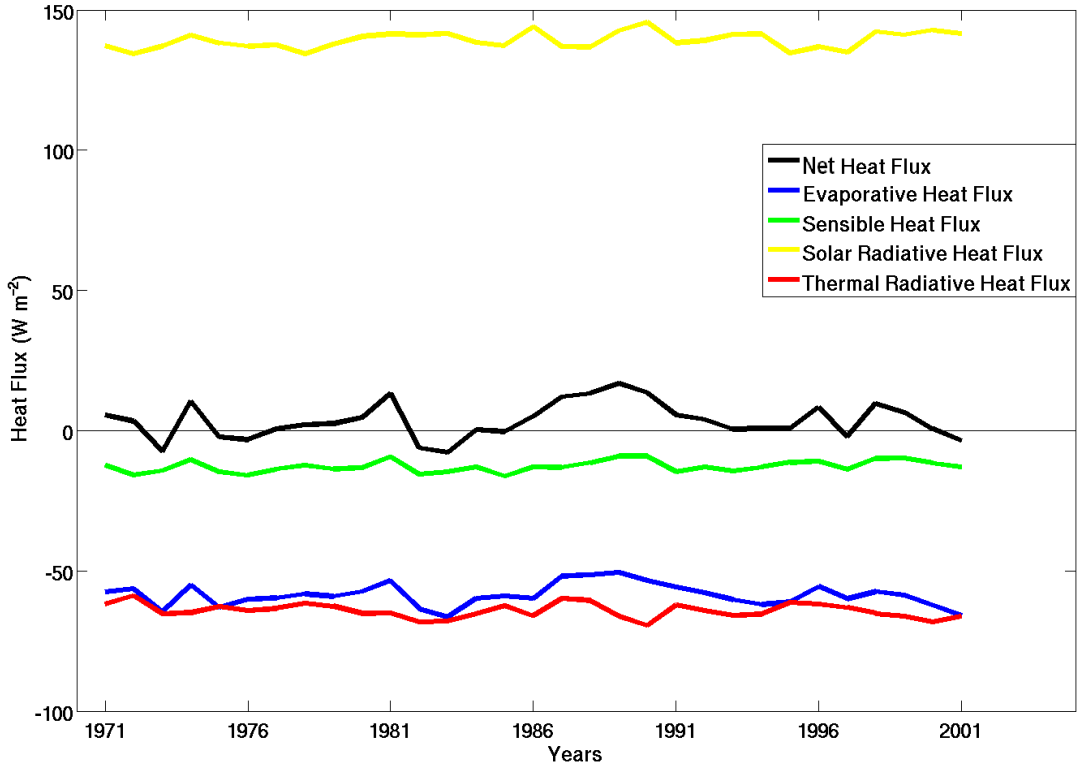


Figure 3.34 Annual mean net heat flux (black), evaporative heat flux (blue), sensible heat flux (green), solar radiative heat flux (yellow), thermal radiative heat flux (red).

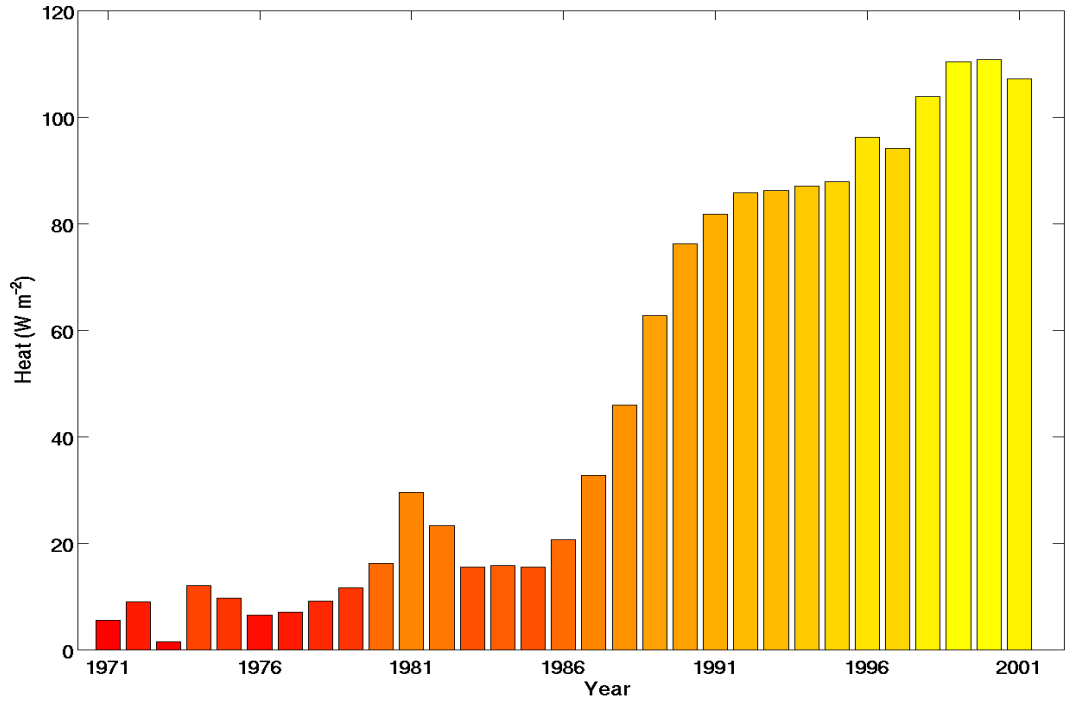


Figure 3.35 Annual heat accumulation of Black Sea.

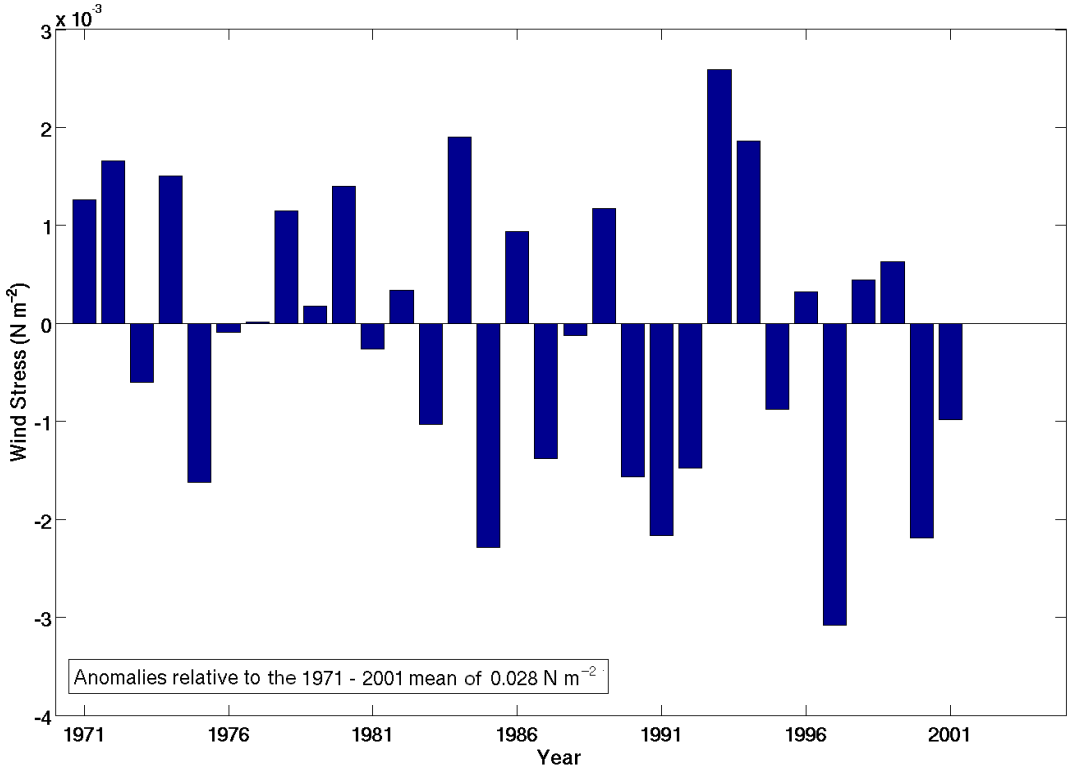


Figure 3.36 Basin averaged annual wind stress anomaly relative to the 1971 – 2001 mean.

### 3.2.5 Summary

Hovmöller plot showing how the stability of the upper 200 m of the water column changes throughout the two model simulations are presented in Figures 3.37 and 3.38. These plots represent the annual formation and breakdown of the seasonal thermocline, with a stability maximum appearing during the summer months between 5 m and 28 m depth (corresponding to a mean summer mixed layer depth of ~17 m). During winter, following erosion of the seasonal thermocline, the water column becomes mixed down to an average depth of ~46 m. The first model simulation exhibits a second relatively minor stability maximum between 52 m and 84 m depth, corresponding to the lower boundary of the CIL. This deeper stability maxima is present during all seasons but appears weakened during the early winter months. Mean CIL upper limit (~31 m) is present around the minimum between two maximums of stability during summer. Intra-annual oscillations below the second stability maximum do not seem to exhibit a seasonal signal. Basin averaged stability from the second model period shows the same seasonal patterns as the first model period between 5 m and 28 m depth, however, there is no distinct deeper stability maximum. Rather, the lower boundary of the CIL seems to overlap the base of the seasonal thermocline, spanning the depth range from 28 – 68 m. The second model simulation exhibits seasonality in water column stability down to depths of at least 68 m.

Between 1971 and 2001 the water column accumulated heat from the atmosphere, maximum SSTs increased and SSS decreased, resulting in a freshening of the surface mixed layer and an increase in the stability of the seasonal thermocline. The above mentioned trends are superimposed on a distinct multiannual variability which is reflected in each of the time series. The period between 1971 and 1981 was characterised by relatively warm and saline surface waters, while the period between 1982 and 1993 was relatively cool and fresh and the period between 1994 and 2001 was warm and fresh. Temperature and salinity conditions within the surface mixed layer influence the stability of the upper water column and the formation of CIL

waters during winter, and consequently the density distribution at the base of the CIL. In order to summarize conditions during the three periods defined above, Table 3.3 includes mean values of key parameters averaged over each of these time periods. Winter minimum SSTs do not exhibit the same warming trend as summer maximum SSTs but rather fluctuate between relatively warm conditions between 1971 and 1981, relatively cool conditions between 1982 and 1993 and warm conditions between 1994 and 2001. The cold intermediate layer appears to reflect the variability in winter SST – between 1971 and 1981 the CIL is relatively thin and warm compared to the period between 1982 and 1993 when the CIL is on average 8 m thicker and the core temperature is on average 0.3 °C cooler than during the earlier period. The NAO index exhibits relatively high positive values between 1982 and 1993 relative to the earlier and later periods, indicative of cool and dry winters during this period. Also, evaporation minus precipitation is higher and as there is less cloud cover, the atmosphere to ocean heat flux is larger during this period.

Mixed-layer depth, CIL upper and lower boundaries and permanent pycnocline depth are plotted together as annual running means in Figure 3.39. The shallowing trend in mixed layer depth is larger than interannual variations throughout both simulation periods (Figure 3.39). Interannual variations in CIL upper and lower boundaries are larger than any existing trend during first model period. As discussed previously, the water column structure produced by the second model simulation is not realistic below the depth of the seasonal mixed layer. Although data from the second model simulation was not used in this thesis to investigate the properties of the CIL, upper and lower boundaries of the CIL and permanent pycnocline (16.2 kg $m^{-3}$ density contour) depth are included in Figure 3.39 (dashed line) in order to demonstrate the existence of physically unrealistic trends in these properties, attributed to model drift. Shallowing of the 16.2 kg $m^{-3}$ density contour throughout the first model simulation may also be a feature of the model or may be related to the increase in the salinity of intermediate water masses, associated with the decrease in salinity of surface waters.

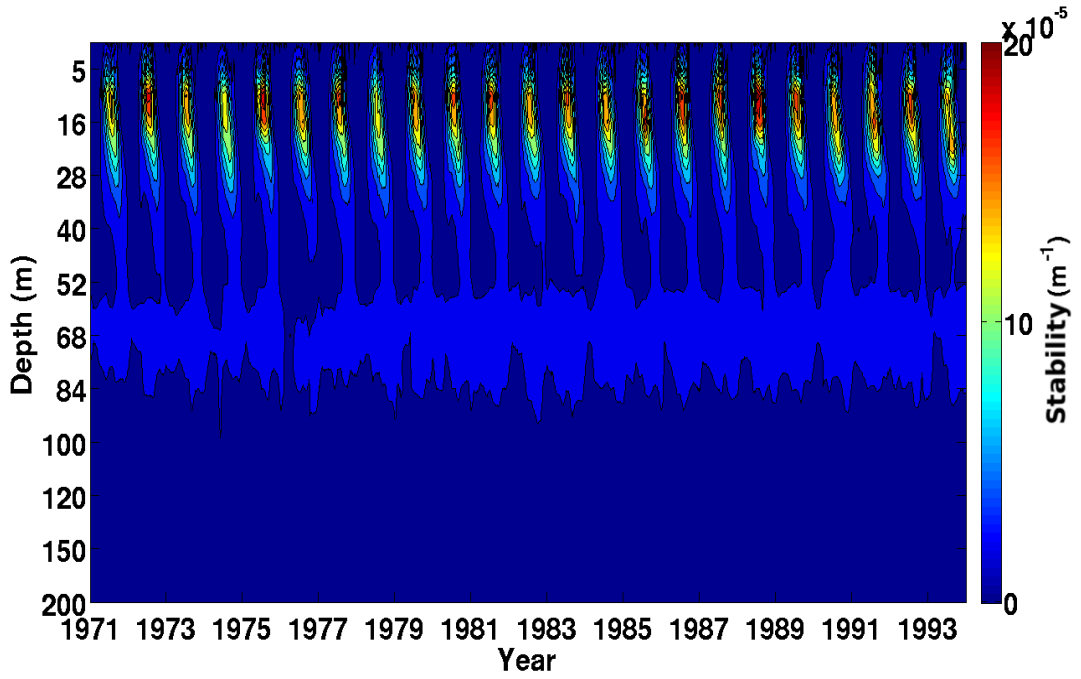


Figure 3.37 Basin mean stability (0 – 200 m) of first model period (1971 – 1993).

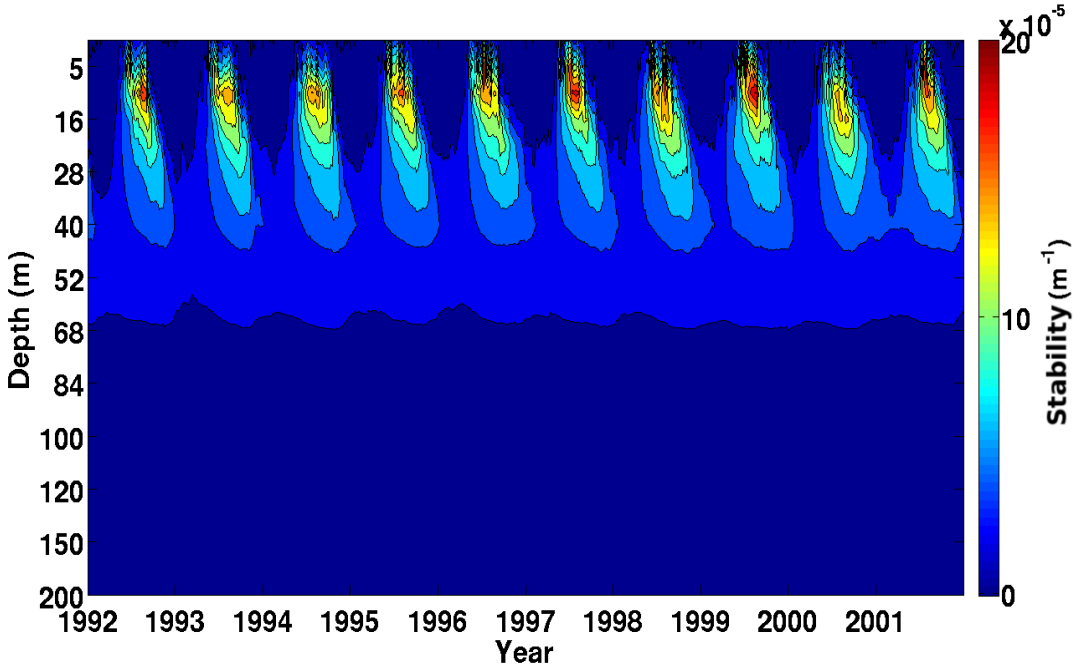


Figure 3.38 Basin mean stability (0 – 200 m) of second model period (1992 – 2001).

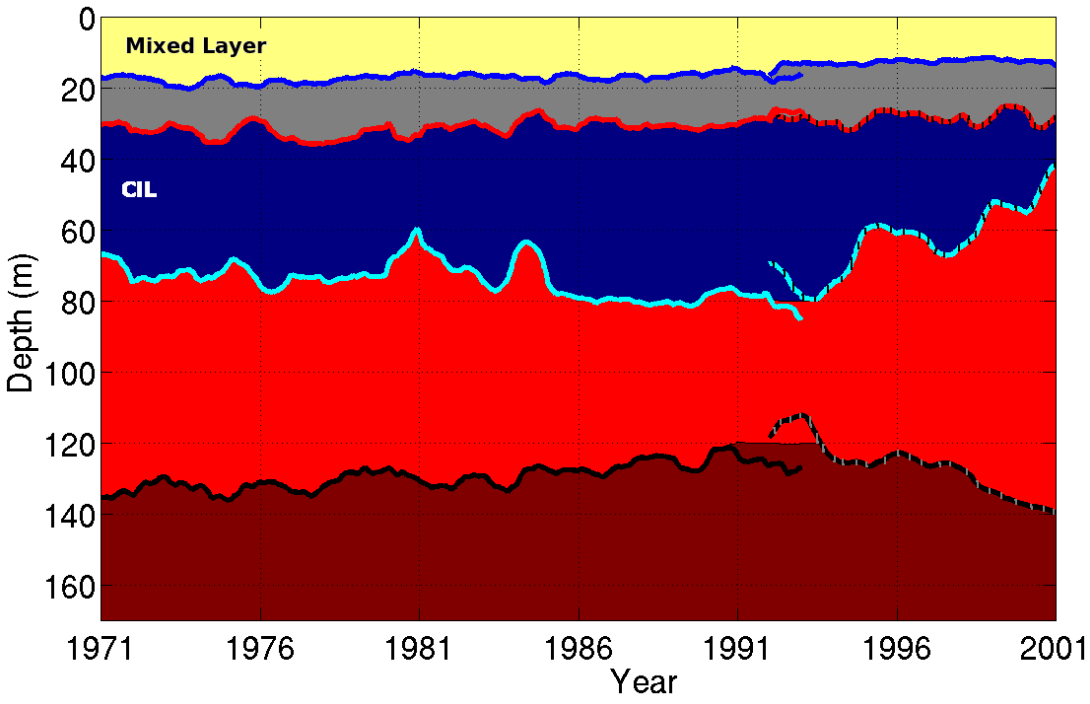


Figure 3. 39 Schematic representation of changes in the mixed layer and CIL from first (1971 – 1993) and second (1992 – 2001) model periods. From top to bottom, solid lines show annual running means of MLD for first and second model period, CIL upper and lower limits, and density level of 16.2 kg $m^{-3}$ for first model period, dashed lines show CIL upper and lower limits and density level of 16.2 kg $m^{-3}$ for second model period.

Table 3.3 Mean values of maximum and minimum SST, annual mean SSD, SSS and MLD, maximum MLD, CIL upper and lower boundary, CIL thickness, CIL core and mean temperature, bulk stability of 0 -46 m and 46 – 200 m layers, net heat flux, wind stress, the NAO and the EA/WR index for 1971 – 1981, 1982 – 1993 and 1994 – 2001.

| | 1971-1981 | 1982-1993 | 1994-2001 | Units |
|---|---|---|---|---|
| Annual SST | 14.55 | 14.37 | 15.17 | $^{o}C$ |
| Maximum SST | 23.80 | 23.96 | 25.01 | $^{o}C$ |
| Minimum SST | 7.08 | 6.68 | 7.34 | $^{o}C$ |
| Annual SSD | 12.87 | 12.80 | 12.50 | kg $m^{-3}$ |
| Annual SSS | 18.07 | 17.94 | 17.74 | - |
| Annual MLD | 17.58 | 16.54 | 12.61 | M |
| Maximum MLD | 47.93 | 45.08 | 32.90 | M |
| CIL Upper Limit | 32.20 | 29.86 | - | M |
| CIL Lower Limit | 70.69 | 76.37 | - | M |
| CIL Thickness | 38.49 | 46.51 | - | M |
| CIL Core Temp. | 7.36 | 7.07 | - | $^{o}C$ |
| CIL Temp. | 7.53 | 7.37 | - | $^{o}C$ |
| Stability (0-46) | $3.15 \times 10^{-5}$ | $3.28 \times 10^{-5}$ | $4.43 \times 10^{-5}$ | $m^{-1}$ |
| Stability (46-200) | $1.29 \times 10^{-5}$ | $1.31 \times 10^{-5}$ | - | $m^{-1}$ |
| Net Heat Flux | 2.68 | 4.73 | 2.62 | W $m^{-2}$ |
| Wind Stress | $2.84 \times 10^{-2}$ | $2.77 \times 10^{-2}$ | $2.75 \times 10^{-2}$ | N $m^{-2}$ |
| NAO | 0.02 | 0.29 | 0.08 | - |
| EA/WR | -0.03 | 0.05 | 0.04 | - |

# CHAPTER 4
# DISCUSSION

The two model reanalyses used in this thesis, when combined, provide a long (32 year) time series of 3-D data, which has been applied here to investigate long term changes in the water column structure of the Black Sea. Both models solve interannual variability and trends in mixed layer properties well (see section 3.1), allowing combination of the two time series to study the effects of climate variability and change on surface layer properties. The second model run, however, was not able to adequately resolve the physical structure of the water column below the surface mixed layer, exhibiting a deepening of the pycnocline and thinning of the CIL (see section 3.1). As the depth of the permanent pycnocline exhibits little variability in observations, the rapid deepening of the pycnocline during the 10 year simulation suggested the model was unstable. As there was no evidence of a similar model drift in the first simulation, which differed only in the data assimilation scheme, it is suggested that the methods used to assimilate altimetry data introduced a drift into the model.

The mechanism leading to the artificial thinning trend in CIL thickness during the second simulation may have been related to the declining density of surface waters. This hinders the formation of dense CIL water because relatively fresh surface waters will not necessarily sink to the depth of the CIL even if the water temperature falls below 8 °C. It is estimated that if the trend towards reduced CIL formation throughout the second simulation was projected forward in time, the CIL would disappear completely within a time scale of a few decades. Since the Black Sea is characterised by shallow mixed layer depths, a model with a higher vertical resolution in the upper layers of the water column may help with reducing the errors of the second model run in forming CIL waters.

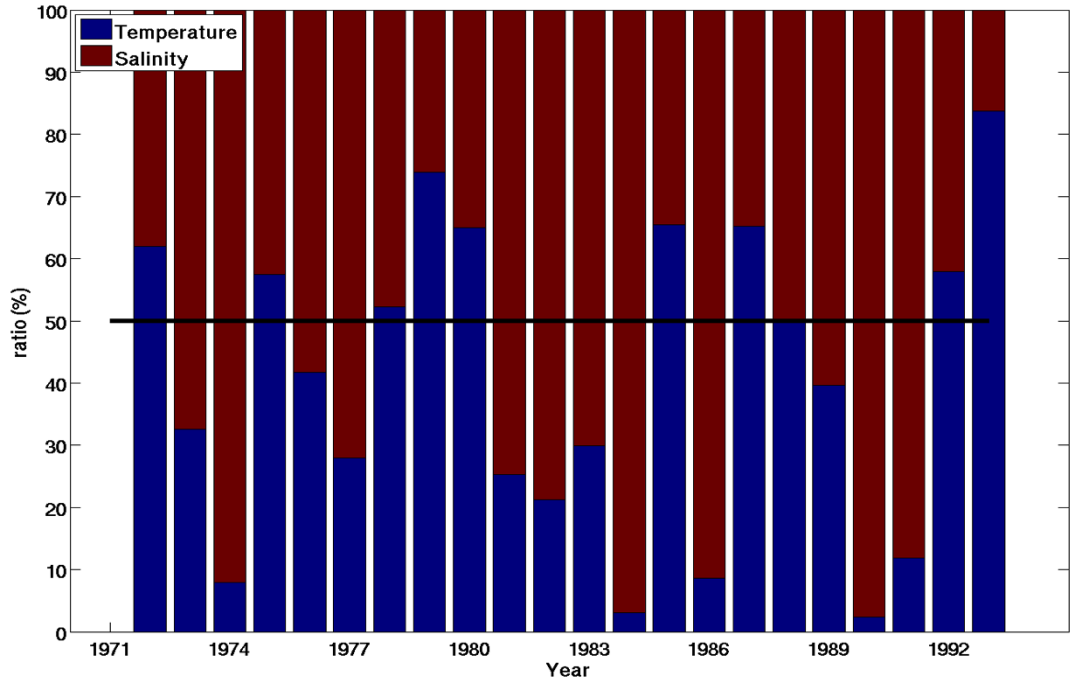


Figure 4.1 Ratio of contribution of surface salinity (red) versus surface temperature (blue) in driving interannual changes in surface density during the first model period.

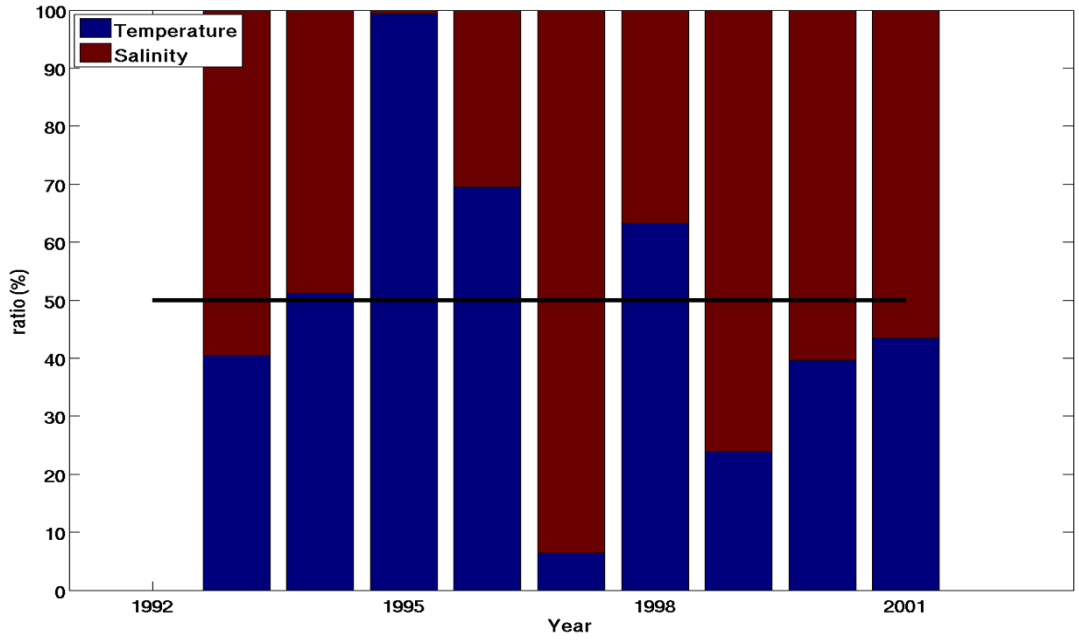


Figure 4.2 Ratio of contribution of surface salinity (red) versus surface temperature (blue) in driving interannual changes in surface density during the second model period.

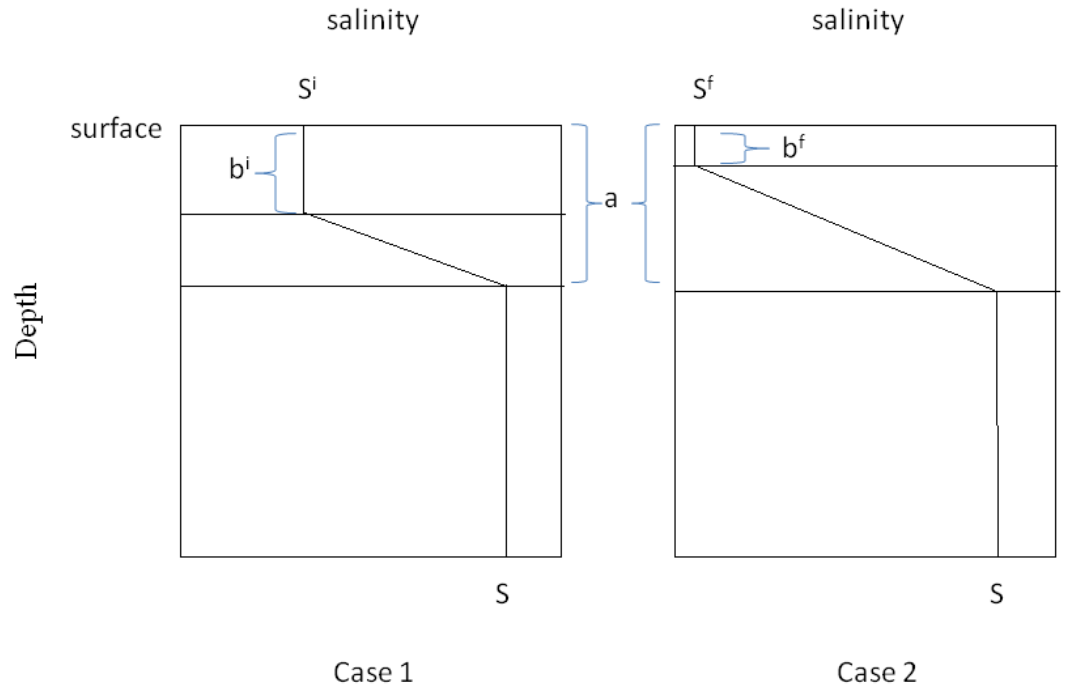


Figure 4.3 Schematic representation of mixed layer depth and surface salinity relationship where a indicates the depth below which salinity does not change, b represents the mixed layer depth, S is salinity and "i" and "f" indicate case 1 and case 2 conditions respectively.

Annual time series of surface salinity shows a higher correlation (0.85) to density than surface temperature (-0.47), suggesting that interannual changes in salinity play a greater role than temperature in modifying interannual variability in the density of the mixed layer. In order to investigate further, the relative contributions of temperature and salinity in modifying year to year changes in surface density were calculated. The first year of the study period, 1971, was taken as a reference case and interannual changes in surface density were then calculated for two different hypothetical cases; constant temperature (1971 annual mean) and varying annual mean salinities, and vice versa. When these two cases are compared it is seen that during most years salinity has more influence on interannual variations in surface density than temperature although both are clearly important (Figure 4.1 and 4.2). As surface salinity and surface density decrease throughout the study period, the mixed layer becomes shallower and the seasonal thermocline becomes increasingly stable. Surface salinity shows a significant correlation with MLD (0.76) and upper layer

stability (-0.73). The above discussion suggests that the freshening trend inn surface salinity is linked to the shallowing trend in MLD. A quantitative relationship between these two properties is proposed below following Figure 4.3. Assuming that the fresh water flux of the basin remains constant and acknowledging that salinity below the permanent pycnocline is believed to remain in steady state over centennial time scales (Ozsoy and Unluata, 1997), a balance is proposed between the salinity content of the mixed layer and the salinity content of the region between the base of the mixed layer and the permanent pycnocline:

$$b^iS^i + ½(a - b^i)(S - S^i) + (a - b^i)S^i = b^fS^f + ½(a - b^f)(S - S^f) + (a - b^f)S^f \qquad (4.1)$$

where a is the depth below which salinity does not change, b is mixed layer depth, S is salinity, i and f indicate case 1 and case 2 conditions respectively, and the total salt content is assumed to be constant. The first term on both sides of equation 4.1 represents the salinity content of the mixed layer and the second two terms on both sides of the equation represent the salinity content of the region between the mixed layer and the permanent pycnocline. This formula introduces a relationship between surface salinity and MLD that is a thinner mixed layer corresponds to a fresher surface layer. If S taken as zero, a simplified version of this formula becomes:

$$S^i(a - b^i) = S^f(a - b^f) \qquad (4.2)$$

This formula not only explains the relationship between MLD and surface salinity but also the relationship between MLD and salinity below the mixed layer. As can be seen in section 3.2.1, during this study salinity below 100 m increases while surface salinity decreases as the mixed layer gets shallower, supporting the theory above.

Even if surface temperatures remain constant, freshening of the surface layer increases the vertical density gradient meaning a larger kinetic energy input is required to mix the water column. If vertical mixing is inhibited, fresh water originating from river inflows remains trapped at the surface and deeper waters are

less diluted. Since the mixed layer depth determines the volume of water which interacts with the atmosphere directly, especially during summer when maximum temperatures are observed, shallower mixed layer depths may contribute to an increase in annual mean SST even if there is no change in the net heat flux this is because there is an increase in the heat flux per unit volume. Since stability increased at the bottom of the mixed layer throughout this study, a stronger mechanical energy input was needed in order to deepen the mixed layer. In other words, even if there was no change in wind stress, mixed layer depth may have continued to decrease because of the positive feedback between MLD, surface salinity, and water column stability.

Interannual variations in the depth of the upper boundary of the CIL exhibit a significant correlation with SST (0.64) and a high correlation with CIL core temperature changes (0.80). During colder winters a larger volume of CIL water is formed, the CIL thickens and its core temperature decreases. During 1975, surface salinity is much lower than during the preceding and following years, a trend which is also reflected in the surface density, mixed-layer depth and water column stability records. This variability is reflected a year later in the CIL upper limit and CIL core temperature time series, probably because winter temperature has a big influence on the CIL characteristics during the following year. CIL core temperature and sea surface salinity show a strong correlation (0.54). While sea surface salinity decreases, colder surface waters are required to sink the relatively fresh water to the density levels of the CIL. Although the CIL core temperature of first model run shows higher correlations with SST (0.88), when the second model run is added, the correlation decreases (0.51). According to data taken from Konovalov and Murray (2001), CIL core temperature continued to decrease between 1960 and 1995 while there were cold and warm periods of SST (Figure 1.14). Furthermore, it should be noted that winter conditions, which are more influenced by atmospheric variability than summer conditions, have most significance to CIL conditions.

Since changes in the depth of the lower boundary of the CIL are larger than changes in the depth of the upper boundary, CIL thickness is mostly determined by the CIL lower limit (correlation coefficient is 0.96). Because of the given surface salinity-MLD relationship, stability between 46 m and 200 m shows high negative correlation (-0.76) with surface salinity. According to equation 4.1, as surface salinity decreases, deeper salinities should increase until a depth where salinity shows no significant change (Figure 4.3).

The study period can be sub-divided into three periods with distinctly different characteristics (Table 3.3). Colder winter SSTs and thicker and colder CIL properties coincide with relatively high NAO and EA/WR periods. So these atmospheric variability patterns may be the dominant modes of interannual and multiannual variability in the Black Sea supporting Oğuz *et al.* (2006). However maximum SST, surface salinity and MLD are not correlated with these indices, exhibiting continuous trends throughout the study period. It has been demonstrated that the modelled increasing trend in SST reflects a net influx of heat to the Black Sea (defined according to the ERA40 reanalysis) which may be related to a global warming trend and assuming that ERA40 heat fluxes are adequate for the Black Sea region. Here, a relationship has been proposed between increasing SST, shallowing MLD, increased thermocline stability and SSS freshening. The response of the Black Sea to global climate change can be linked to the formation of seasonal thermocline and shallow mixed layers during summer, when maximum temperatures are observed. As summer temperatures increases year by year with the increased heat accumulation, the summer mixed layers gets increasingly shallower and more stable. Any trend associated with global warming in winter mean properties is masked by the larger interannual and multiannual variability associated with oscillations in atmospheric forcing. Atmospheric climate oscillations (NAO and the EA/WR) have a stronger signal during winter when the atmospheric circulation is stronger and influence the summer conditions of the Black Sea to a lesser extent. Because the surface mixed layer gets more stable over time, stronger winter convection and/or more kinetic energy input are required to break down the seasonal thermocline and deepen the

mixed-layer during winter. As the mixed layer gets shallower, surface waters gets fresher which further increases stability so a positive feedback mechanism is formed.

Effects of the NAO and the EA/WR on the winter (minimum) and annual surface temperatures in interannual and multiannual timescales is in line with previous studies (Gündüz and Özsoy, 2005; Oğuz *et.al*., 2006), showing that higher values of these indices corresponds with lower surface temperatures. However EOF analysis of surface salinity shows that surface salinity around Danube discharge increases while around the Kerch Strait it decreases relative to their mean values during cold periods. Unlike mean salinity of first 200 m (Oğuz *et.al.,* 2006), which reflects climate variability, freshening of surface waters may be a reflection of current climate change.

Increased surface temperatures and shallower mixed layer depths are accepted as climate change signals (Hardy, 2003). For this reason, the impact of global warming on MLD and water column stability is a focus of many current research projects and this thesis work contributes to increase the understanding of these processes. Furthermore, as this study suggests the existence of a multidecadal scale shallowing trend in the mixed-layer depth of the Black Sea, the Black Sea basin provides an ideal location to study the effects of shallowing mixed-layer depths on biogeochemical cycling and ecosystem functioning. Understanding the impacts of global warming on MLD and stability is important because vertical chemical and biological distributions are influenced by water column stability. In the Black Sea, the mixed layer depth and seasonal thermocline formation determine the amount of nutrient rich deep waters mixed with euphotic waters, while CIL formation and winter convection influence deep ventilation. Hence interannual changes in the stability and position of CIL affect sulphide production and oxidation at the base of the suboxic zone.

The Black Sea is characterized by shallow mixed layer depths and anoxic deep waters. Shallowing of the mixed layer, increased water column stability and

decreased oxygen pumping to deeper regions may cause anaerobic life forms to move to shallower depths (Dawson and Spannagle, 2008). Another possible effect of shallowing of the MLD and increased stratification may be a decrease of upward nutrient pumping (Dawson and Spannagle, 2008). However, with the help of increased stratification, river originated nutrients can be distributed horizontally better since sinking will probably take more time. Since the Black Sea has its own unique biochemical structure, more and careful modelling studies and experiments are needed to understand climate implications for biochemical cycling and ecosystem functioning in more detail.

It should be considered that, using annual and basin mean properties are not appropriate to understand changes in spatial distribution and seasonal cycles. This thesis work can be improved by investigating more spatial patterns and seasonal cycles. Surface and sub surface currents, sea surface height, heat content of the mixed layer and the CIL should also be analyzed in order to have a more complete picture of the Black Sea.

# CHAPTER 5

# CONCLUSION

This thesis provides an analysis of interannual and multiannual variability of physical water column characteristics of the Black Sea for the period 1971 – 2001 with the use of a three dimensional hydrodynamical model. This study helps to understand atmosphere-ocean (Black Sea) relationships in the interannual to multiannual time scales and also analyses the impact of global climate change on the Black Sea by focusing on the observed trends in surface salinity and mixed layer depths. This work provides new ideas on the relationship between surface layer properties of the Black Sea (e.g. surface salinity and MLD relationship).

Model results analysed in this thesis well reproduce observed surface and mixed layer properties. First model period (1971 – 1993) CIL results are better than the second model period (1992 – 2001) results. Results of both model periods are validated using CTD data from the Black Sea data base, AVHRR SST and HadSST2 SST data. Qualitative validation of model outputs is also carried out for surface currents and vertical profiles. These studies show that SST trends and variations in the model outputs are supported by the observations. However, the second model period reflects possible artificial trends for CIL properties. Although there is an artificial thinning trend in CIL thickness for the second model period, results point out a possible negative effect of freshening of surface waters together with shallowing of mixed layer, on CIL formation.

The most prominent results of this work is that increasing maximum (summer) surface temperatures (1.7 $^{o}$C) and freshening trend of surface waters (-0.4) with shallowing trend of mixed layer (-6.3 m) as a possible consequence of global climate change between 1971 and 2001. As a result of increased surface temperatures and fresher surface waters, surface density also decreased (-0.5 kg m$^{-3}$) while increasing

the density difference between upper and lower layers so that stability of water column increased ($8.9\ 10^{-6}\ m^{-1}$).

Another prominent outcome of this study is a possible relationship between mixed layer depth and surface salinity. As the annual mean mixed layer depth of the Black Sea became shallower, surface waters became less saline throughout the study period, which increased the stability of the upper water column. As a result, fresher surface waters originating from river runoff remain trapped at the surface, further increasing the stability of the water column and reducing the rate at which deeper waters are diluted. According to the results of this work, the freshening trend of surface waters may also be a reason for the cooling trend of CIL waters and increased CIL stability. Although there is no observed trend in the net heat flux, as the annual mean heat flux is positive, accumulation of heat throughout the study period may be a reason for the observed warming trend.

In conclusion this study provided a better understanding of the physical characteristics relationships of vertical physical properties of the Black Sea as well as their relations with atmospheric forcing and climate change over interannual and multiannual time scales. However, understanding the implications of these results on the chemical and biological structure of the Black Sea requires further research.

## REFERENCES


Barnston, A.G. and Livezey, R.E., 1987. Classification, seasonality, and persistence of low-frequency atmosphere circulation patterns. Monthly Weather Review 115, pp. 1083–1123.

Belokopytov, V., 1998. On Hydrometeorological Conditions of Cold Intermediate Water Renewal in Northern Part of the Black Sea. In: L. Ivanov, T. Oguz (eds.) Ecosystem Modelling as a Management Tool for the Black Sea, Kluwer Academic Publishes, Dordrecht, Vol.2, 47 - 52.

Blumberg, A. F. and G. L. Mellor, A description of a three-dimensional coastal ocean circulation model, Three-Dimensional Coastal ocean Models, edited by N. Heaps, 208 pp., American Geophysical Union, 1987.

Buesseler, K. O., Livingston, H. D., & Casso, S. A. 1991. Mixing between oxic and anoxic waters of the Black Sea as traced by Chernobyl cesium isotopes. Deep-Sea Research I, 38, S725ÐS745

Cannaby,H.2005 The Physical Limnology of Lough Corrib. Phd Thesis. National University of Ireland.

Casper,J.K.2010.Changing Ecosystems: Effects of Global Warming. Facts On File, Inc. An imprint of Infobase Publishing 132 West 31st Street New York NY 10001.pp:169-197.

Chen C.A. and Millero F.J.1986. Precise thermodynamic properties for natural waters covering only the limnological range. Limnology and Oceanography, 31, pp.657-662

Codispoti, L.A., G.E. Friederich, J.W. Murray, and C.M. Sakamoto, 1991. Chemical variability in the Black Sea: implications of continuous vertical profiles that penetrated the oxic/anoxic interface. Deep-Sea Res. I, 38, Suppl.2, S691-S710.

Dawson.B.,Spannagle.M.2009.The Complete Guide to Climate Change. Routledge 2 Park Square, Milton Park, Oxon OX14 4RN.pp:190-193,258-263,292,293.

Demyshev, S.G., 1992. A numerical experiment on computations of the Black Sea density fields and current velocities during summer. Sov. J. Phys. Oceanogr. 3, 293-298.

Dzhioev, T.K., Sarkisyan, A.S., 1976. Numerical computations of the Black Sea currents. Izv. Atmos., Oceanic Phys. 6,217-223.

Eremeev, V.N., Ivanov, L.M., Kochergin, S.V., Mel'nichenko, O.V., 1992. Analysis of observations and methods of calculating oceanic hydrophysical fields. Sov. J. Phys. Oceanogr. 3, 193-209.

Flippov, D.M., 1965. The Cold Intermediate Layer in the Black Sea. Oceanology 5, 47-52.

Fotonoff N.P. and Millard Jr. R.C. 1983. Alghoritms for computation of fundemental properties of sea water. Division of Marine Sciences UNESCO, Paris, France.

Goosse H., P.Y. Barriat, W. Lefebvre, M.F. Loutre, and V. Zunz (2009). Introduction to climate dynamics and climate modeling. Online textbook available at http://www.climate.be/textbook. pp:114,115.

Gücü, A.C., 2002. Can overfishing be responsible for the successful development of Mnemiopsis? Estuarine, Coastal and Shelf Science, 54, 439–451.

Gündüz M, Özsoy E. 2005. Effects of the North Sea Caspian pattern on surface fluxes of Euro-Asian-Mediterranean seas. *Geophysical Research Letters* **32**: 1–4.

Hannachi.A.2004.A Primer for EOF Analysis of Climate Data. From http://www.met.rdg.ac.uk/:_han/ Monitor/eofprimer.pdf

Hardy.J.T.2003. Climate Change: Causes, Effects, and Solutions. John Wiley & Sons Ltd, The Atrium, Southern Gate, Chichester,West Sussex PO19 8SQ, England pp:131-148.

Henderson-Sellers, B. (1984), Development and application of U.S.E.D.: a hydroclimate lake stratification model, Ecological Modelling, 21(4), 233-246

Humborg, C., V. Ittekkot, A. Cociasu, and B. Bodungen, 1997. Effect of Danube River dam on Black Sea biogeochemistry and ecosystem structure. Nature, 386, 385–388.

Hurrell.J.W., Deser.C.2009. North Atlantic climate variability: The role of the North Atlantic Oscillation. In: Journal of Marine Systems Volume 79, Issues 3-4, 10 February 2010, Pages 231-244

Imberger,J and G. Parker (1985) Mixed layer Dynamics in a lake exposed to a spatially variable wind field. Limnology and oceanography, 30, 473-478.

Ivanov, L., Besiktepe, S., Ozsoy, E., 1997. Physical oceanographic variability in the Black Sea pycnocline. In: Ozsoy, E., Mikaelyan, A. (Eds.), Sensitivity to Change: Black Sea, Baltic Sea and North Sea. NATO ASI Series 2, Environment 27. Kluwer, Dordrecht, pp. 265-274.

Ivanov.L.,Konovalov.S.,Melnikov.V.,Mikaelyan.A.,Yunev.O.,Basturk.O.,Belokopitov.V.,Besiktepe.S.,Bodeanu.N.,Bologa.A.,Cociasu,.A.,Diakonu.V.,Kamburska.L.,Kid

eys.A.,Mankovsky.V.,Moncheva.S.,Nezlin.N.,Niermann.U.,Petranu.A.,Shalovenkov.N.,Shuskina.E.,Salihoglu.I.,Senichkina.L.,Uysal.Z.,Vedernikov.V.,Yakubenko.V.,Yakushev.E., Yilmaz. A.1998a. Physical, chemical and biological data sets of the TU Black Sea data base: description and evaluation. In: L.I. Ivanov and T. Oguz, Editors, Ecosystem Modelling as a Management Tool for the Black SeaNATO ASI Series vol. 1, Kluwer, Dordrecht (1998), pp. 11–38.

Ivanov.L.I.,Konovalov.S.K.,Belokopytov.V.,Ozsoy.E.,1998b.Regional peculiarities of physical and chemical responses to changes in external conditions within the Black Sea pycnocline: cooling phase. In: L. Ivanov and T. O uz, Editors, NATO TU-Black Sea Project: Ecosystem Modelling as a Management Tool for the Black Sea, Symposium on Scientific ResultsNATO ASI Ser. vol. 2, Kluwer Academic Publishers, Dordrecht (1998), pp. 53–68.

Kideys, E.A., and Z.A. Romanova, 2001. Distribution of gelatinous macrozooplankton in the southern Black Sea during 1996–1999, Mar. Biol., 139, 535–547.

Klimok, V.I., Makeshov, K.K., 1993. Numerical modeling of the seasonal variability of hydrophysical fields in the Black Sea. Sov. J. Phys. Oceanogr. 4. 27-33.

Konovalov.S.K., Murray.J.W.2001.Variations in the chemistry of the Black Sea on a time scale of decades (1960–1995). J Mar Syst 31:217–243.

Kovalev, A.V., U., Neirman, V.V., Melnikov, V., Belokopytov, Z., Uysal, A.E., Kideys, M., Unsal, and D., Altukov, 1998. Long term changes in the Black Sea zooplankton: the role of natural and anthropogenic factors. In: Ecosystem Modeling as a Management Tool for the Black Sea. L. Ivanov and T. Oguz, eds. NATO ASI Series 2, Environment-Vol.47, Kluwer Academic Publishers, Vol. 1, pp. 221– 234.

Latif, M.A., O&z, T., Sur, H.j., Besiktepe, S., Ozsoy, E., Unluata, U., 1990. Oceanography of the Turkish Straits - 3rd Annual Report, Vol. I. Physical Oceanography of the Turkish Straits. Inst. Mar. Sci., METU, Erdemli, Icel.

Letcher.T.M.2009. Climate Change Observed Effects on Planet Earth. Elsevier Radarweg 29, PO Box 211, 1000 AE Amsterdam, The Netherlands Linacre House, Jordan Hill, Oxford OX2 8DP, UK pp:103-123,233-279.

Lorenz, E. N., 1956: Empirical orthogonal functions and statistical weather prediction. Statistical Forecasting Scientific Rep. 1, Department of Meteorology, Massachusetts Institute of Technology, Cambridge, MA, 57 pp

Marchuk G.I., Kordzadze, A.A., Skiba, Y.N., 1975. Calculation of the basic hydrological fields in the Black Sea. Atmos., Ocean Phys. 11 (4), 379-393.

Mikaelyan, A. S., 1997. Long-term variability of phytoplankton communities in open Black Sea in relation to environmental changes. In: Sensitivity to change: Black Sea,

Baltic Sea and North Sea, NATO Sci. Partnership Sub-series 2, vol. 27, E. Ozsoy and A. Mikaelyan, eds., Kluwer Acad., Norwell, Mass., pp. 105–116.

Moncheva, S., A., Krastev, 1997. Some aspects of phytoplankton long-term alterations off Bulgarian Black Sea Shelf. In: Sensitivity to Change: Black Sea, Baltic Sea and North Sea, E. Ozsoy, A. Mikaelyan, eds. NATO ASI Series, Vol. 27. Kluwer Academic Publishers, Dordrecht, pp. 79–94.

Montegut B.C. Madec G. Fischer A.S. Lazar A. Iudicone D. 2004. Mixed layer depth over the global ocean: An examination of profile data and a profile-based climatology. Journal of Geophysical Research, vol. 109. Paris, France.

Moskalenko, L.V., 1976. Calculation of stationary wind-driven currents in the Black Sea. Oceanology 15, 168-171.

Murray, J. W., Z. Top, and E. Ozsoy, 1991. Hydrographic properties and ventilation of the Black Sea.Deep-Sea Res., 38, Suppl.2A, p.p.663–690.

Neumann, G., 1942. Die Absolute Topografie des Physikalischen Meeresniveaus und die Oberflachen-Stromungen des Schwarzen Meeres. Ann. Hydrogr. Berlin 70, 265-282.

Oguz, T., Latun, VS., Latif, M.A., Vladimirov, V.V., Sur, H.I., Markov, A.A., Ozsoy, E., Kotovshchikov, B.B., Eremeev, V.V., Unluata, U., 1993. Circulation in the surface and intermediate layers of the Black Sea. Deep-Sea Research I 40, 1597-1612.

Oguz, T., Aubrey, D.G., Latun, V.S., Demirov, E., Koveshnikov L., Sur, H.I., Diaconu, V., Besiktepe, S., Duman, M., Limeburner, R., Eremeev, V., 1994. Mesoscale circulation and thermohaline structure of the Black Sea observed during Hydroblack ‘91. Deep-Sea Research I. 41, 603-628.

Oguz T. and Tugrul S. 1998. A look at the general oceanography of the Turkish Seas In: Gorur N. (Ed) Geology of Turkish Seas and surroundings. Istanbul. p.p.1-21

Oguz, T., S., Besiktepe, 1999. Observations on the Rim Current structure, CIW formation and transport in the western Black Sea. Deep-Sea Research.I, 46, 1733.1753.

Oguz, T., J. W. Murray, and A. E. Callahan, 2001. Modeling redox cycling across the suboxic-anoxic interface zone in the Black Sea. Deep-Sea Research I., 48, 761–787.

Oğuz, T., T. Cokacar, P. Malanotte-Rizzoli, and H. W. Ducklow, 2003. Climatic warming and accopanying changes in the ecological regime of the Black Sea during 1990s. Global Biogeochem. Cycles, 17(3), 1088, doi: 10.1029/2003.

Oğuz,T., Tuğrul,S.,Kıdeys,A.E.,Ediger,V.,Kubilay,N.2004. Physical and Biological Characteristics of the Black Sea. In: Robinson, A.R., Brink, K. (Eds.), The Sea. Vol. 14. pp. 1331–1369 (Chapter 33).

Oguz T. Tugrul S. Kideys A.E. Ediger V. Kubilay N. 2005 Physical and biogeochemical characteristics of the Black Sea. The Sea, Vol. 14, Chapter 33, 1331-1369.

Oguz, T. 2005. Black Sea ecosystem response to climatic variations. Oceanography, 18(2), 122-133.

Oğuz,T., Gilbert,D.2006. Abrupt transitions of the top-down controlled Black Sea pelagic ecosystem during 1960-2000: Evidence for regime-shifts under strong fishery exploitation and nutrient enrichment modulated by climate-induced variations. In: Deep Sea Research Part I: Oceanographic Research Papers Volume 54, Issue 2, February 2007, Pages 220-242

Oğuz.T., Dippner.J.W.,Kaymaz.Z.,2006. Climatic regulation of the Black Sea hydro-meteorological and ecological properties at interannual-to-decadal time scales.In: Deep Sea Research Part II: Topical Studies in Oceanography Volume 53, Issues 17-19, August-September 2006, Pages 1923-1933

Ottersen.G.,Planque.B.,Belgrano.A.,Post.E.,Reid.P.C.,StensethN.C.2001. Ecological effects of the North Atlantic Oscillation. In: OECOLOGIA Volume 128, Number 1, 1-14,

Ovchinnikov, I.M., Popov, Yu.I., 1987. Evolution of the Cold Intermediate Layer in the Black Sea. Oceanology 27, 555-560.

Ozsoy, E., Oguz, T., Latif, M.A., Unluata, U., 1986. Oceanography of the Turkish Straits - 1st Annual Report, Vol. I, Physical Oceanography of the Turkish Straits. Inst. Mar. Sci., METU, Erdemli, Icel,p. 223

Ozsoy, E., Oguz, T., Latif, M.A., Unluata, U., Sur, HI., Besiktepe. S., 1988. Oceanography of the Turkish Straits - 2nd Annual Report, Vol. I. Physical Oceanography of the Turkish Straits. Inst. Mar. Sci., METU, Erdemli, Icel.

Ozsoy, E. and U. Unluata, 1997. Oceanography of the Black Sea: a review of some recent results. Earth Sci.Rev., 42, 231–272.

Ozsoy.E.1999. Sensitivity to global change in temperate Euro-Asian Seas (The Mediterranean, Black Sea and Caspian Sea): a review. In: P. Malanotte-Rizzoli and V. Eremeev, Editors, The Eastern Mediterranean as a Laboratory Basin for the Assessment of Contrasting Ecosystems, NATO Sci. Partnership Sub-ser., 2 vol. 51, Kluwer Academic Publishers (1999), pp. 281–300.

Philander.S.G.2008. Encyclopedia of Global Warming and Climate Change. SAGE Publications, Inc. 2455 Teller Road Thousand Oaks, California 91320.pp:456-460,619,620.

Porumb F., 1989. The influence of eutrophication on zooplankton communities in the Black Sea waters. Certerari Marine, 22, 233.246.

Rachev, N.H., E.V. Stanev, 1997. Eddy processes in semi-enclosed seas. A case study for the Black Sea. J. Phys. Oceanogr., 27, 1581–1601.

Rass, T.S., 1992. Changes in the fish resources of the Black Sea. Oceanology (Eng. Trans.), 32, 197–153.

Rayner N.A. Brohan P. Parker D.E. Folland C.K. Kennedy J.J. Vanicek M. Ansell T. and Tett S.F.B.2005. Improved analyses of changes and uncertainties in sea surface temperature measured in situ since the mid-nineteenth century: the HadSST2 data set. Hadley Centre for Climate Prediction and Research, U.K.

Reva.Yu.A.1997.Interannual oscillations of the Black Sea level. Oceanology (Eng. Transl.) 37, 193–200.

Rimbu.N.,Dima.M.,Lohmann.G.,Stefan.S..2004. Impacts of the North Atlantic oscillation and the El Nino-southern oscillation on Danube river flow variability, Geophs. Res. Lett. 31 (2004), p. L23203.

Robert H.S.2009,Introduction to Physical Oceanography, Open Source Textbook. Chapter 8 - Equations of Motion With Viscosity. Department of Oceanography, Texas A&M University, taken from http://oceanworld.tamu.edu/resources/ocng_textbook/chapter08/chapter08_04.htm updated on February 4

Ross D.A. and E.T. Degens, 1974. Recent sediments of the Black Sea. In: The Black Sea-Geology, Chemistry, and Biology, Degens.E.T and Ross.D.A, eds, American Association of Petroleum Geologists Memoir Vol.20, Tulsa, Oklahoma, U.S.A., pp. 183–199.

Sahney, S., and Benton, M. J., 2008, Recovery from the most profound mass extinction of all time: Proceedings of the Royal Society of London B, 275. 759-765.

Shaffer, G., 1986: Phosphate pumpsand shuttles in the Black Sea. Nature, 321, 515–517.

Shaviv, N.J., and Veizer, J., 2003, Celestial driver of Phanerozoic climate?: GSA Today, v. 13, no. 7, p. 4–10

Shiganova, T.A., 1998: Invasion of the Black Sea by the ctenophore Mnemiopsis leidyi and recent changes in pelagic community structure, Fish. Oceanogr., 7, 305–310.

Shushkina, E.A., M.E. Vinogradov, L.P. Lebedeva, T. Oguz, N.P. Nezlin, V. Yu. Dyakonov, and L.L. Anokhina, 1998: Studies of structural parameters of planktonic communities of the open part of the Black Sea relevant to ecosystem modeling. In: Ecosystem Modeling as a Management Tool for the Black Sea, vol. 1, NATO Sci. Partnership Sub-ser., 2, vol. 47, L.I. Ivanov, and T. Oguz, eds. Kluwer Acad., Norwell, Mass., pp. 311–326.

Solomon, S., D. Qin, M. Manning, Z. Chen, M. Marquis, K.B. Averyt, M. Tignor and H.L. Miller (eds.) Cambridge University Press, Cambridge, United Kingdom and New York, NY, USA.

Stanev, E.V., Trukhchev, D.I., Roussenov, V.M., 1988. The Black Sea Circulation and Numerical Modeling of the Black Sea Currents. Sofia University Press, Sofia, 222 pp. (in Russian).

Stanev, E.V., 1990. On the mechanisms of the Black Sea circulation. Earth-Sci. Rev. 28, 285-319.

Stanev.E.V.,Peneva.E.L.2002.Regional sea level response to global climatic change: Black Sea examples. In Global and Planetary Change Volume 32, Issue 1, December 2001, Pages 33-47

Stenseth.N.C.,Ottersen.G.,Hurrell.J.W.,Belgrano.A.2005.Marine Ecosystems and Climate Variation. Published in the United States by Oxford University Press Inc..New York.

Suga, T., K. Motoki, Y. Aoki, and A. M. Macdonald (2004), The North Pacific climatology of winter mixed layer and mode waters, J. Phys. Oceanogr., 34, 3 – 22.

Sur H.I., 2004. On the physical oceanography of the Black Sea. In:Celikkale M.S.(Ed.),Workshop: A Glance to the Black Sea, Istanbul, Turkiye, p.18

Taylor, K.E.: Summarizing multiple aspects of model performance in a single diagram. J. Geophys. Res., 106, 7183-7192, 2001

Tolmazin, D., 1985. Changing coastal oceanography of the Black Sea, I. Northwestern Shelf. Prog. Oceanogr. 15, 217-276.

Trukhchev, D.I., Demin, Y.L., 1992. The Black Sea general circulation and climatic temperature and salinity fields. CoMS-Black 92-010 Tech. Rep. WHOI-92-34.

Tsimplis and Josey, 2001 M.N. Tsimplis and S.A. Josey, Forcing of the Mediterranean Sea by atmospheric oscillations over the North Atlantic, Geophys. Res. Lett. 28 (2001), pp. 803–806.

Tsimplis, M.N. and Rixen, M. 2003 Variability of Mediterranean and Black Sea sea level and its forcing. In,Yilmaz, A. (ed.) Oceanography of the Eastern Mediterranean and Black Sea: similarities and differences of two interconnected basins, Proceedings

of the 2nd International Conference on..., Ankara, Turkey, 14-18 October 2002. 2nd International Conference on Oceanography of the Eastern Mediterranean and Black Sea: similarities and differences of two interconnected basins Ankara, Turkey, Tubitak Publishers, 137-144

Tsimplis, et al, 2004 art. no. C08015 M.N. Tsimplis, S.A. Josey, M. Rixen and E.V. Stanev, On the forcing of sea level in the Black Sea, J. Geophys. Res. (Oceans) 109 (C8) (2004).

Tugrul.S.,Basturk.O.,Saydam.C.Yilmaz.A.,1992.Changes in the hydrochemistry of the Black Sea inferred from water density profiles. In: Nature 359, 137 - 139

Unllata, O., Oguz, T., Latif, M.A., Ozsoy, E., 1990. On the physical oceanography of the Turkish Straits. In: Pratt, L.J. (Ed.), The Physical Oceanography of Sea Straits. NATO/AS1 Series, Kluwer, Dordrecht, pp. 25-60.

Uysal, Z., A. E. Kideys, L. Senichkina, L. Georgieva, D. Altukhov, L. Kuzmenko, L. Manjos, and E. Eker, 1998. Phytoplankton patches formed along the southern Black Sea coast in spring and summer 1996. In: Ecosystem Modeling as a Management Tool for the Black Sea, L. I. Ivanov and T. Oguz, eds. vol 1, Kluwer Academic Publishers, Netherlands, pp. 151–162.

Ward.P.D.2007.Under a Green Sky: Global Warming, The Mass Extinctions of The Past, and What They Mean for Our Future.Harper Collins, NY 2007.

## APPENDIX A

## Calculation of thermal expantion coefficient (α)

Thermal expansion coefficient (α) is calculated following Chen and Millero (1986):

$$\alpha \times 10^6 = -68.00 + 18.2091 \times T - 0.30866 \times T^2 + 5.3445 \times 10^{-3} \times T^3$$
$$-6.0721 \times 10^{-5} \times T^4 + 3.1441 \times 10^{-7} \times T^5$$
$$+(4.599 - 0.1999 \times T + 2.790 \times 10^{-3} \times T^2) \times S \qquad \text{(app.A.1)}$$
$$+(0.3682 - 1.520 \times 10^{-2} \times T + 1.91 \times 10^{-4} \times T^2 - 4.613 \times 10^{-3} \times S) \times P$$

with a standard deviation of $\pm 0.3 \times 10^{-6}$ $^{o}$C where T is temperature of water, S is salinity and P is pressure.

## APPENDIX B

## Time series difference of modelled and observed data

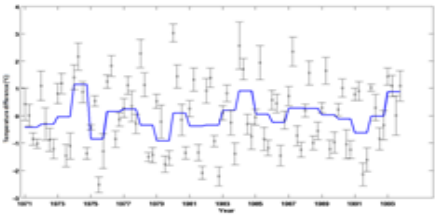

(a) Temperature difference
(1971 - 1993)

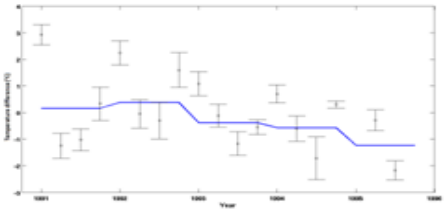

(b) Temperature difference
(1992 - 1996)

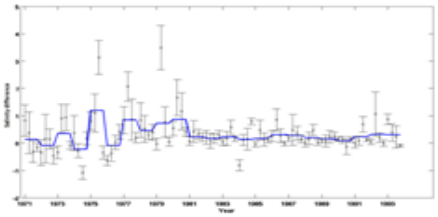

(c) Salinity difference
(1971 - 1993)

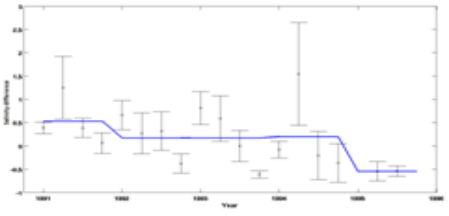

(d) Salinity difference
(1992 - 1996)

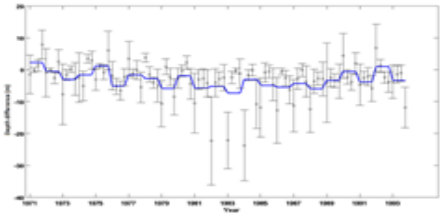

(e) MLD difference
(1971 - 1993)

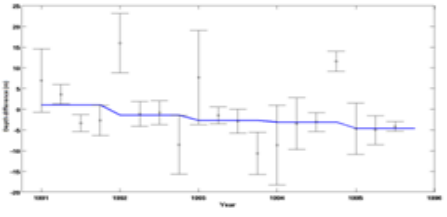

(f) MLD difference
(1992 - 1996)

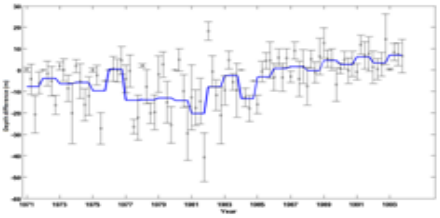

(g) CIL upper boundary difference
(1971 - 1993)

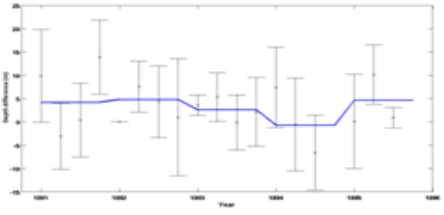

(h) CIL upper boundary difference
(1992 - 1996)

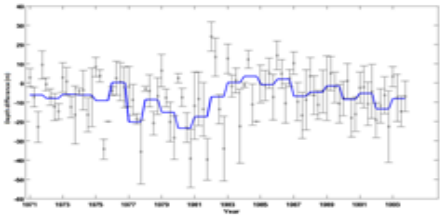

(i) CIL lower boundary difference
(1971 - 1993)

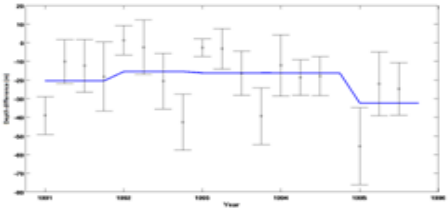

(j) CIL lower boundary difference
(1992 - 1996)

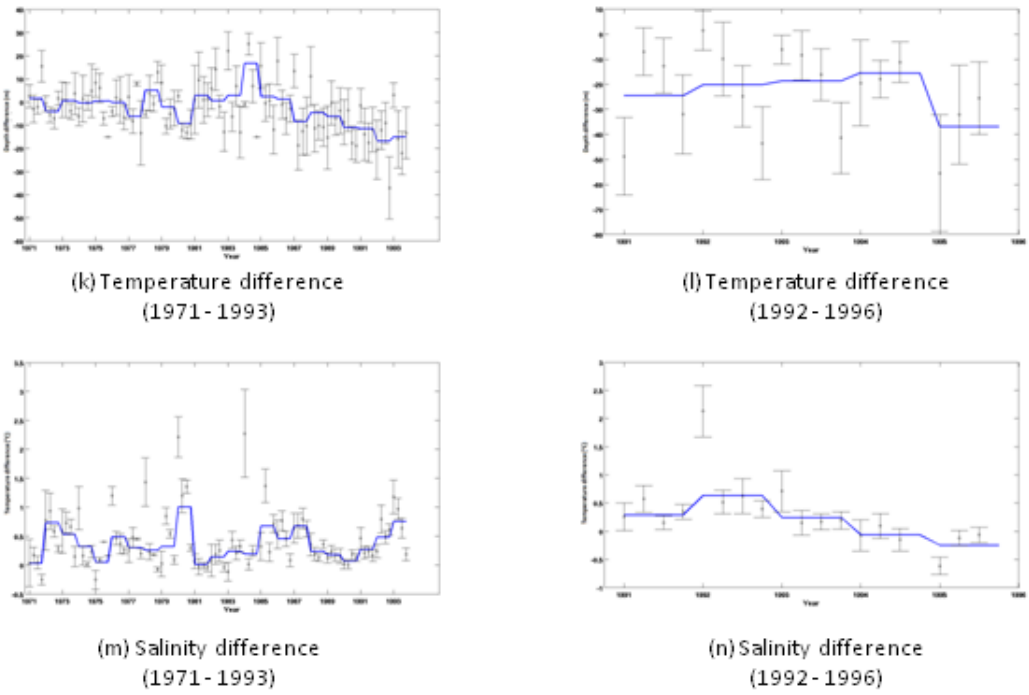


Figure app.B.1 Time series basin averaged difference between modelled and observed variables (model result minus observation) (a) SST (1971 – 1993), (b) SST (1992 – 1996), (c) SSS (1971 – 1993), (d) SSS (1992 – 1996), (e) MLD (1971 – 1993), (f) MLD (1992 – 1996), (g) CIL upper boundary (1971 – 1993), (h) CIL upper boundary (1992 – 1996), (i) CIL lower boundary (1971 – 1993), (j) CIL lower boundary (1992 – 1996), (k) CIL thickness (1971 – 1993) (l) CIL thickness (1992 – 1996), (m) CIL mean temperature (1971 – 1993) and (n) CIL mean temperature (1992 – 1996). Solid blue line represents annual mean errors and circles represent seasonal mean errors. Bars shows seasonal error scatter. The number of stations and total number of observations included in each of the maps can be seen in table 3.1.

## APPENDIX C

## Mean surface currents and density of first model period (1971 – 2001)

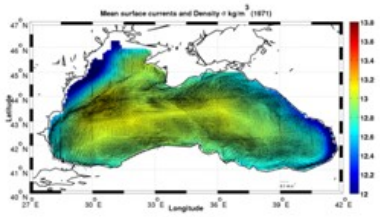
(a) 1971

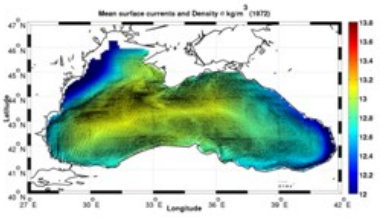
(b) 1972

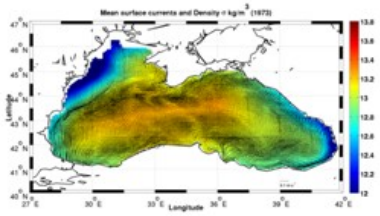
(c) 1973

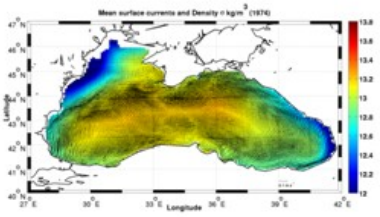
(d) 1974

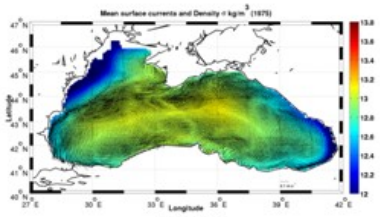
(e) 1975

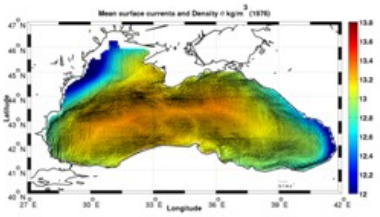
(f) 1976

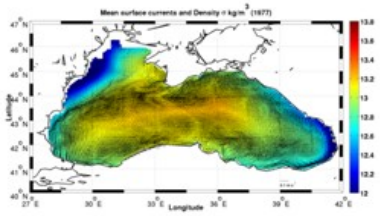
(g) 1977

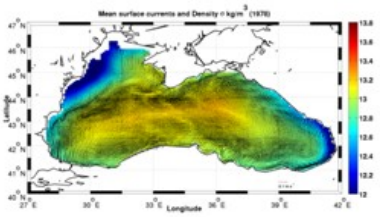
(h) 1978

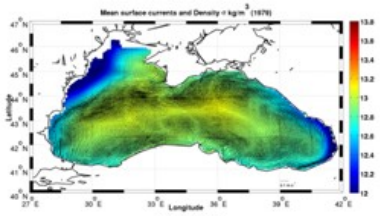
(i) 1979

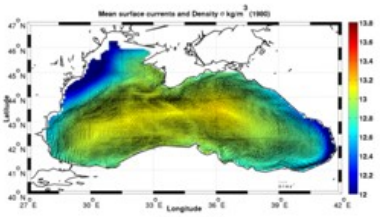
(j)1980

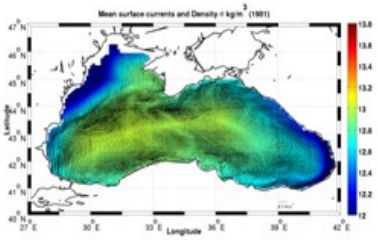


(k) 1981

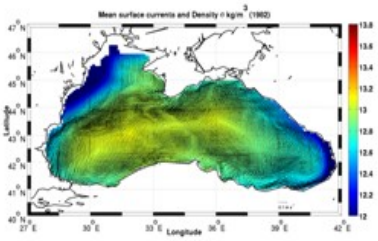


(l) 1982

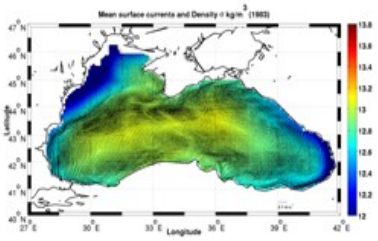


(m) 1983

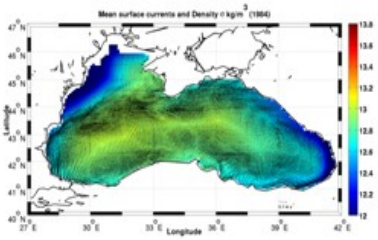


(n) 1984

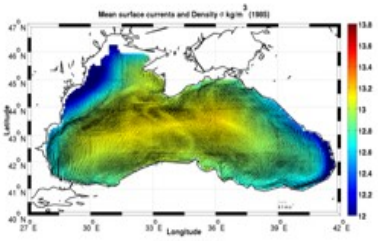


(o) 1985

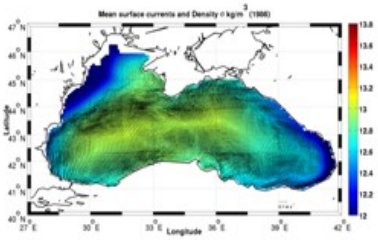


(p) 1986

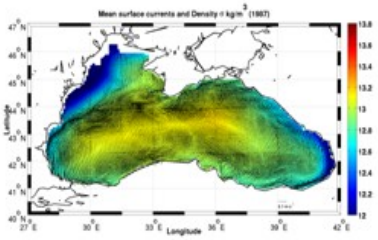


(q) 1987

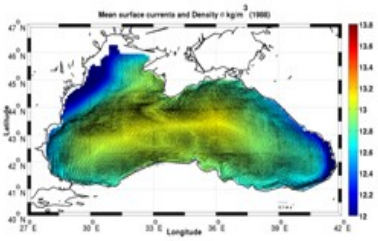


(r) 1988

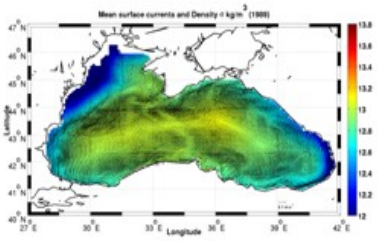


(s) 1989

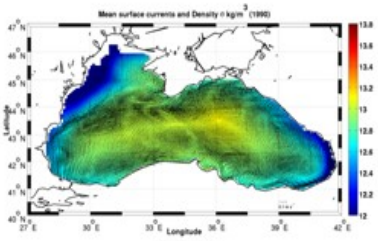


(t)1990

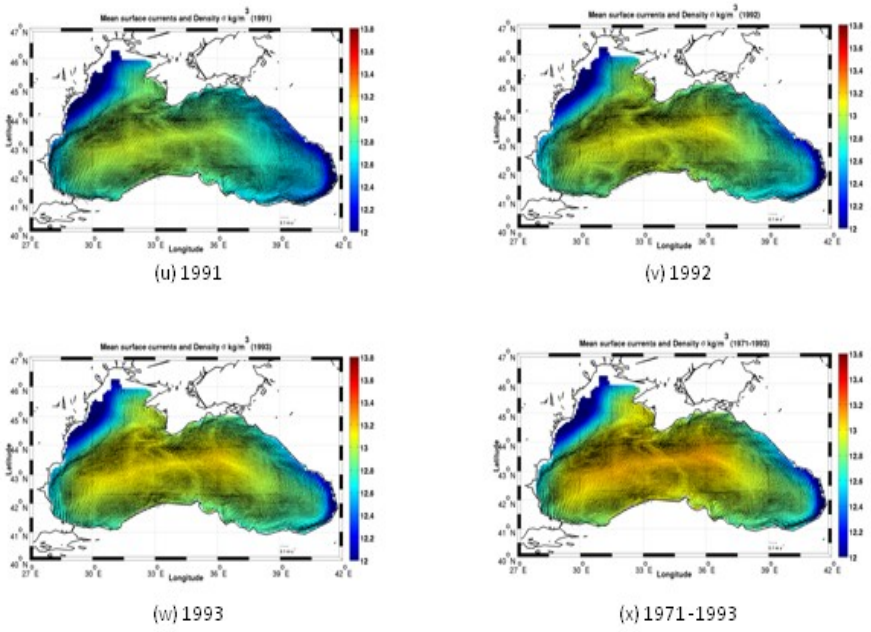


Figure app.C.1 Annual mean surface currents and surface density of first model period (from 1971 to 2001 from (a) to (w)) and first model period mean of surface currents and density (x).